REPORT DOCUMENTATION PAGE

Form Approved OMB NO. 0704-0188

1. REPORT DATE (DD-MM-YYYY)	2. REPORT TYPE	3. DATES COVERED (From - To)
09-09-2012	Final Report	1-Oct-2008 - 30-Jun-2012

4. TITLE AND SUBTITLE

Theoretical Study of Operational Limits of High-Speed Quantum Dot Lasers

5a. CONTRACT NUMBER
W911NF-08-1-0462

5b. GRANT NUMBER

5c. PROGRAM ELEMENT NUMBER
611102

6. AUTHORS

Levon V. Asryan

5d. PROJECT NUMBER

5e. TASK NUMBER

5f. WORK UNIT NUMBER

7. PERFORMING ORGANIZATION NAMES AND ADDRESSES

Virginia Polytechnic Institute & State University
Office of Sponsored Programs
Virginia Polytechnic Institute and State University
Blacksburg, VA 24060 -

8. PERFORMING ORGANIZATION REPORT NUMBER

9. SPONSORING/MONITORING AGENCY NAME(S) AND ADDRESS(ES)

U.S. Army Research Office
P.O. Box 12211
Research Triangle Park, NC 27709-2211

10. SPONSOR/MONITOR'S ACRONYM(S)
ARO

11. SPONSOR/MONITOR'S REPORT NUMBER(S)
54975-EL.18

12. DISTRIBUTION AVAILIBILITY STATEMENT

Approved for Public Release; Distribution Unlimited

13. SUPPLEMENTARY NOTES

The views, opinions and/or findings contained in this report are those of the author(s) and should not contrued as an official Department of the Army position, policy or decision, unless so designated by other documentation.

14. ABSTRACT

A comprehensive theory of the modulation response of quantum dot (QD) lasers is developed. The factors limiting the modulation bandwidth are identified and the highest possible bandwidth is calculated.

The highest bandwidth increases directly with overlap integral of the electron and hole wave functions in a QD, number of QD-layers, and surface density of QDs in a layer, and is inversely proportional to the inhomogeneous line broadening caused by the QD-size dispersion. At 10% dispersion and 100% overlap, the upper limit for the

15. SUBJECT TERMS

semiconductor lasers, quantum dot lasers, quantum well lasers, modulation response, modulation bandwidth, upper limit for the modulation bandwidth, decay rate and frequency of relaxation oscillations, inhomogeneous line broadening, carrier capture delay

16. SECURITY CLASSIFICATION OF:			17. LIMITATION OF ABSTRACT	15. NUMBER OF PAGES	19a. NAME OF RESPONSIBLE PERSON
a. REPORT	b. ABSTRACT	c. THIS PAGE			Levon Asryan
UU	UU	UU	UU		19b. TELEPHONE NUMBER: 540-231-7033

Report Title

Theoretical Study of Operational Limits of High-Speed Quantum Dot Lasers

ABSTRACT

A comprehensive theory of the modulation response of quantum dot (QD) lasers is developed. The factors limiting the modulation bandwidth are identified and the highest possible bandwidth is calculated.

The highest bandwidth increases directly with overlap integral of the electron and hole wave functions in a QD, number of QD-layers, and surface density of QDs in a layer, and is inversely proportional to the inhomogeneous line broadening caused by the QD-size dispersion. At 10% dispersion and 100% overlap, the upper limit for the modulation bandwidth in a single QD-layer laser is as high as 60 GHz.

The carrier capture from the waveguide region into QDs strongly limits the modulation bandwidth. As a function of the capture cross-section, the modulation bandwidth asymptotically approaches its highest value when the cross-section increases infinitely (the case of instantaneous capture). With reducing the capture cross-section, the modulation bandwidth decreases and becomes zero at a certain nonvanishing value of the cross-section. The use of multiple-layers with QDs significantly enhances the modulation bandwidth.

The internal optical loss, which increases with carrier density in the waveguide region, considerably reduces the modulation bandwidth. With internal loss cross-section increasing and approaching its maximum tolerable value, the modulation bandwidth decreases and becomes zero.

Enter List of papers submitted or published that acknowledge ARO support from the start of the project to the date of this printing. List the papers, including journal references, in the following categories:

(a) Papers published in peer-reviewed journals (N/A for none)

Received		Paper
2012/08/29 0	17	Z. N. Sokolova, I. S. Tarasov, L. V. Asryan. Effect of the number of quantum wells in the active region on the linearity of the light-current characteristic of a semiconductor laser, Semiconductors, (08 2012): 1044. doi: 10.1134/S1063782612080222
2012/03/27 0	16	Yuchang Wu, Robert A. Suris, Levon V. Asryan. Effect of internal optical loss on the modulation bandwidth of a quantum dot laser, Applied Physics Letters, (03 2012): 0. doi: 10.1063/1.3697683
2012/03/02 0	15	Z. N. Sokolova, I. S. Tarasov, L. V. Asryan. Capture of charge carriers and output power of a quantum well laser, Semiconductors, (11 2011): 0. doi: 10.1134/S1063782611110261
2011/08/10 2	14	Levon Asryan, Yuchang Wu, Robert Suris. Carrier capture delay and modulation bandwidthin an edge-emitting quantum dot laser, Proc. International Symposium “Nanostructures: Physics and Technology”, (06 2011): 19. doi:
2011/04/07 2	13	Levon V. Asryan, Yuchang Wu, and Robert A. Suris. Carrier capture delay and modulation bandwidth in an edge-emitting quantum dot laser, Applied Physics Letters, (03 2011): . doi:
2011/04/07 2	12	Levon V. Asryan, Yuchang Wu, and Robert A. Suris. Capture delay and modulation bandwidth in a quantum dot laser, Proc. SPIE Photonic West, (01 2011): . doi:
2011/04/07 1	11	Levon V. Asryan. Double Tunneling-Injection Quantum Dot Laser: Temperature-Stable, High-Power, and High-Speed Operation, Proceedings of IEEE Photonics Society Winter Topical Meetings, (01 2010): . doi:
2010/07/22 2	10	Levon V. Asryan, Robert A. Suris. Maximum modulation bandwidth of a quantum dot laser, Proc. International Symposium "Nanostructures: Physics and Technology", (06 2010): . doi:
2010/06/07 1	9	Levon V. Asryan, Robert A. Suris. Upper limit for the modulation bandwidth of a quantum dot laser, Applied Physics Letters, (06 2010): . doi:
2010/04/15 0	8	Levon V. Asryan, Robert A. Suris. Theory of relaxation oscillations and modulation response of a quantum dot laser, Proceedings of the Society for Photo-Optical Instrumentation Engineering, (01 2010): . doi:
2010/04/15 0	7	Dae-Seob Han, Levon V. Asryan. Double tunneling-injection quantum dot laser: Effect of the wetting layer, Proceedings of the Society for Photo-Optical Instrumentation Engineering, (01 2010): . doi:
2010/04/14 2	6	Dae-Seob Han, Levon V Asryan. Output power of a double tunneling-injection quantum dot laser, Nanotechnology, (01 2010): . doi:
2010/04/14 2	5	Dae-Seob Han, Levon V. Asryan. Effect of the Wetting Layer on the Output Power of a Double Tunneling-Injection Quantum-Dot Laser, IEEE Journal of Lightwave Technology, (12 2009): . doi:

TOTAL: 13

Number of Papers published in peer-reviewed journals:

(b) Papers published in non-peer-reviewed journals (N/A for none)

Received	Paper
2010/04/14 2: 4	Levon V. Asryan. Theory of Semiconductor Quantum Dot Lasers, Electrochemical Society Transactions, (01 2009): . doi:
2010/04/14 2: 3	L. V. Asryan. Theory of high performance tunneling-injection quantum dot lasers, Proc. International Symposium "Nanostructures: Physics and Technology", (06 2009): . doi:
2010/04/14 2: 2	Li Jiang, Levon V. Asryan. Spatial hole burning and optical power in a quantum dot laser, Proceedings of SPIE, (01 2009): . doi:
2010/04/14 2: 1	Levon V. Asryan. Theoretical investigation of factors controlling the operating characteristics of quantum dot lasers: a review, Journal of Nanophotonics, (01 2009): . doi:

TOTAL: 4

Number of Papers published in non peer-reviewed journals:

(c) Presentations

[1] L. V. Asryan, "Tunneling-injection of electrons and holes into quantum dots as a tool for high-power lasing," Symposium on "Semiconductor Lasers: Physics and Technology," Saint Petersburg, Russia, Nov. 5-7, 2008.

[2] L. V. Asryan and R. A. Suris, "Maximum possible modulation bandwidth of a quantum dot laser," Symposium on "Semiconductor Lasers: Physics and Technology," Saint Petersburg, Russia, Nov. 10-12, 2010.

[3] L. V. Asryan, "Double tunneling-injection quantum dot laser," International Workshop "Photonics and Micro- and Nano-structured materials", Yerevan, Armenia, June 28-30, 2011.

Number of Presentations: 3.00

Non Peer-Reviewed Conference Proceeding publications (other than abstracts):

Received	Paper

TOTAL:

Number of Non Peer-Reviewed Conference Proceeding publications (other than abstracts):

Peer-Reviewed Conference Proceeding publications (other than abstracts):

Received	Paper

TOTAL:

Number of Peer-Reviewed Conference Proceeding publications (other than abstracts):

(d) Manuscripts

Received	Paper

TOTAL:

Number of Manuscripts:

Books

Received	Paper

TOTAL:

Patents Submitted

Patents Awarded

Awards

Elected by the Bureau of the Division of Physical Sciences of the Russian Academy of Sciences as a Member of the Editorial Board of "Semiconductors" – Russia's leading peer-reviewed journal in the field of semiconductor physics and technology (translated into English).

Graduate Students

NAME	PERCENT_SUPPORTED	Discipline
Yuchang Wu	1.00	
Dae-Seob Han	0.33	
FTE Equivalent:	**1.33**	
Total Number:	**2**	

Names of Post Doctorates

NAME	PERCENT_SUPPORTED
FTE Equivalent:	
Total Number:	

Names of Faculty Supported

NAME	PERCENT_SUPPORTED	National Academy Member
Levon Asryan	0.05	No
FTE Equivalent:	**0.05**	
Total Number:	**1**	

Names of Under Graduate students supported

NAME	PERCENT_SUPPORTED
FTE Equivalent:	
Total Number:	

Student Metrics

This section only applies to graduating undergraduates supported by this agreement in this reporting period

The number of undergraduates funded by this agreement who graduated during this period:	0.00
The number of undergraduates funded by this agreement who graduated during this period with a degree in science, mathematics, engineering, or technology fields:.....	0.00
The number of undergraduates funded by your agreement who graduated during this period and will continue to pursue a graduate or Ph.D. degree in science, mathematics, engineering, or technology fields:.....	0.00
Number of graduating undergraduates who achieved a 3.5 GPA to 4.0 (4.0 max scale):	0.00
Number of graduating undergraduates funded by a DoD funded Center of Excellence grant for Education, Research and Engineering:	0.00
The number of undergraduates funded by your agreement who graduated during this period and intend to work for the Department of Defense	0.00
The number of undergraduates funded by your agreement who graduated during this period and will receive scholarships or fellowships for further studies in science, mathematics, engineering or technology fields:	0.00

Names of Personnel receiving masters degrees

NAME
Total Number:

Names of personnel receiving PHDs

NAME
Dae-Seob Han
Total Number: 1

Names of other research staff

NAME	PERCENT_SUPPORTED
FTE Equivalent:	
Total Number:	

Sub Contractors (DD882)

Inventions (DD882)

Scientific Progress

See also Attachment
---

1) A comprehensive theory of the modulation response of quantum dot (QD) lasers is developed. The factors limiting the modulation bandwidth of QD lasers are identified and the highest possible bandwidth is calculated.

A closed-form expression is derived for the upper limit for the modulation bandwidth. The highest bandwidth increases directly with overlap integral of the electron and hole wave functions in a QD, number of QD-layers, and surface density of QDs in a layer, and is inversely proportional to the inhomogeneous line broadening caused by the QD-size dispersion. At 10% dispersion and 100% overlap, the upper limit for the modulation bandwidth in a single QD-layer laser is as high as 60 GHz.

The carrier capture from the waveguide region into QDs is shown to strongly limit the modulation bandwidth. As a function of the capture cross-section, the modulation bandwidth asymptotically approaches its highest value when the cross-section increases infinitely (the case of instantaneous capture). With reducing the capture cross-section, the modulation bandwidth decreases and becomes zero at a certain nonvanishing value of the cross-section. The use of multiple-layers with QDs significantly enhances the modulation bandwidth.

The internal optical loss, which increases with carrier density in the waveguide region, is shown to considerably reduce the modulation bandwidth. With internal loss cross-section increasing and approaching its maximum tolerable value, the modulation bandwidth decreases and becomes zero.

The theory of the modulation response developed during the performance of this project provides insights into the physical principles dominating the behavior of lasers with nanosize active regions. It serves as the basis for improving such lasers for the use in high-speed communication systems.

2) A comprehensive theory of a double tunneling-injection (DTI) QD laser is developed. In such a laser, both electrons and holes are injected into QDs by tunneling from two separate quantum wells (QWs). Close-to-ideal operating characteristics are predicted for a DTI QD laser. In particular, even in the presence of out-tunneling leakage from QDs and in the presence of the wetting layer, the light-current characteristic (LCC) of a DTI QD laser exhibits a remarkable feature distinguishing such a laser from other types of injection lasers - the LCC becomes increasingly linear and the slope efficiency grows closer to unity at high injection currents.

3) The effect of noninstantaneous capture of carriers from the waveguide region into QWs on the power characteristics of QW lasers is studied. The carrier capture delay into QWs is shown to lead to reduction of the internal quantum efficiency and to sublinearity of the LCC of the laser. It is shown that the use of two QWs as an active region leads to a considerable increase of the internal quantum efficiency and a significantly higher linearity of the LCC compared to a single-well structure. The use of three or more QWs provides, however, only an insignificant improvement of the laser power characteristics as compared to a double-well structure. Hence, from the viewpoint of high output powers and ease of growth, a double-well structure is the most optimum.

Technology Transfer

Attachment

Theoretical Study of Operational Limits of High-Speed Quantum Dot Lasers

Levon V. Asryan

Virginia Polytechnic Institute and State University, Blacksburg, VA 24061

Phone: (540) 231-7033

E-mail: asryan@vt.edu

http://www.mse.vt.edu/people/faculty/asryan.html

Table of Contents

I. Statement of the problem studied

The **objective of this project** was to explore the potential of semiconductor quantum dot (QD) lasers for high-frequency direct modulation of the optical output by injection current. A comprehensive theoretical model for the modulation response of QD lasers was developed, which was based on the small-signal analysis of rate equations for carriers localized in QDs, free carriers in the waveguide region, and photons. The following major factors affecting the modulation bandwidth were considered:

- inhomogeneous line broadening caused by QD-size nonuniformity;
- carrier capture delay from the waveguide region into QDs;
- thermal escape from QDs;
- parasitic recombination outside QDs;
- internal optical loss in the waveguide region.

II. Summary of the most important results

The most important results of this project were published in peer-reviewed journals [1]–[8] and conference proceedings [C1]–[C9]. The papers [1]–[7] and conference proceedings [C1] and [C3] are appended to the end of this attachment.

In [1], [C1], and [C2], the frequency and decay rate of relaxation oscillations, the modulation response, and the modulation bandwidth are calculated as functions of the dc component of the injection current density, cavity length, and parameters of the QD laser structure. A closed-form expression is derived for the upper limit for the modulation bandwidth. The highest possible bandwidth increases directly with overlap integral of the electron and hole wave functions in a QD, number of QD-layers, and surface density of QDs in a layer, and is inversely proportional to the inhomogeneous line broadening caused by the QD-size dispersion. At 10% QD-size fluctuations and 100% overlap, the upper limit for the modulation bandwidth in a single QD-layer laser is as high as 60 GHz.

In [2], [C3], and [C4], it is shown that the carrier capture from the optical confinement layer into QDs strongly limits the modulation bandwidth $\omega_{-3\,\mathrm{dB}}$ of a QD laser. Closed-form analytical expressions are obtained for $\omega_{-3\,\mathrm{dB}}$ in the limiting cases of fast and slow capture. As a function of the cross-section σ_n of carrier capture into a QD, $\omega_{-3\,\mathrm{dB}}$ asymptotically approaches its highest value when $\sigma_\mathrm{n} \to \infty$ (the case of instantaneous capture). With reducing σ_n, $\omega_{-3\,\mathrm{dB}}$ decreases and becomes zero at a certain non-vanishing $\sigma_\mathrm{n}^{\min}$. This $\sigma_\mathrm{n}^{\min}$ presents the minimum tolerable capture cross-section for the lasing to occur at a given dc component j_0 of the injection current density. The higher is j_0, the smaller is $\sigma_\mathrm{n}^{\min}$ and hence the direct modulation of the output power is possible at a slower capture. The use of multiple-layers with QDs significantly enhances the modulation bandwidth – $\omega_{-3\,\mathrm{dB}}$ is considerably higher in a multilayer structure as compared to a single-layer structure at the same dc current. At a plausible value of $\sigma_\mathrm{n} = 10^{-11}\,\mathrm{cm}^2$, $\omega_{-3\,\mathrm{dB}}$ as high as 19 GHz is attainable in a 5-QD-layer structure.

In [3], it is shown that the internal optical loss, which increases with free-carrier density in the waveguide region, considerably reduces the modulation bandwidth $\omega_{-3\,\mathrm{dB}}$ of a QD laser. At a certain optimum value j_0^{opt} of the dc component of the injection current density, the maximum bandwidth $\omega_{-3\,\mathrm{dB}}^{\mathrm{max}}$ is attained and the modulation response function becomes as flat as possible. With internal loss cross-section σ_{int} increasing and approaching its maximum tolerable value, $\omega_{-3\,\mathrm{dB}}^{\mathrm{max}}$ decreases and becomes zero. As with j_0^{opt}, there also exists the optimum cavity length, at which $\omega_{-3\,\mathrm{dB}}$ is highest; the larger is σ_{int}, the longer is the optimum cavity.

In [4], [C5], and [C6], a comprehensive theoretical model is developed for a double tunneling-injection (DTI) QD laser. In a DTI QD laser, both electrons and holes are injected into QDs by tunneling from two separate quantum wells (QWs). It is shown that the light-current characteristic (LCC) of a DTI QD laser exhibits a remarkable feature distinguishing this laser from other types of injection lasers — it becomes increasingly linear, and the slope efficiency grows closer to unity at high injection currents. The linearity is due to the fact that the current paths connecting the opposite sides of the structure lie entirely within QDs — in view of the three-dimensional confinement in QDs, the out-tunneling fluxes of carriers from dots are limited.

In [5] and [C7], the LCC of a DTI QD laser is studied in the presence of the wetting layer (WL). Since *(i)* the opposite sides of a DTI structure are only connected by the current paths through QDs and *(ii)* the WL is located in the n-side of the structure, the only source of holes for the WL is provided by QDs. It is shown that, due to the zero-dimensional nature of QDs, the rate of the hole supply to the WL remains limited with increasing injection current. For this reason, as in the other parts of the structure outside QDs (QWs and optical confinement layer), the parasitic electron-hole recombination remains restricted in the WL. As a result, even in the presence of the WL, the LCC of a DTI QD laser becomes increasingly linear at high injection currents, which is a further demonstration of the potential of such a laser for high-power operation.

In [6], the effect of noninstantaneous capture of carriers from the waveguide region into a QW on the power characteristics of a single QW laser is studied. The main parameter of the theoretical model is the velocity of carrier capture from the waveguide region into a QW. A delayed capture of carries into a QW is shown to lead to reduction of the internal differential quantum efficiency and to sublinearity of the LCC of the laser. A comparison of theoretical and experimental LCCs for a structure considered as an example shows that a good agreement between them (up to a very high injection current density 45 kA/cm^2) is attained at the capture velocity value 2×10^6 cm/s. The findings of this work may be used for optimization of QW lasers for generation of high optical powers.

In [7], the LCC of a semiconductor laser with multiple QWs is calculated taking into account the carrier capture delay from the waveguide region into the wells. It is shown that the use of two QWs as an active region leads to a considerable increase of the internal quantum efficiency of stimulated emission and a significantly higher linearity of the laser LCC compared to a single-well structure. The use of three or more QWs provides, however, only an insignificant improvement of the laser power characteristics as compared to a double-well structure. Hence, from the viewpoint of high output powers and ease of growth, a double-well structure is the most optimum.

III. List of papers published in peer reviewed journals

[1] L. V. Asryan and R. A. Suris, "Upper limit for the modulation bandwidth of a quantum dot laser," ***Appl. Phys. Lett.***, vol. 96, no. 22, Art. no. 221112, May 2010.

[2] L. V. Asryan, Y. Wu, and R. A. Suris, "Carrier capture delay and modulation bandwidth in an edge-emitting quantum dot laser," ***Appl. Phys. Lett.***, vol. 98, no. 13, Art. no. 131108, Mar. 2011.

[3] Y. Wu, R. A. Suris, and L. V. Asryan, "Effect of internal optical loss on the modulation bandwidth of a quantum dot laser," ***Appl. Phys. Lett.***, vol. 100, no. 13, Art. no. 131106, Mar. 2012.

[4] D.-S. Han and L. V. Asryan, "Output power of a double tunneling-injection quantum dot laser," ***Nanotechnology***, vol. 21, no. 1, Art. no. 015201, 14 pages, Jan. 2010.

[5] D.-S. Han and L. V. Asryan, "Effect of the wetting layer on the output power of a double tunneling-injection quantum-dot laser," ***J. Lightw. Technol.***, vol. 27, no. 24, pp. 5775-5782, Dec. 2009.

[6] Z. N. Sokolova, I. S. Tarasov, and L. V. Asryan, "Capture of charge carriers and output power of a quantum well laser," ***Semicond.***, vol. 45, no. 11, pp. 1494–1500, Nov. 2011.

[7] Z. N. Sokolova, I. S. Tarasov, and L. V. Asryan, "Effect of the number of quantum wells in the active region on the linearity of the light–current characteristic of a semiconductor laser," ***Semicond.***, vol. 46, no. 8, pp. 1044–1050, Aug. 2012.

[8] L. V. Asryan, "Theoretical investigation of factors controlling the operating characteristics of quantum dot lasers: A review," ***J. Nanophoton.***, vol. 3, Art. no. 031601, 25 pages, Jan. 2009.

IV. List of conference proceeding publications

[C1] L. V. Asryan and R. A. Suris, "Theory of relaxation oscillations and modulation response of a quantum dot laser," ***Proc. SPIE***, vol. 7610, pp. 76100R-1--76100R-7, Jan. 2010.

[C2] L. V. Asryan and R. A. Suris, "Maximum modulation bandwidth of a quantum dot laser," ***Proc. 18th International Symposium "Nanostructures: Physics and Technology,"*** June 21–26, 2010, St. Petersburg, Russia. pp. 18-20.

[C3] L. V. Asryan, Y. Wu, and R. A. Suris, "Capture delay and modulation bandwidth in a quantum dot laser," ***Proc. SPIE***, vol. 7947, pp. 794708-1--794708-8, Jan. 2011.

[C4] L. V. Asryan, Y. Wu, and R. A. Suris, "Carrier capture delay and modulation bandwidth in an edge-emitting quantum dot laser," ***Proc. 19th International Symposium***

"Nanostructures: Physics and Technology," June 20–25, 2011, Ekaterinburg, Russia. pp. 19-20.

[C5] L. V. Asryan, “Theory of high performance tunneling-injection quantum dot lasers,” ***Proc. 17th International Symposium "Nanostructures: Physics and Technology,"*** June 22-26, 2009, Minsk, Belarus. pp. 16-18.

[C6] L. V. Asryan, “Double Tunneling-Injection Quantum Dot Laser: Temperature-Stable, High-Power, and High-Speed Operation,” ***Proc. IEEE Photonics Society Winter Topical Meeting***, Keystone, CO, Jan. 10-12, 2011, pp. 41-42.

[C7] D.-S. Han and L. V. Asryan, “Double tunneling-injection quantum dot laser: Effect of the wetting layer,” ***Proc. SPIE***, vol. 7610, pp. 76100T-1--76100T-12, Jan. 2010.

[C8] L. Jiang and L. V. Asryan, “Spatial hole burning and optical power in a quantum dot laser,” ***Proc. SPIE***, vol. 7224, pp. 72240R-1--72240R-7, Jan. 2009.

[C9] L. V. Asryan, "Theory of semiconductor quantum dot lasers - Invited Talk," ***ECS (Electrochemical Society) Trans.***, vol. 25, no. 11, pp. 9-23, Sept. 2009.

V. Appendixes

See appended the papers published in peer reviewed journals.

Upper limit for the modulation bandwidth of a quantum dot laser

Levon V. Asryan[1,a)] and Robert A. Suris[2,b)]
[1]*Virginia Polytechnic Institute and State University, Blacksburg, Virginia 24061, USA*
[2]*Ioffe Physico-Technical Institute, Saint Petersburg 194021, Russia*

(Received 25 April 2010; accepted 17 May 2010; published online 4 June 2010)

We derive a closed-form expression for the upper limit for the modulation bandwidth of a semiconductor quantum dot (QD) laser. The highest possible bandwidth increases directly with overlap integral of the electron and hole wave functions in a QD, number of QD-layers, and surface density of QDs in a layer, and is inversely proportional to the inhomogeneous line broadening caused by the QD-size dispersion. At 10% QD-size fluctuations and 100% overlap, the upper limit for the modulation bandwidth in a single QD-layer laser can be as high as 60 GHz. © *2010 American Institute of Physics*. [doi:10.1063/1.3446968]

Due to the capability of direct modulation of the optical output by electric current, semiconductor lasers are extensively used in high-speed fiber networks. In quantum dot (QD) lasers, the stimulated emission is produced in nanosize regions confining the charge carriers in all three spatial dimensions.[1] A discrete energy spectrum of carriers in QDs enables lasing with low threshold current[2–4] and high temperature-stability.[5] The modulation bandwidth of QD lasers, however, needs to be enhanced.

In this work, we study the modulation bandwidth of semiconductor lasers with a quantum-confined active region. Although our analysis and derivations are general and apply also to quantum well and quantum wire lasers, our focus here is on a QD laser. We estimate the highest possible intrinsic bandwidth attainable in a coupled electron-photon system of a laser. For this purpose, we do not consider a transport delay across the optical confinement layer (OCL) and a capture delay from the OCL to the active region. For the same purpose, we do not also consider the gain compression with increasing optical power.

We use the small-signal analysis of rate equations.[6–12] While we assume instantaneous carrier injection into the active region, our model includes the carrier population and recombination in the OCL. In the simplest model, three equations are used—for carriers outside the active region (in the OCL), those in the active region, and photons. The assumptions of no transport and capture delay effectively reduce the number of equations to two. These equations are

$$\frac{\partial}{\partial t}(\delta n) = \frac{\delta j}{eb} - \delta R_{\text{non-stim}} - \delta R_{\text{stim}}, \tag{1}$$

$$\frac{\partial}{\partial t}\left(\frac{\delta N}{V}\right) = \delta R_{\text{stim}} - \delta R_{\text{loss}}, \tag{2}$$

where $\delta(\ldots)$ means a small variation of $(\ldots)$, $n=n_{\text{act}}+n_{\text{OCL}}$ is the total carrier density (including the active region and OCL), j is the injection current density, N is the number of photons in the lasing mode, and b and V are the OCL thickness and volume, respectively, $R_{\text{non-stim}}$ is the total rate of nonstimulated recombination processes (including the active region and OCL), R_{stim} is the stimulated recombination rate, and R_{loss} is the photon loss rate.

Assuming a small time-harmonic ac injection current density $\delta j=\delta j_{\text{m}}\exp(i\omega t)$ and correspondingly looking for the solutions of Eqs. (1) and (2) in the form of $\delta n=\delta n_{\text{m}}(\omega)\exp(i\omega t)$ and $\delta N=\delta N_{\text{m}}(\omega)\exp(i\omega t)$, we obtain for the modulation response function

$$H(\omega) = \left|\frac{\delta N_{\text{m}}(\omega)}{\delta N_{\text{m}}(0)}\right|^2 = \frac{\omega_0^4}{(\omega^2-\omega_0^2)^2+4\Gamma_{\text{dec}}^2\omega^2}. \tag{3}$$

The shape of $H(\omega)$ depends strongly on the dc component j_0 of the injection current density. For a certain range of values of j_0 (see below), $H(\omega)$ has a peak (Fig. 1) obtained at

$$\omega_{\text{peak}} = \sqrt{\Omega_{\text{osc}}^2-\Gamma_{\text{dec}}^2} = \sqrt{\omega_0^2-2\Gamma_{\text{dec}}^2}, \tag{4}$$

where Ω_{osc} and Γ_{dec} are the angular frequency and decay rate of relaxation oscillations,

$$\Omega_{\text{osc}} = \sqrt{\omega_0^2-\Gamma_{\text{dec}}^2}, \tag{5}$$

$$\Gamma_{\text{dec}} = \frac{1}{2}\left(\frac{1}{\tau_{\text{non-stim}}^{\text{dif}}} + v_g\frac{G^{\text{dif}}}{V}N_0\right), \tag{6}$$

and ω_0 is given as

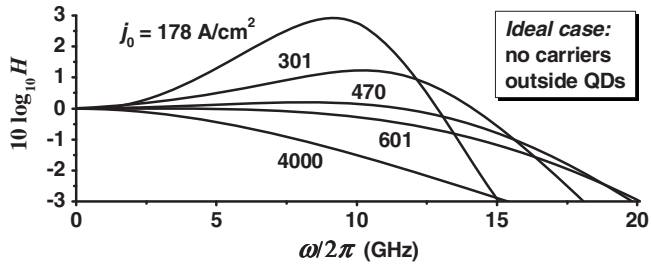

FIG. 1. Response function in the ideal case of no carriers outside QDs at different values of the dc component of the injection current density. In Figs. 1–4, a GaInAsP structure of Ref. 13 lasing at $T=300$ K near 1.55 μm is considered. $Z_{\text{L}}=1$, $(\Delta\varepsilon)_{\text{inhom}}=7$ meV (10% QD-size fluctuations), $N_{\text{S}}=6.11\times10^{10}$ cm^{-2}, and $I_{\text{overlap}}=1$; $g^{\max}=29.52$ cm^{-1} and $G_{\text{act}}^{\text{dif}}=1.36\times10^{-14}$ cm^2. The cavity length $L=1.139$ mm. At these parameters, $\omega_{-3\text{ dB}}^{\max}/2\pi=20$ GHz and $j_{\text{opt}}=601$ A/cm^2 (see also Fig. 2).

a)Electronic mail: asryan@mse.vt.edu.
b)Electronic mail: suris@theory.ioffe.ru.

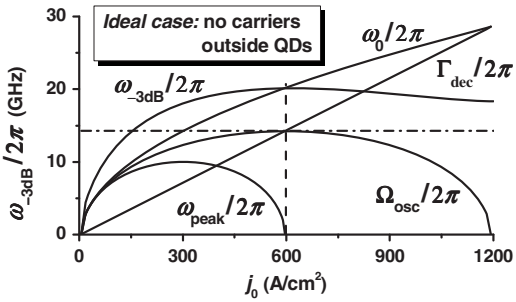

FIG. 2. Modulation bandwidth $\omega_{-3\,\mathrm{dB}}/2\pi$, peak frequency of the response function $\omega_{\mathrm{peak}}/2\pi$, relaxation oscillation frequency $\Omega_{\mathrm{osc}}/2\pi$, $\Gamma_{\mathrm{dec}}/2\pi$, and $\omega_0/2\pi$ vs dc component of the injection current density in the ideal case of no carriers outside QDs. The vertical dashed line marks j_{opt}.

$$\omega_0 = \sqrt{\mathrm{v_g}\frac{G^{\mathrm{dif}}}{V}N_0\frac{1}{\tau_{\mathrm{ph}}}}. \tag{7}$$

In the above equations, $\mathrm{v_g}$ is the group velocity of light, N_0 is the dc number of photons in the lasing mode, which is related to j_0 by the steady-state light-current characteristic, $\tau_{\mathrm{ph}}=(L/\mathrm{v_g})/\ln(1/R)$ is the photon lifetime in the cavity, L is the cavity length, and R is the mirror reflectivity.

The *effective differential gain* G^{dif} is calculated as the derivative of the modal gain g with respect to the *total carrier density* $n=n_{\mathrm{act}}+n_{\mathrm{OCL}}$,

$$G^{\mathrm{dif}} = \frac{\partial g}{\partial n} = \frac{\partial n_{\mathrm{act}}}{\partial n}G^{\mathrm{dif}}_{\mathrm{act}} \ll G^{\mathrm{dif}}_{\mathrm{act}}, \tag{8}$$

where $G^{\mathrm{dif}}_{\mathrm{act}}=\partial g/\partial n_{\mathrm{act}}$. Due to the fact that $\partial n_{\mathrm{act}}/\partial n \ll 1$, $G^{\mathrm{dif}} \ll G^{\mathrm{dif}}_{\mathrm{act}}$ and, as discussed below, the practically achievable modulation bandwidth of the laser can be significantly reduced.

In Eq. (6), the effective differential non-stimulated recombination time $\tau^{\mathrm{dif}}_{\mathrm{non\text{-}stim}}=(\partial R_{\mathrm{non\text{-}stim}}/\partial n)^{-1}$ is expressed in terms of such times in and outside the active region.

The most important dynamic characteristic is the -3 dB bandwidth (referred to as the modulation bandwidth $\omega_{-3\,\mathrm{dB}}/2\pi$ here)—the frequency at which the response function $H(\omega)$ has fallen to half its dc ($\omega=0$) value. The equation for $\omega_{-3\,\mathrm{dB}}$ is

$$\omega_{-3\,\mathrm{dB}} = \sqrt{\omega^2_{\mathrm{peak}} + \sqrt{\omega^4_{\mathrm{peak}} + (r-1)\omega_0^4}}, \tag{9}$$

where $r=10^{0.3}\approx 1.995$.

The relaxation oscillations are only possible [Ω_{osc} should be real—see Eq. (5)] for a certain range of values of N_0, i.e., of dc component j_0 of the injection current density. For such j_0, Ω_{osc} increases from zero, approaches its maximum value, and then decreases to zero (Fig. 2). The peak of the response function also exists for its own range of j_0 [ω_{peak} should be real—see Eq. (4)]; ω_{peak} behaves similarly to Ω_{osc} with increasing j_0 (Fig. 2)—what this means is, at a certain j_0, the peak of $H(\omega)$ appears at $\omega_{\mathrm{peak}}=0$, then it moves to higher frequencies with increasing j_0, and then moves back to lower frequencies and finally disappears at $\omega_{\mathrm{peak}}=0$ (Fig. 2). At j_0 value, at which the peak of $H(\omega)$ disappears, Ω_{osc} is maximum (Fig. 2).

As a function of j_0, the modulation bandwidth also has a maximum (Fig. 2). The maximum of $\omega_{-3\,\mathrm{dB}}$ is obtained at approximately the same value j_{opt} of j_0, at which the peak of the response function disappears (Fig. 2). At $j_0=j_{\mathrm{opt}}$, $H(\omega)$ is most flat (Fig. 1); although Ω_{osc} is maximum at $j_0=j_{\mathrm{opt}}$, the relaxation oscillations are strongly damped at this current ($\Gamma_{\mathrm{dec}}=\Omega^{\mathrm{max}}_{\mathrm{osc}}\approx 1/\tau_{\mathrm{ph}}$—see Fig. 2). On further increase in j_0 beyond j_{opt}, $\omega_{-3\,\mathrm{dB}}$ decreases and asymptotically approaches its saturation value $\omega_{-3\,\mathrm{dB}}|_{j_0\to\infty}\approx 1/\tau_{\mathrm{ph}}$. The maximum values of ω_{peak}, Ω_{osc}, and $\omega_{-3\,\mathrm{dB}}$ are all controlled by the reciprocal photon lifetime in the cavity,

$$\omega^{\mathrm{max}}_{-3\,\mathrm{dB}} \approx \sqrt{2}\Omega^{\mathrm{max}}_{\mathrm{osc}} \approx \sqrt{2}\left(\sqrt{2}\omega^{\mathrm{max}}_{\mathrm{peak}}\right) \approx \frac{\sqrt{2}}{\tau_{\mathrm{ph}}} = \sqrt{2}\frac{\mathrm{v_g}}{L}\ln\frac{1}{R}. \tag{10}$$

The shorter the cavity, the higher $\omega^{\mathrm{max}}_{-3\,\mathrm{dB}}$. The shortest cavity length L^{min} is controlled by the maximum modal gain g^{max} through the lasing condition (equality of the loss to the gain),

$$\frac{1}{L^{\mathrm{min}}}\ln\frac{1}{R} = g^{\mathrm{max}}. \tag{11}$$

Using L^{min} for L in Eq. (10), we find that *the highest possible bandwidth increases directly with* g^{max} *and is not affected by the differential gain* G^{dif},

$$\omega^{\mathrm{highest}}_{-3\,\mathrm{dB}} = \sqrt{2}\mathrm{v_g}g^{\mathrm{max}}. \tag{12}$$

While $\omega^{\mathrm{highest}}_{-3\,\mathrm{dB}}$ is controlled by merely g^{max}, and $\omega^{\mathrm{max}}_{-3\,\mathrm{dB}}$ by L, the optimum current densities j_{opt}, at which they are obtained, are controlled by G^{dif} as well. Indeed, the condition for the maximum bandwidth ($\omega_{\mathrm{peak}}=0$) is obtained when $\omega_0^2=2\Gamma^2_{\mathrm{dec}}$—see Eq. (4). As seen from Eqs. (6) and (7), both ω_0 and Γ_{dec} are controlled by the product of N_0 and G^{dif}. Hence, the lower G^{dif}, the higher will be the photon number $N_0=N_0^{\mathrm{opt}}$, at which $\omega_0^2=2\Gamma^2_{\mathrm{dec}}$, i.e., the higher will be j_{opt}. As a result, the practically achievable bandwidth will be reduced compared to Eq. (12) and even Eq. (10).

The above analysis and equations are general and apply to semiconductor lasers with any type of a quantum-confined active region assuming that the carrier transport to and exchange with the latter are instantaneous. In what follows, we focus on QD lasers. Using the expression for g^{max} for a QD laser,[13,14] we obtain from Eq. (12)

$$\frac{1}{2\pi}\omega^{\mathrm{highest}}_{-3\,\mathrm{dB}} = \frac{2}{3}\sqrt{2}\xi\frac{\alpha}{\sqrt{\epsilon_{\mathrm{g}}}}\left(\frac{P}{\hbar}\right)^2\left(\frac{\lambda_0}{\sqrt{\epsilon}}\frac{1}{\mathcal{L}}\right) \times I_{\mathrm{overlap}}Z_{\mathrm{L}}N_{\mathrm{S}}\frac{\hbar}{(\Delta\varepsilon)_{\mathrm{inhom}}}, \tag{13}$$

where $\xi=1/\sqrt{2\pi}$ or $1/\pi$ for Gaussian or Lorentzian QD-size distributions, respectively, $\alpha=e^2/\hbar c$ is the fine structure constant, $\sqrt{\epsilon_{\mathrm{g}}}$ and $\sqrt{\epsilon}$ are the group and refractive indices of the dispersive OCL material, P is Kane's parameter [$P/\hbar$ has the dimension of a velocity—see Eq. (3) in Ref. 13], λ_0 is the lasing wavelength, $\mathcal{L}$ is the characteristic length of the light confinement in the transverse direction in the waveguide [see Eq. (9) in Ref. 15], I_{overlap} is the overlap integral of the electron and hole wave functions in a QD, Z_{L} is the number of QD-layers, N_{S} is the surface density of QDs in one layer, and $(\Delta\varepsilon)_{\mathrm{inhom}}$ is the inhomogeneous line broadening (measured in units of energy) caused by the QD-size dispersion.

The absence of carriers in the OCL would be the best-case scenario not only for the threshold and power characteristics but for the modulation characteristics as well. For such an ideal case, Figs. 1 and 2 show the response function

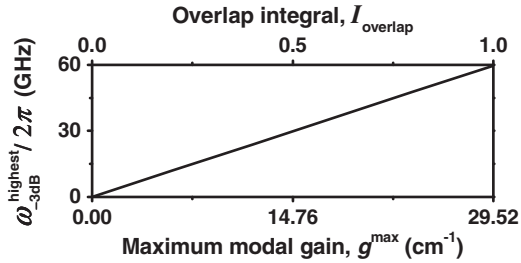

FIG. 3. The upper limit for the modulation bandwidth of a single QD-layer laser vs maximum modal gain and overlap integral of the electron and hole wave functions in a QD.

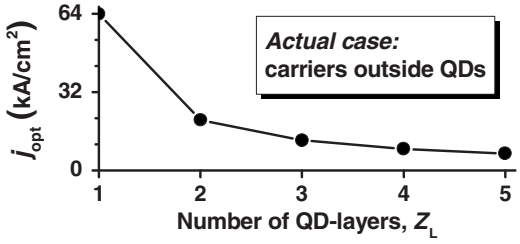

FIG. 4. Optimum dc injection current density maximizing the modulation bandwidth ($\omega_{-3\,dB}^{max}/2\pi=20$ GHz at $L=1.139$ mm) vs number of QD-layers in the actual case of carriers outside QDs.

and the modulation bandwidth $\omega_{-3\,dB}/2\pi$ versus dc current density j_0. The parameters of a specific structure used for an illustration of the results are presented in the caption to Fig. 1. As seen from the figures, $\omega_{-3\,dB}^{max}$ is attained at a fairly low j_{opt} (601 A/cm^2). This is because G^{dif} is high in this case: $G^{dif}=G_{act}^{dif}=1.36\times10^{-14}$ cm^2.

Figure 3 shows the upper limit for the modulation bandwidth $\omega_{-3\,dB}^{highest}/2\pi$ versus maximum modal gain g^{max} in a single QD-layer laser. The top axis illustrates the situation when g^{max} is varied through changing $I_{overlap}$. At 10% QD-size fluctuations [$(\Delta\varepsilon)_{inhom}=7$ meV], $N_S=6.11\times10^{10}$ cm^{-2}, and ideal overlap of the electron and hole wave functions in a QD ($I_{overlap}=1$), the maximum gain is $g^{max}=29.52$ cm^{-1}, and the shortest cavity length is $L^{min}=386$ μm. At these parameters, *the highest possible modulation bandwidth in a single QD-layer laser* is

$$\omega_{-3\,dB}^{highest}/2\pi\approx 60\ \text{GHz}. \tag{14}$$

If the overlap is poor or the QD-size dispersion is large, g^{max} will be low and so will be $\omega_{-3\,dB}^{highest}/2\pi$. Thus, $g^{max}=4.4$ cm^{-1} and $\omega_{-3\,dB}^{highest}/2\pi\approx9$ GHz if $I_{overlap}=0.15$. One way to increase $I_{overlap}$ is the use of more symmetrical (e.g., truncated or disk-shape) QDs.[14]

As seen from Eq. (13), the use of multiple layers with QDs can effectively enhance the modulation bandwidth thus compensating for a poor overlap of the electron and hole wave functions in a QD or for a large QD-size dispersion. The use of submonolayer QDs was also reported to allow for a higher surface density N_S of QDs in a layer.[16]

In the presence of carriers in the OCL, all the above expressions hold. At the same time, G^{dif} [see Eq. (8)] is considerably reduced as compared to G_{act}^{dif}. Due to this, $\omega_{-3\,dB}^{max}$ (and the more so $\omega_{-3\,dB}^{highest}$) becomes unattainable at practical values of the pump current density in a single QD-layer laser. In such a specific laser structure considered here, $\partial n_{act}/\partial n=0.009$, i.e., G^{dif} is about two orders of magnitude lower than G_{act}^{dif} [see Eq. (8)]: $G^{dif}=1.27\times10^{-16}$ cm^2. Hence, the photon number $N_0=N_0^{opt}$, at which $\omega_{-3\,dB}^{max}$ is obtained [see the discussion following Eq. (12)], is two orders of magnitude higher than in the ideal case of no carriers in the OCL, and so is j_{opt} (64 kA/cm^2). Figure 4 shows the optimum dc current density $j_0=j_{opt}$ maximizing $\omega_{-3\,dB}$ versus number of QD-layers. While j_{opt} is very high even for $Z_L=2$, the use of four or five layers makes $\omega_{-3\,dB}^{max}$ practically attainable thus compensating for the adverse effect of carriers in the OCL.

In conclusion, we derived a closed-form expression for the upper limit for the modulation bandwidth of a QD laser. The highest possible bandwidth increases with increasing overlap integral of the electron and hole wave functions in a QD, number of QD-layers and surface density of QDs in a layer, and with reducing QD-size dispersion. At 10% QD-size fluctuations and 100% overlap, the upper limit for the bandwidth in a single QD-layer laser can be as high as 60 GHz.

L.V.A. acknowledges the U.S. Army Research Office (Grant No. W911-NF-08-1-0462) and R.A.S. acknowledges the Russian Foundation for Basic Research (Grant No. 08-02-01337) for support of this work.

[1]Y. Arakawa and H. Sakaki, Appl. Phys. Lett. **40**, 939 (1982).
[2]G. Park, O. B. Shchekin, D. L. Huffaker, and D. G. Deppe, IEEE Photonics Technol. Lett. **12**, 230 (2000).
[3]P. G. Eliseev, H. Li, A. Stintz, G. T. Liu, T. C. Newell, K. J. Malloy, and L. F. Lester, Appl. Phys. Lett. **77**, 262 (2000).
[4]I. C. Sandall, P. M. Smowton, C. L. Walker, H. Y. Liu, M. Hopkinson, and D. J. Mowbray, IEEE Photonics Technol. Lett. **18**, 965 (2006).
[5]S. Fathpour, Z. Mi, P. Bhattacharya, A. R. Kovsh, S. S. Mikhrin, I. L. Krestnikov, A. V. Kozhukhov, and N. N. Ledentsov, Appl. Phys. Lett. **85**, 5164 (2004).
[6]T. Ikegami and Y. Suematsu, Proc. IEEE **55**, 122 (1967).
[7]T. L. Paoli and J. E. Ripper, Proc. IEEE **58**, 1457 (1970).
[8]M. J. Adams, Opto-electronics (London) **5**, 201 (1973).
[9]R. F. Kazarinov and R. A. Suris, Sov. Phys. JETP **39**, 522 (1974).
[10]C. B. Su and V. A. Lanzisera, IEEE J. Quantum Electron. **22**, 1568 (1986).
[11]R. Olshansky, P. Hill, V. Lanzisera, and W. Powazinik, IEEE J. Quantum Electron. **23**, 1410 (1987).
[12]R. Nagarajan, M. Ishikawa, T. Fukushima, R. S. Geels, and J. E. Bowers, IEEE J. Quantum Electron. **28**, 1990 (1992).
[13]L. V. Asryan and R. A. Suris, Semicond. Sci. Technol. **11**, 554 (1996).
[14]L. V. Asryan, M. Grundmann, N. N. Ledentsov, O. Stier, R. A. Suris, and D. Bimberg, J. Appl. Phys. **90**, 1666 (2001).
[15]L. V. Asryan, S. Luryi, and R. A. Suris, IEEE J. Quantum Electron. **39**, 404 (2003).
[16]N. N. Ledentsov, F. Hopfer, and D. Bimberg, Proc. IEEE **95**, 1741 (2007).

Carrier capture delay and modulation bandwidth in an edge-emitting quantum dot laser

Levon V. Asryan,[1,a)] Yuchang Wu,[1,b)] and Robert A. Suris[2,c)]
[1]*Virginia Polytechnic Institute and State University, Blacksburg, Virginia 24061, USA*
[2]*Ioffe Physico-Technical Institute, Saint Petersburg 194021, Russia*

(Received 1 March 2011; accepted 8 March 2011; published online 30 March 2011)

We show that the carrier capture from the optical confinement layer into quantum dots (QDs) can strongly limit the modulation bandwidth $\omega_{-3\ \mathrm{dB}}$ of a QD laser. As a function of the cross-section σ_n of carrier capture into a QD, $\omega_{-3\ \mathrm{dB}}$ asymptotically approaches its highest value when $\sigma_n \to \infty$ (the case of instantaneous capture). With reducing σ_n, $\omega_{-3\ \mathrm{dB}}$ decreases and becomes zero at a certain nonvanishing $\sigma_n^{\min}$. The use of multiple-layers with QDs significantly improves the laser modulation response—$\omega_{-3\ \mathrm{dB}}$ is considerably higher in a multilayer structure as compared to a single-layer structure at the same dc current. © *2011 American Institute of Physics*. [doi:10.1063/1.3571295]

Due to the quantum-size effect, reducing dimensionality of the active region has been a key to developing low-threshold semiconductor lasers.[1,2] In commercial diode lasers, a two-dimensional (2D) active region [quantum well (QW)] is used.[3,4] In quantum dot (QD) lasers, an ultimate case of a zero-dimensional active region is realized.[5,6] The interesting physics involved and the potential for wide range of applications have motivated extensive studies of QD lasers. However, in contrast to the steady-state characteristics, the dynamic properties of QD lasers need to be further scrutinized. In particular, the potential of QD lasers for high-speed direct modulation of the output optical power by injection current should be clarified.

In Ref. 7, the highest modulation bandwidth attainable in QD lasers was estimated. For this purpose, an idealized situation of instantaneous carrier capture into QDs was assumed. In actual semiconductor lasers, carriers are not directly injected into the quantum-confined active region—they are first injected into the optical confinement layer (OCL) and then captured into the active region (Fig. 1). Indirect injection adversely affects the laser operating characteristics—the threshold current is increased[8] and more temperature-sensitive,[9] and the output optical power is decreased.[10,11] Due to a transport delay across the OCL and a capture delay from the OCL into the active region, the bandwidth of direct modulation of the output power by injection current is also reduced (see, e.g., Ref. 12 for QW lasers).

In this letter, we briefly report on the effect of noninstantaneous capture of carriers into QDs on the modulation bandwidth of an edge-emitting QD laser. Our model is based on the following set of three coupled rate equations for free carriers in the OCL, carriers confined in QDs, and photons:

$$\frac{\partial n_{\mathrm{OCL}}}{\partial t} = \frac{j}{eb} - \sigma_n \mathrm{v}_n \frac{N_S}{b}(1-f_n)n_{\mathrm{OCL}} + \sigma_n \mathrm{v}_n n_1 \frac{N_S}{b} f_n - Bn_{\mathrm{OCL}}^2, \quad (1)$$

$$\frac{\partial}{\partial t}\left(2\frac{N_S}{b}f_n\right) = \sigma_n \mathrm{v}_n \frac{N_S}{b}(1-f_n)n_{\mathrm{OCL}} - \sigma_n \mathrm{v}_n n_1 \frac{N_S}{b} f_n - \frac{N_S}{b}\frac{f_n^2}{\tau_{\mathrm{QD}}} - \mathrm{v}_g g^{\max}(2f_n - 1)n_{\mathrm{ph}}, \quad (2)$$

$$\frac{\partial n_{\mathrm{ph}}}{\partial t} = \mathrm{v}_g g^{\max}(2f_n - 1)n_{\mathrm{ph}} - \mathrm{v}_g \beta n_{\mathrm{ph}}, \quad (3)$$

where n_{OCL} is the free carrier density in the OCL, j is the injection current density, b is the OCL thickness, σ_n is the cross-section of carrier capture into a QD, v_n is the carrier thermal velocity, N_S is the surface density of QDs, f_n is the occupancy of the energy-level of a carrier confined in a QD, B is the spontaneous radiative recombination constant for the OCL, τ_{QD} is the spontaneous radiative time in a QD, v_g is the group velocity of light, $g^{\max}$ is the maximum modal gain,[8] n_{ph} is the photon density (per unit volume of the OCL) in the lasing mode, $\beta = (1/L)\ln(1/R)$ is the mirror loss, L is the cavity length, and R is the facet reflectivity.

In Eqs. (1) and (2), the quantity $n_1 = N_c^{3D}\exp(-E_n/T)$ characterizes the carrier thermal escape from a QD to the OCL, where N_c^{3D} is the effective density of states in the OCL, E_n is the carrier thermal excitation energy from a QD, and T is the temperature (in units of energy).

Strictly speaking, σ_n is the only parameter adequately describing the capture/escape into/from a QD. Using σ_n, two distinct characteristic times can be introduced—the capture time into an unoccupied QD ensemble[11] and the thermal escape time from an individual QD,[8,11]

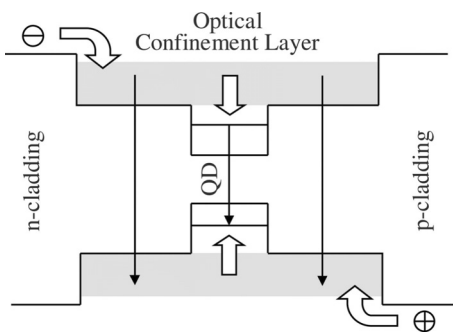

FIG. 1. Indirect injection into the active region of a QD laser.

a)Electronic mail: asryan@vt.edu.
b)Electronic mail: yuchangw@vt.edu.
c)Electronic mail: suris@theory.ioffe.ru.

$$\tau_{\mathrm{capt},0}=\left(\sigma_{\mathrm{n}}\mathrm{v}_{\mathrm{n}}\frac{N_{\mathrm{S}}}{b}\right)^{-1},\quad \tau_{\mathrm{esc}}=(\sigma_{\mathrm{n}}\mathrm{v}_{\mathrm{n}}n_1)^{-1}. \tag{4}$$

In a specific structure considered below, $\tau_{\mathrm{capt},0}=1.63$ ps and $\tau_{\mathrm{esc}}=0.07$ ps at $\sigma_{\mathrm{n}}=10^{-11}$ cm^2.

We consider the spontaneous radiative recombination as the only mechanism of nonstimulated recombination in the OCL and QDs. The inclusion of the nonradiative Auger recombination will increase the threshold current density and the steady-state carrier density in the OCL, and, within the framework of the small-signal analysis, will decrease the differential nonstimulated recombination time, while not otherwise affecting the main derivations of this letter.

Our model does not include the wetting layer (WL), which is inherently present in self-assembled Stranski–Krastanow grown QD structures. The WL can affect the carrier capture into QDs. In addition to the direct capture from the bulk OCL into QDs, carriers will also be captured from the OCL into the 2D WL and then from the WL into QDs. The inclusion of the WL will thus require a careful consideration of all these capture processes.

Due to inhomogeneous broadening of the transition energy in a QD-ensemble in an edge-emitting laser, we do not also consider the optical mode resonance with the QD-transition. This resonance in the context of QD nanocavity lasers was considered in Ref. 13.

Applying the small-signal analysis of rate equations, we consider the injection current density in Eq. (1) in the form of $j=j_0+(\delta j_{\mathrm{m}})\exp(i\omega t)$, where j_0 is the dc component and the amplitude δj_{m} of the time-harmonic ac component is small ($\delta j_{\mathrm{m}}\ll j_0-j_{\mathrm{th}}$, where j_{th} is the threshold current density). We correspondingly look for n_{OCL}, f_{n}, and n_{ph} in Eqs. (1)–(3) in the form of $n_{\mathrm{OCL}}=n_{\mathrm{OCL},0}+(\delta n_{\mathrm{OCL-m}})\exp(i\omega t)$, $f_{\mathrm{n}}=f_{\mathrm{n},0}+(\delta f_{\mathrm{n-m}})\exp(i\omega t)$, and $n_{\mathrm{ph}}=n_{\mathrm{ph},0}+(\delta n_{\mathrm{ph-m}})\exp(i\omega t)$, where $n_{\mathrm{OCL},0}$, $f_{\mathrm{n},0}$, and $n_{\mathrm{ph},0}$ are the solutions of the steady-state rate equations at $j=j_0$.[10,11] In particular,

$$f_{\mathrm{n},0}=\frac{1}{2}\left(1+\frac{\beta}{g^{\max}}\right)=\frac{1}{2}\left(1+\frac{1}{\tau_{\mathrm{ph}}\mathrm{v}_{\mathrm{g}}g^{\max}}\right), \tag{5}$$

where the photon lifetime in the cavity is

$$\tau_{\mathrm{ph}}=\frac{1}{\mathrm{v}_{\mathrm{g}}\beta}=\frac{L}{\mathrm{v}_{\mathrm{g}}\ln(1/R)}. \tag{6}$$

As seen from Eq. (5), the confined-carrier level-occupancy $f_{\mathrm{n},0}$ in a QD at the steady-state is pinned at its threshold value and does not change with j_0 above the lasing threshold. In contrast to $f_{\mathrm{n},0}$, the steady-state free-carrier density $n_{\mathrm{OCL},0}$ in the OCL is not pinned—it rises with j_0 above the lasing threshold. It should be emphasized that it is the noninstantaneous capture of carriers from the OCL into QDs that causes this rise in $n_{\mathrm{OCL},0}$ above the lasing threshold.[10,11]

We obtain from Eqs. (1)–(3) a set of algebraic equations in the frequency-dependent small amplitudes $\delta n_{\mathrm{OCL-m}}$, $\delta f_{\mathrm{n-m}}$, and $\delta n_{\mathrm{ph-m}}$, the solution of which yields the modulation response function $H(\omega)=|\delta n_{\mathrm{ph-m}}(\omega)/\delta n_{\mathrm{ph-m}}(0)|^2$. Finally, we arrive at a cubic equation for the square of the modulation bandwidth $\omega_{-3\ \mathrm{dB}}$—the frequency, at which $H(\omega)$ has fallen to half its dc ($\omega=0$) value.

For an illustration of our results, room-temperature operation of a GaInAsP heterostructure lasing near 1.55 μm (Ref. 8) is considered here. We assume 10% QD-size fluctuations, the surface density of QDs in a single-layer $N_{\mathrm{S}}=6.11\times10^{10}$ cm^{-2}, and an ideal overlap between the electron and hole wave functions in a QD. At these parameters, the maximum modal gain in a single-QD-layer structure $g^{\max}=29.52$ cm^{-1}. The OCL thickness $b=0.28$ μm and the cavity length $L=1.1$ mm (at this L and the as-cleaved facet reflectivity $R=0.32$, the mirror loss $\beta=10$ cm^{-1}).

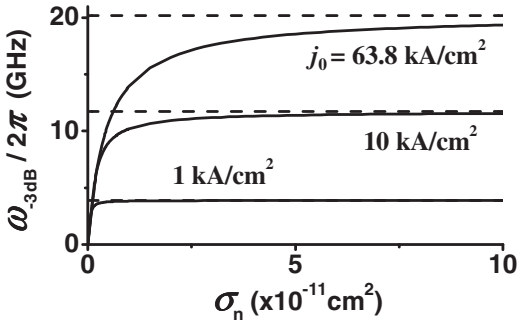

FIG. 2. Modulation bandwidth vs capture cross-section into a QD at different values of the dc component j_0 of the injection current density in a single-layer structure. The horizontal dashed lines show $\omega_{-3\ \mathrm{dB}}$ for the case of instantaneous capture [Eq. 9 of Ref. 7]. 63.8 kA/cm^2 is the optimum value of j_0 maximizing $\omega_{-3\ \mathrm{dB}}$ for the case of instantaneous capture and, correspondingly, the top horizontal line shows $\omega_{-3\ \mathrm{dB}}^{\max}$ for that case [Eq. (11)]. $T=300$ K and $L=1.1$ mm.

The modulation bandwidth depends strongly on the capture cross-section σ_{n}. At a fixed j_0, with making slower the capture into QDs (reducing σ_{n}), $\omega_{-3\ \mathrm{dB}}$ decreases and finally becomes zero (Figs. 2 and 3).

As seen from Fig. 3, $\omega_{-3\ \mathrm{dB}}=0$ at a certain nonvanishing value $\sigma_{\mathrm{n}}^{\min}$. This is due to the fact that, at a given j_0, no lasing is attainable in the structure if $\sigma_{\mathrm{n}}<\sigma_{\mathrm{n}}^{\min}$. Indeed, while j_0 is fixed, the threshold current density increases with decreasing σ_{n} (the curve corresponding to the left axis),

$$j_{\mathrm{th}}=\frac{eN_{\mathrm{S}}}{\tau_{\mathrm{QD}}}f_{\mathrm{n0}}^2+ebB\left(n_1\frac{f_{\mathrm{n0}}}{1-f_{\mathrm{n0}}}+\frac{1}{\sigma_{\mathrm{n}}\mathrm{v}_{\mathrm{n}}\tau_{\mathrm{QD}}}\frac{f_{\mathrm{n0}}^2}{1-f_{\mathrm{n0}}}\right)^2, \tag{7}$$

where $f_{\mathrm{n},0}$ is given by Eq. (5). In order for the lasing to occur, j_0 should be higher than j_{th}. At a certain $\sigma_{\mathrm{n}}^{\min}$, j_{th} becomes equal to j_0 (Fig. 3). At $\sigma_{\mathrm{n}}\le\sigma_{\mathrm{n}}^{\min}$, $j_{\mathrm{th}}\ge j_0$, which means that there can be no lasing and hence no direct modulation in the structure (the shaded region in Fig. 3).

The minimum tolerable σ_{n} for the lasing to occur at j_0 is found from the condition $j_{\mathrm{th}}=j_0$ and is given by

$$\sigma_{\mathrm{n}}^{\min}(j_0)=\frac{1}{\mathrm{v}_{\mathrm{n}}\tau_{\mathrm{QD}}}\frac{f_{\mathrm{n0}}^2}{1-f_{\mathrm{n0}}}\sqrt{ebB}\frac{\sqrt{j_0-\frac{eN_{\mathrm{S}}}{\tau_{\mathrm{QD}}}f_{\mathrm{n0}}^2}+\sqrt{j_{\mathrm{th}}^{\mathrm{eq}}-\frac{eN_{\mathrm{S}}}{\tau_{\mathrm{QD}}}f_{\mathrm{n0}}^2}}{j_0-j_{\mathrm{th}}^{\mathrm{eq}}}, \tag{8}$$

where $j_{\mathrm{th}}^{\mathrm{eq}}$ is j_{th} for the case of instantaneous capture [$j_{\mathrm{th}}^{\mathrm{eq}}$ is obtained using $\sigma_{\mathrm{n}}=\infty$ in Eq. (7)].

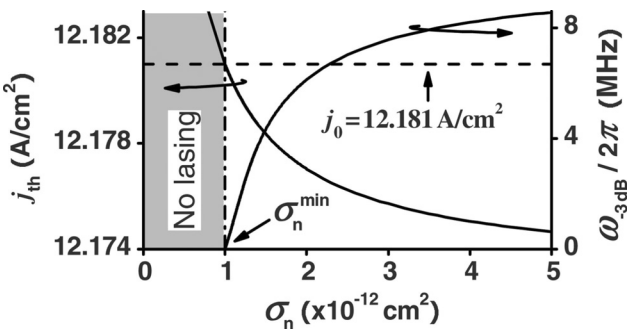

FIG. 3. Modulation bandwidth (at a very low j_0) and threshold current density vs capture cross-section into a QD in a single-layer structure.

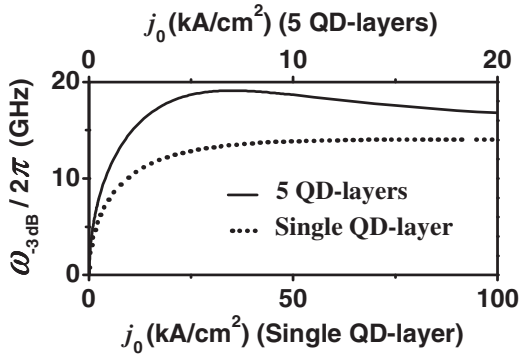

FIG. 4. Modulation bandwidth vs dc component of the injection current density in single- and 5-QD-layer-structures. A plausible value $\sigma_n = 10^{-11}$ cm^2 (Refs. 14 and 15) of the capture cross-section is used.

As seen from Eq. (8), when j_0 decreases and approaches j_{th}^{eq}, σ_n^{min} increases infinitely, i.e., no lasing is attainable at $j_0 \le j_{th}^{eq}$ even if the carrier capture into QDs is instantaneous.

With increasing j_0, σ_n^{min} becomes smaller, i.e., the lasing can occur and hence the direct modulation of the output power is possible at a slower capture. At high j_0 (when $\sigma_n^{min} \to 0$), the asymptotic expression for $\omega_{-3\ dB}$ for σ_n in the vicinity of σ_n^{min} $[(\sigma_n - \sigma_n^{min})/\sigma_n^{min} \ll 1]$ is

$$\omega_{-3\ dB} \approx 2\sqrt{r-1}\, v_g g^{max} \frac{f_{n0}(1-f_{n0})}{2-f_{n0}} \frac{\sigma_n - \sigma_n^{min}}{\sigma_n^{min}}, \tag{9}$$

where the numerical parameter $r = 10^{0.3} \approx 1.995$ originates from the definition of the -3 dB bandwidth, $10 \log_{10} H(\omega_{-3\ dB}) = -3$.

As a function of the dc component j_0 of the injection current density, $\omega_{-3\ dB}$ has a maximum (Fig. 4). In a single-QD-layer structure (the dotted curve), the optimum value j_{opt} of j_0, at which $\omega_{-3\ dB}^{max}$ is attained, is very high, i.e., $\omega_{-3\ dB}^{max}$ is unattainable. As seen from the figure, there are the following two advantages in a multi-QD-layer structure (the solid curve) as compared to a single-layer structure: (i) $\omega_{-3\ dB}$ is considerably higher at the same j_0 and (ii) j_{opt} is considerably reduced, which means that $\omega_{-3\ dB}^{max}$ is practically attainable.

At large σ_n, when $\tau_{capt,0}/\tau_{ph} \ll 1$ [$\tau_{capt,0}$ and τ_{ph} are given by Eqs. (4) and (6), respectively], both $\omega_{-3\ dB}$ at a given j_0 (Fig. 2) and $\omega_{-3\ dB}^{max}$ (Fig. 5) asymptotically approach their saturation values (the horizontal dashed lines) corresponding to the case of instantaneous capture into QDs,

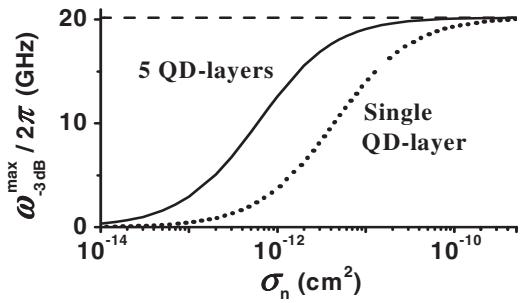

FIG. 5. Maximum modulation bandwidth vs capture cross-section into a QD. The horizontal dashed line shows $\omega_{-3\ dB}^{max}$ for the case of instantaneous capture into QDs [Eq. (11)].

$$(\omega_{-3\ dB}|_{\sigma_n=\infty} - \omega_{-3\ dB}), \quad (\omega_{-3\ dB}^{max}|_{\sigma_n=\infty} - \omega_{-3\ dB}^{max}) \propto \frac{\tau_{capt,0}}{\tau_{ph}} \propto \frac{1}{\sigma_n}, \tag{10}$$

where $\omega_{-3\ dB}|_{\sigma_n=\infty}$ is given by Eq. 9 of Ref. 7 and

$$\omega_{-3\ dB}^{max}|_{\sigma_n=\infty} \approx \frac{\sqrt{2}}{\tau_{ph}}. \tag{11}$$

As seen from Fig. 5, while the saturation value of $\omega_{-3\ dB}^{max}$ at $\sigma_n \to \infty$ and at a fixed L [Eq. (11)] does not depend on the number of QD-layers, $\omega_{-3\ dB}^{max}$ at a given finite σ_n is higher in a multilayer structure as compared to a single-layer structure.

In conclusion, we have shown that the carrier capture from the OCL into QDs can strongly limit the modulation bandwidth $\omega_{-3\ dB}$ of a QD laser. $\omega_{-3\ dB}$ is highest in the case of instantaneous capture into QDs, when the cross-section of carrier capture into a QD $\sigma_n = \infty$. With reducing σ_n, $\omega_{-3\ dB}$ decreases and becomes zero at a certain nonvanishing σ_n^{min}. This σ_n^{min} presents the minimum tolerable σ_n for the lasing to occur at a given dc component j_0 of the injection current density. The use of multiple-layers with QDs has been shown to significantly improve the modulation response of the laser—$\omega_{-3\ dB}$ is considerably higher in a multilayer structure as compared to a single-layer structure at the same j_0. At a plausible cross-section $\sigma_n = 10^{-11}$ cm^2,[14,15] $\omega_{-3\ dB}$ as high as 19 GHz can be obtained in a 5-QD-layer structure with the cavity length $L = 1.1$ mm at a practical value of $j_0 = 7$ kA/cm^2. Our analysis provides a basis for optimizing the QD laser design for high-speed operation.

L.V.A. and Y.W. acknowledge the U.S. Army Research Office (Grant No. W911-NF-08-1-0462), Y.W. also acknowledges the China Scholarship Council, and R.A.S. acknowledges the Russian Foundation for Basic Research (Grant No. 08-02-01337) and the Program "Fundamental Research in Nanotechnology and Nanomaterials" of the Presidium of the Russian Academy of Sciences for support of this work.

[1]R. Dingle and C. H. Henry, U.S. Patent No. 3982207 (21 September 1976).
[2]Zh. I. Alferov, Rev. Mod. Phys. **73**, 767 (2001).
[3]W. T. Tsang, Appl. Phys. Lett. **40**, 217 (1982).
[4]P. S. Zory, Jr., *Quantum Well Lasers* (Academic, Boston, 1993).
[5]Y. Arakawa and H. Sakaki, Appl. Phys. Lett. **40**, 939 (1982).
[6]A. E. Zhukov, A. R. Kovsh, S. S. Mikhrin, A. P. Vasil'ev, E. S. Semenova, N. A. Maleev, V. M. Ustinov, M. M. Kulagina, E. V. Nikitina, I. P. Soshnikov, Y. M. Shernyakov, D. A. Livshits, N. V. Kryjanovskaya, D. S. Sizov, M. V. Maximov, A. F. Tsatsul'nikov, N. N. Ledentsov, D. Bimberg, and Zh. I. Alferov, Physica E **17**, 589 (2003).
[7]L. V. Asryan and R. A. Suris, Appl. Phys. Lett. **96**, 221112 (2010).
[8]L. V. Asryan and R. A. Suris, Semicond. Sci. Technol. **11**, 554 (1996).
[9]L. V. Asryan and R. A. Suris, IEEE J. Quantum Electron. **34**, 841 (1998).
[10]L. V. Asryan, S. Luryi, and R. A. Suris, Appl. Phys. Lett. **81**, 2154 (2002).
[11]L. V. Asryan, S. Luryi, and R. A. Suris, IEEE J. Quantum Electron. **39**, 404 (2003).
[12]R. Nagarajan, M. Ishikawa, T. Fukushima, R. S. Geels, and J. E. Bowers, IEEE J. Quantum Electron. **28**, 1990 (1992).
[13]M. Lorke, T. R. Nielsen, and J. Mørk, Appl. Phys. Lett. **97**, 211106 (2010).
[14]O. Engström, M. Kaniewska, Y. Fu, J. Piscator, and M. Malmkvist, Appl. Phys. Lett. **85**, 2908 (2004).
[15]S. K. Zhang, H. J. Zhu, F. Lu, Z. M. Jiang, and X. Wang, Phys. Rev. Lett. **82**, 2622 (1999).

Effect of internal optical loss on the modulation bandwidth of a quantum dot laser

Yuchang Wu,[1,a)] Robert A. Suris,[2,b)] and Levon V. Asryan[1,c)]
[1]*Virginia Polytechnic Institute and State University, Blacksburg, Virginia 24061, USA*
[2]*Ioffe Physico-Technical Institute, St. Petersburg 194021, Russia*

(Received 10 February 2012; accepted 6 March 2012; published online 26 March 2012)

We show that the internal optical loss, which increases with free-carrier density in the waveguide region, considerably reduces the modulation bandwidth $\omega_{-3\,\mathrm{dB}}$ of a quantum dot laser. At a certain optimum value j_0^{opt} of the dc component of the injection current density, the maximum bandwidth $\omega_{-3\,\mathrm{dB}}^{\mathrm{max}}$ is attained and the modulation response function becomes as flat as possible. With internal loss cross-section σ_{int} increasing and approaching its maximum tolerable value, $\omega_{-3\,\mathrm{dB}}^{\mathrm{max}}$ decreases and becomes zero. As with j_0^{opt}, there also exists the optimum cavity length, at which $\omega_{-3\,\mathrm{dB}}$ is highest; the larger is σ_{int}, the longer is the optimum cavity. © *2012 American Institute of Physics*. [http://dx.doi.org/10.1063/1.3697683]

The optical output in edge-emitting semiconductor lasers is provided by photons leaving the cavity through its mirrors. In addition to this useful output loss, there is also parasitic loss of photons, which occurs within the laser cavity and, for this reason, is termed internal optical loss. There can be several mechanisms for internal loss,[1–6] such as free-carrier absorption, intervalence band absorption, and scattering at rough surfaces. While there have been studies of the effect of internal loss on the threshold and power characteristics of semiconductor lasers with a quantum-confined active region and, particularly, quantum dot (QD) lasers,[7–9] no consideration of the dynamic properties of QD lasers in the presence of internal loss has been given so far. In this work, we study the modulation response of a QD laser taking into account the carrier-density-dependent internal loss in the optical confinement layer (OCL). To mainly focus on the effect of internal loss, we do not consider here some other factors, among them the carrier capture delay from the OCL into QDs,[10] which also affect the modulation bandwidth of a laser.

To consider a direct modulation of the laser output by alternating current (ac), we use the small-signal analysis[11–17] and hence we assume that the ac component δj of the injection current density is small. For small variations $\delta\ldots$ of the corresponding quantities (around their steady-state values) caused by δj, we have the following rate equations:

$$\frac{\partial}{\partial t}(\delta n) = \frac{\delta j}{eb} - \delta R_{\mathrm{non-stim}} - \delta R_{\mathrm{stim}}, \tag{1}$$

$$\frac{\partial}{\partial t}(\delta n_{\mathrm{ph}}) = \delta R_{\mathrm{stim}} - \delta R_{\mathrm{loss}}, \tag{2}$$

where $n = n_{\mathrm{act}} + n_{\mathrm{OCL}}$, n_{act} and n_{OCL} are the carrier densities in the active region and OCL, respectively, n_{ph} is the photon density (per unit volume of the OCL) in the lasing mode, e is the electron charge, b is the thickness of the OCL, and $R_{\mathrm{non-stim}}$ is the rate of the processes of non-stimulated recombination of carriers in the active region and OCL.

In Eqs. (1) and (2), the rate of stimulated recombination of carriers, which is the same as the rate of stimulated emission of photons, is

$$R_{\mathrm{stim}} = \mathrm{v_g} g n_{\mathrm{ph}}, \tag{3}$$

where $\mathrm{v_g}$ is the group velocity of light and g is the modal gain of the laser.

The photon loss rate in Eq. (2) is the sum of the useful output (mirror) and parasitic (internal) loss rates,

$$R_{\mathrm{loss}} = \mathrm{v_g}(\beta + \alpha_{\mathrm{int}}) n_{\mathrm{ph}}, \tag{4}$$

where $\beta = (1/L)\ln(1/R)$ is the mirror loss coefficient, L is the cavity length, and R is the mirror reflectivity.

In the general case, the internal loss coefficient can be presented as[7–9]

$$\alpha_{\mathrm{int}} = \alpha_0 + \sigma_{\mathrm{int}} n_{\mathrm{OCL}}, \tag{5}$$

where the constant component α_0 accounts for scattering at rough surfaces and free-carrier absorption in the cladding layers, and the component $\sigma_{\mathrm{int}} n_{\mathrm{OCL}}$ describes free-carrier and intervalence band absorption in the OCL with σ_{int} being the effective cross-section for these absorption loss processes.

As seen from Eq. (5), α_{int} will vary with time through such variation in the free-carrier density n_{OCL} caused by the ac current. Hence, as seen from Eqs. (4) and (5), the temporal variation of the photon loss rate will be due to such variation of not only the photon density n_{ph} but n_{OCL} as well.

Considering a time-harmonic ac injection current density, $\delta j = \delta j_{\mathrm{m}} \exp(i\omega t)$, we find from Eqs. (1) and (2) the frequency-dependent amplitude $\delta n_{\mathrm{ph-m}}(\omega)$ of the time-harmonic photonic density and then the modulation response function $H(\omega)$,

$$H(\omega) = \left|\frac{\delta n_{\mathrm{ph-m}}(\omega)}{\delta n_{\mathrm{ph-m}}(0)}\right|^2 = \frac{\omega_0^4}{(\omega^2 - \omega_0^2)^2 + 4\Gamma_{\mathrm{dec}}^2 \omega^2}. \tag{6}$$

a)Electronic mail: yuchangw@vt.edu.
b)Electronic mail: suris@theory.ioffe.ru.
c)Electronic mail: asryan@vt.edu.

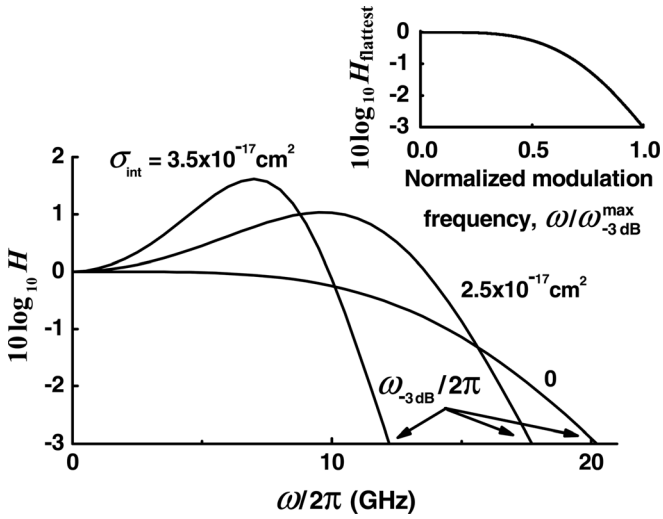

FIG. 1. Modulation response function at different values of the internal loss cross-section σ_{int}. For our calculations, room-temperature operation of a GaInAsP structure of Ref. 20 with a single layer of QDs lasing near 1.55 μm is considered; 10% QD-size fluctuations are assumed; $g^{max} = 29.52\,cm^{-1}$. $\alpha_0 = 0$ and $L = 1.139$ mm. For all the three curves, the dc component of the injection current density $j_0 = 64\,kA/cm^2$; for the case of no internal loss, this value of j_0 is equal to j_0^{opt} and that is why the response function is flattest. The inset shows the flattest response function given by Eq. (15) vs. normalized modulation frequency $\omega/\omega^{max}_{-3\,dB}$; using this universal dependence and Eq. (12) for $\omega^{max}_{-3\,dB}$, the flattest response function at a non-zero σ_{int} can be easily plotted.

While the shape of $H(\omega)$ depends strongly on the internal loss (Fig. 1), as a function of the frequency ω of direct modulation and parameters Γ_{dec} and ω_0, expression (6) is the same as for the case of no internal loss.[18]

The decay rate of relaxation oscillations is given by

$$\Gamma_{dec} = \frac{1}{2}\left(\frac{1}{\tau^{dif}_{non-stim}} + v_g G^{dif} n_{ph,0}\right), \tag{7}$$

where $\tau^{dif}_{non-stim} = (\partial R_{non-stim,0}/\partial n_0)^{-1}$ is the effective differential non-stimulated recombination time, $G^{dif} = \partial g_0/\partial n_0$ is the effective differential gain, $g_0 = g^{max}(2f_{n,0} - 1)$ is the modal gain, g^{max} is the maximum value of the modal gain, and $f_{n,0}$ is the confined-carrier level occupancy in a QD. Except for α_0 and ω_0, "0" in the subscripts of all the other quantities denotes their steady-state values.

In terms of the quantities $\tau^{dif}_{non-stim}$, G^{dif}, and $n_{ph,0}$, expression (7) is also the same as for the case of no internal loss.[18] Each of these quantities is, however, affected by the internal loss.

For ω_0 entering into Eq. (6), we have

$$\omega_0 = \sqrt{v_g G^{dif} n_{ph,0} \frac{1}{\tau_{ph,0}}}\ \sqrt{1 - \frac{\partial \alpha_{int,0}}{\partial g_0}}, \tag{8}$$

where $\tau_{ph,0}$ is the photon lifetime in the cavity,

$$\tau_{ph,0} = \frac{1}{v_g(\beta + \alpha_{int,0})} = \frac{1}{v_g(\beta + \alpha_0 + \sigma_{int} n_{OCL,0})}. \tag{9}$$

Due to the internal loss, $\tau_{ph,0}$ depends on the free-carrier density $n_{OCL,0}$ in the OCL.

For the modulation bandwidth, which is defined as the -3 dB bandwidth [$10\log_{10} H(\omega_{-3\,dB}) = -3$, see Fig. 1], we derived

$$\omega_{-3\,dB} = \sqrt{\sqrt{\omega^4_{peak} + (r-1)\omega_0^4} + \omega^2_{peak}}$$
$$= \sqrt{\sqrt{(\omega_0^2 - 2\Gamma^2_{dec})^2 + (r-1)\omega_0^4} + (\omega_0^2 - 2\Gamma^2_{dec})}, \tag{10}$$

where $r = 10^{0.3} \approx 1.995$ and

$$\omega_{peak} = \sqrt{\omega_0^2 - 2\Gamma^2_{dec}}. \tag{11}$$

The steady-state photon density $n_{ph,0}$, entering into Eqs. (7) and (8), is a function of the dc component j_0 of the injection current density (the relationship between $n_{ph,0}$ and j_0 is given by the light-current characteristic). Consequently, all the quantities Γ_{dec}, ω_0, ω_{peak}, $\omega_{-3\,dB}$, and the response function $H(\omega)$ depend on j_0 as well.

When $H(\omega)$ has a peak (which occurs only for a certain range of values of the dc component j_0 of the injection current density), Eq. (11) presents the frequency of the peak. Equation (10) for $\omega_{-3\,dB}$ holds also for those j_0 at which there is no peak in $H(\omega)$ – in that case too, ω_{peak} is formally given by Eq. (11) but the difference $\omega_0^2 - 2\Gamma^2_{dec}$ in Eq. (11) is negative.

With increasing j_0 above the threshold current density j_{th}, the modulation bandwidth increases from zero, approaches its maximum value $\omega^{max}_{-3\,dB}$ (marked by the symbol "x" in Fig. 2) at a certain optimum dc current density j_0^{opt}, then decreases and will asymptotically approach its saturation value. At $j_0 = j_0^{opt}$, when the maximum bandwidth $\omega^{max}_{-3\,dB}$ is attained, the peak of the response function occurs at $\omega_{peak} = 0$ and the response function becomes as flat as possible (Fig. 1).

Analyzing Eq. (10) for $\omega_{-3\,dB}$ as a function of j_0, we obtained the following expression for $\omega^{max}_{-3\,dB}$:

$$\omega^{max}_{-3\,dB} \approx \frac{\sqrt{2}}{\tau_{ph,0}}\left(1 - \frac{\partial \alpha_{int,0}}{\partial g_0}\right) = \frac{\sqrt{2}}{\tau_{ph,0}}\left[1 - \frac{\sigma_{int} n_1}{2g^{max}(1 - f_{n,0})^2}\right], \tag{12}$$

where we used Eq. (5) for α_{int} and the equation $n_{OCL} = n_1 f_n/(1 - f_n)$ (Eq. (3) of Ref. 19) relating the free-carrier

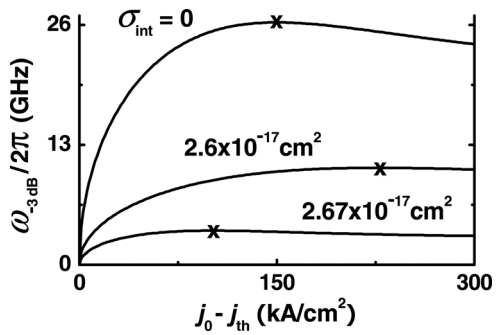

FIG. 2. Modulation bandwidth $\omega_{-3\,dB}/2\pi$ vs. excess of the dc component of the injection current density over the threshold current density at different values of σ_{int}. $\alpha_0 = 3\,cm^{-1}$ and $L = 1.139$ mm. The "x" symbol marks the maximum point (j_0^{opt}, $\omega^{max}_{-3\,dB}$) on each curve.

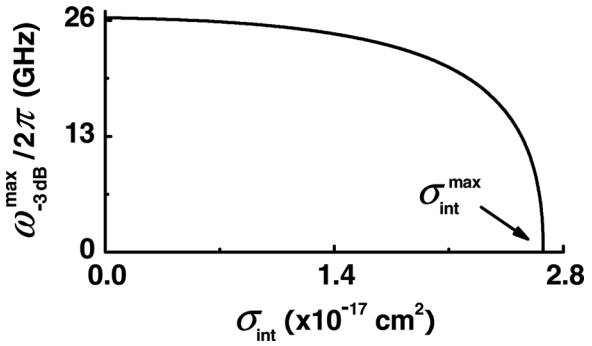

FIG. 3. Maximum modulation bandwidth $\omega^{max}_{-3\,dB}/2\pi$ vs. internal loss cross-section σ_{int}. $\alpha_0 = 3\,cm^{-1}$ and $L = 1.139$ mm; $\sigma^{max}_{int} = 2.677 \times 10^{-17}$ cm^2.

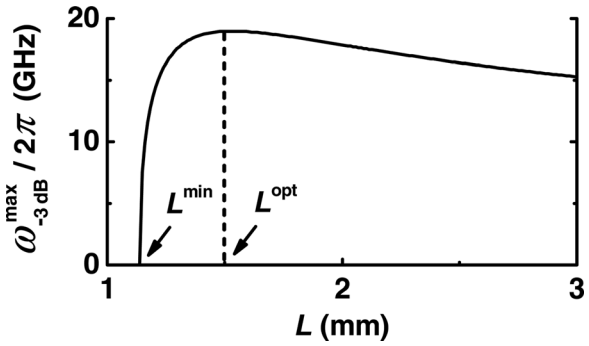

FIG. 4. Maximum modulation bandwidth $\omega^{max}_{-3\,dB}/2\pi$ vs. cavity length L. $\alpha_0 = 3\,cm^{-1}$ and $\sigma_{int} = 2.67 \times 10^{-17}$ cm^2; $L^{opt} = 1.5$ mm.

density in the OCL n_{OCL} to the confined-carrier level occupancy in a QD f_n. The quantity $n_1 = N_c^{OCL}\exp(-E_n/T)$ characterizes the intensity of thermally excited escape of carriers from a QD to the OCL, N_c^{OCL} is the effective density of states in the OCL, E_n is the carrier excitation energy from a QD, and T is the temperature (in units of energy).

Due to the free-carrier-density-dependent internal loss, the confined-carrier level occupancy in a QD $f_{n,0}$ entering into Eq. (12) is itself a function of σ_{int}. In Ref. 7, the following expression was derived for $f_{n,0}$ from the steady-state lasing condition (equality of the gain to the total loss):

$$f_{n,0} = \frac{1}{4}\left(3 + \frac{\beta + \alpha_0 - \sigma_{int} n_1}{g^{max}}\right) - \sqrt{\frac{1}{16}\left(3 + \frac{\beta + \alpha_0 - \sigma_{int} n_1}{g^{max}}\right)^2 - \frac{1}{2}\left(1 + \frac{\beta + \alpha_0}{g^{max}}\right)}. \quad (13)$$

Fig. 3 shows $\omega^{max}_{-3\,dB}/2\pi$ vs. σ_{int}. As seen from Eq. (12), Fig. 3 and also Fig. 2, $\omega^{max}_{-3\,dB}$ is highest for the case of no free-carrier-density-dependent internal loss ($\sigma_{int} = 0$). With σ_{int} increasing and approaching a certain maximum tolerable value σ^{max}_{int}, $\omega^{max}_{-3\,dB}$ decreases and becomes zero. Using Eq. (13) for $f_{n,0}$ in Eq. (12) for $\omega^{max}_{-3\,dB}$ and equalizing the latter to zero, we obtain the following expression for the critical tolerable cross-section of internal loss (see also Ref. 19):

$$\sigma^{max}_{int} = \frac{\left(\sqrt{2g^{max}} - \sqrt{\beta + \alpha_0 + g^{max}}\right)^2}{n_1}. \quad (14)$$

For $\sigma_{int} > \sigma^{max}_{int}$, the lasing is not attainable in the structure and, naturally, no direct modulation is possible.

While $\omega^{max}_{-3\,dB}$ depends strongly on σ_{int}, the flattest response function (the response function at $j_0 = j_0^{opt}$) is universal in terms of the normalized modulation frequency $\omega/\omega^{max}_{-3\,dB}$ (the inset in Fig. 1),

$$H_{flattest}(\omega/\omega^{max}_{-3\,dB}) = \frac{1}{1 + (\omega/\omega^{max}_{-3\,dB})^4}. \quad (15)$$

As seen from Fig. 4, as a function of the cavity length, $\omega^{max}_{-3\,dB}$ has a maximum. With increasing L from the shortest tolerable cavity length required for lasing,[19] $\omega^{max}_{-3\,dB}$ increases from zero, approaches its highest value $\omega^{highest}_{-3\,dB}$ at a certain optimum cavity length L^{opt}, and then decreases. L^{opt} depends on σ_{int} – the larger is σ_{int}, the longer should be the optimum cavity. When σ_{int} is small [so small that the second terms in the brackets in the right-hand sides of Eqs. (16) and (17) are much less compared to unity], the analysis of Eq. (12) for $\omega^{max}_{-3\,dB}$ as a function of L yields the following expressions for L^{opt} and $\omega^{highest}_{-3\,dB}$:

$$L^{opt} \approx L_0^{min}\left(1 + \frac{g^{max}}{g^{max} - \alpha_0}\sqrt[3]{\frac{4\sigma_{int} n_1}{g^{max}}}\right) = \frac{\ln(1/R)}{g^{max} - \alpha_0}\left(1 + \frac{g^{max}}{g^{max} - \alpha_0}\sqrt[3]{\frac{4\sigma_{int} n_1}{g^{max}}}\right), \quad (16)$$

$$\omega^{highest}_{-3\,dB} \approx \omega^{highest}_{-3\,dB}\Big|_{\sigma_{int}=0}\left(1 - \frac{3}{2}\sqrt[3]{\frac{4\sigma_{int} n_1}{g^{max}}}\right) = \sqrt{2}v_g g^{max}\left(1 - \frac{3}{2}\sqrt[3]{\frac{4\sigma_{int} n_1}{g^{max}}}\right), \quad (17)$$

where L_0^{min} and $\omega^{highest}_{-3\,dB}|_{\sigma_{int}=0}$ are the shortest tolerable cavity length and the highest bandwidth, respectively, when $\sigma_{int} = 0$.

The highest modulation bandwidth $\omega^{highest}_{-3\,dB}/2\pi$ is shown against σ_{int} in Fig. 5. As seen from the figure, in the ideal case of no free-carrier-density-dependent internal loss in the OCL (and also no carrier capture delay from the OCL into QDs), $(\omega^{highest}_{-3\,dB}|_{\sigma_{int}=0})/2\pi$ is about 60 GHz in a GaInAsP structure of Ref. 20 used for our calculations here. In the presence of such a loss, $\omega^{highest}_{-3\,dB}/2\pi$ is, however, considerably reduced and becomes vanishing as σ_{int} approaches its maximum tolerable value (Fig. 5).

In conclusion, the free-carrier-density-dependent internal optical loss in the waveguide region has been shown to

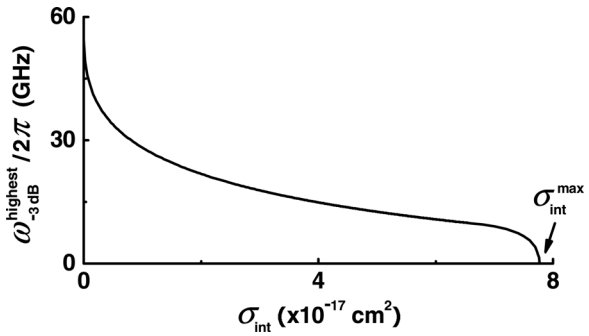

FIG. 5. Highest modulation bandwidth $\omega^{highest}_{-3\,dB}/2\pi$ vs. internal loss cross-section σ_{int}. $\alpha_0 = 3\,cm^{-1}$. σ^{max}_{int} in the figure corresponds to $L = \infty$ and that is why it is larger than in Fig. 3.

considerably reduce the modulation bandwidth $\omega_{-3\,\mathrm{dB}}$ of a QD laser. At a certain optimum value j_0^{opt} of the dc component of the injection current density, the maximum bandwidth $\omega_{-3\,\mathrm{dB}}^{\mathrm{max}}$ is attained and the response function becomes as flat as possible. While $\omega_{-3\,\mathrm{dB}}^{\mathrm{max}}$ depends strongly on the effective cross-section σ_{int} of internal absorption loss processes (decreases and becomes zero at the maximum tolerable value of σ_{int}), the flattest response function is universal in terms of the normalized modulation frequency $\omega/\omega_{-3\,\mathrm{dB}}^{\mathrm{max}}$. As with j_0^{opt}, there also exists the optimum cavity length, at which $\omega_{-3\,\mathrm{dB}}$ is highest; the larger is σ_{int}, the longer should be the optimum cavity.

L.V.A. and Y.W. acknowledge the U.S. Army Research Office (Grant No. W911-NF-08-1-0462), Y.W. also acknowledges the China Scholarship Council, and R.A.S. acknowledges the Russian Foundation for Basic Research (Grant No. 11-02-00573) and the Program "Fundamental Research in Nanotechnology and Nanomaterials" of the Presidium of the Russian Academy of Sciences for support of this work.

[1]G. P. Agrawal and N. K. Dutta, *Long-Wavelength Semiconductor Lasers* (Van Nostrand, New York, 1986), p. 474.
[2]D. Z. Garbuzov, A. V. Ovchinnikov, N. A. Pikhtin, Z. N. Sokolova, I. S. Tarasov, and V. B. Khalfin, Sov. Phys. Semicond. **25**, 560 (1991).
[3]C. H. Henry, R. A. Logan, F. R. Merritt, and J. P. Luongo, IEEE J. Quantum Electron. **19**, 947 (1983).
[4]M. Asada, A. Kameyama, and Y. Suematsu, IEEE J. Quantum Electron. **20**, 745 (1984).
[5]J. J. Lee, L. J. Mawst, and D. Botez, J. Cryst. Growth **249**, 100 (2003).
[6]D. A. Ackerman, G. E. Shtengel, M. S. Hybertsen, P. A. Morton, R. F. Kazarinov, T. Tanbun-Ek, and R. A. Logan, IEEE J. Sel. Top. Quantum Electron. **1**, 250 (1995).
[7]L. V. Asryan and S. Luryi, Appl. Phys. Lett. **83**, 5368 (2003).
[8]L. V. Asryan, Appl. Phys. Lett. **88**, 073107 (2006).
[9]L. Jiang and L. V. Asryan, Laser Phys. Lett. **4**, 265 (2007).
[10]L. V. Asryan, Y. Wu, and R. A. Suris, Appl. Phys. Lett. **98**, 131108 (2011).
[11]T. Ikegami and Y. Suematsu, Proc. IEEE **55**, 122 (1967).
[12]T. L. Paoli and J. E. Ripper, Proc. IEEE **58**, 1457 (1970).
[13]M. J. Adams, Opto-electronics **5**, 201 (1973).
[14]R. F. Kazarinov and R. A. Suris, Sov. Phys. JETP **39**, 522 (1974).
[15]C. B. Su and V. A. Lanzisera, IEEE J. Quantum Electron. **22**, 1568 (1986).
[16]R. Olshansky, P. Hill, V. Lanzisera, and W. Powazinik, IEEE J. Quantum Electron. **23**, 1410 (1987).
[17]R. Nagarajan, M. Ishikawa, T. Fukushima, R. S. Geels, and J. E. Bowers, IEEE J. Quantum Electron. **28**, 1990 (1992).
[18]L. V. Asryan and R. A. Suris, Appl. Phys. Lett. **96**, 221112 (2010).
[19]L. V. Asryan and S. Luryi, IEEE J. Quantum Electron. **40**, 833 (2004).
[20]L. V. Asryan and R. A. Suris, Semicond. Sci. Technol. **11**, 554 (1996).

Theory of relaxation oscillations and modulation response of a quantum dot laser

Levon V. Asryan[*a)] and Robert A. Suris[**b)]

[a)] Virginia Polytechnic Institute and State University, Blacksburg, VA 24061

[b)] Ioffe Physical-Technical Institute, Saint Petersburg, Russia

ABSTRACT

Dynamic effects in a quantum dot (QD) laser are studied theoretically. The frequency and decay rate of relaxation oscillations, and the modulation response are calculated as functions of injection current density, cavity length, and parameters of the QD structure. The highest possible bandwidth is calculated and shown to increase with increasing overlap integral between the electron and hole wave functions in a QD, number of QD-layers and surface density of QDs in a layer, and with reducing QD-size dispersion.

Keywords: Modulation bandwidth, quantum dot lasers, relaxation oscillations

1. INTRODUCTION

Due to the compactness and capability of direct modulation of the optical output by electric current, semiconductor lasers are extensively used in high-speed fiber networks. In quantum dot (QD) lasers, the stimulated emission is produced in nanosize regions confining the charge carriers in all three spatial dimensions [1]. A discrete energy spectrum of carriers in QDs enables lasing [2] at low threshold current [3] and with high temperature-stability [4]. At the same time, even with advanced technologies for QD structures growth and fabrication, the modulation bandwidth of QD lasers is still below that of quantum well (QW) lasers [5]. In this work, dynamic effects in a QD laser are studied theoretically and the factors limiting its modulation bandwidth are identified. The highest possible bandwidth is calculated.

2. THEORETICAL MODEL

The carrier injection into a quantum-confined active region of semiconductor lasers is indirect – carriers are first injected into the reservoir [optical confinement layer (OCL)] and then captured into the active region. Reservoir-mediated injection adversely affects the laser operating characteristics – the threshold current is increased [6] and more temperature-sensitive [7, 8], and the output optical power is decreased [9, 10]. Due to a transport delay across the OCL and a capture delay from the OCL into the active region, the bandwidth of direct modulation of the output power by injection current is also reduced. The main objective of this work is to estimate the highest possible modulation bandwidth of a laser. For this purpose, we assume instantaneous carrier injection into the active region, i.e., we assume that both the transport across the OCL to the active region and exchange between the OCL and the active region are instantaneous. At the same time, our model includes the carrier population and recombination in the OCL. Although our analysis and derivations are general and apply also to QW and quantum wire lasers, our focus here is on QD lasers.

We use the small-signal analysis of rate equations [11]–[17]. In the general case, three equations should be used – for carriers outside the active region (in the OCL), those in the active region, and photons. The above assumptions of no transport and capture delay allow us to effectively reduce the number of equations to two. These equations are

[*] E-mail: asryan@mse.vt.edu; Web: http://www.mse.vt.edu/people/faculty/asryan.html; Telephone: 1 (540) 231-7033

[**] E-mail: suris@theory.ioffe.ru; Web: http://www.ioffe.rssi.ru/Dep_TM/suris.html; Telephone: 7 (812) 292-7367

Quantum Dots and Nanostructures: Synthesis, Characterization, and Modeling VII,
edited by Kurt G. Eyink, Frank Szmulowicz, Diana L. Huffaker, Proc. of SPIE Vol. 7610,
76100R · © 2010 SPIE · CCC code: 0277-786X/10/$18 · doi: 10.1117/12.842907

$$\frac{\partial}{\partial t}(\delta n) = \frac{\delta j}{eb} - \delta R_{\text{spon}} - \delta R_{\text{stim}}, \tag{1}$$

$$\frac{\partial}{\partial t}\left(\frac{\delta N}{V}\right) = \delta R_{\text{stim}} - \delta R_{\text{loss}}, \tag{2}$$

where $\delta(...)$ means a small variation of (…), $n = n_{\text{act}} + n_{\text{OCL}}$ is the total carrier density (including the active region and OCL), j is the injection current density, N is the number of photons in the lasing mode, b and V are the OCL thickness and volume, respectively, R_{spon} is the total spontaneous recombination rate (including the active region and OCL), R_{stim} is the stimulated recombination rate, and R_{loss} is the photon loss rate.

Assuming time-harmonic ac current density $\delta j = (\delta j_{\text{m}})\exp(i\omega t)$ and correspondingly looking for the solutions of (1) and (2) in the form of $\delta n = (\delta n_{\text{m}})\exp(i\omega t)$ and $\delta N = (\delta N_{\text{m}})\exp(i\omega t)$, we calculate the modulation response function

$$H(\omega) = \left|\frac{\delta N_{\text{m}}(\omega)}{\delta N_{\text{m}}(0)}\right|^2. \tag{3}$$

Depending on the dc component j_0 of the injection current density, $H(\omega)$ may have a peak (Fig. 1), which is obtained at the frequency

$$\omega_{\text{peak}} = \sqrt{\Omega_{\text{osc}}^2 - \Gamma_{\text{dec}}^2} = \sqrt{\omega_0^2 - 2\Gamma_{\text{dec}}^2}, \tag{4}$$

where Ω_{osc} and Γ_{dec} are the frequency and decay rate of relaxation oscillations,

$$\Omega_{\text{osc}} == \sqrt{\omega_0^2 - \Gamma_{\text{dec}}^2}, \tag{5}$$

$$\Gamma_{\text{dec}} = \frac{1}{2}\left(\frac{1}{\tau_{\text{spon}}^{\text{dif}}} + \text{v}_{\text{g}}\frac{G^{\text{dif}}}{V}N_0\right), \tag{6}$$

and ω_0 is given as

$$\omega_0 = \sqrt{\text{v}_{\text{g}}\frac{G^{\text{dif}}}{V}N_0\frac{1}{\tau_{\text{ph}}}}. \tag{7}$$

In the above equations, N_0 is the dc number of photons in the lasing mode, v_{g} is the group velocity of light, and τ_{ph} is the photon lifetime in the cavity,

$$\frac{1}{\tau_{\text{ph}}} = \text{v}_{\text{g}}\left(\frac{1}{L}\ln\frac{1}{R}\right), \tag{8}$$

where L is the cavity length and R is the mirror reflectivity.

The *effective differential gain* G^{dif} in the above equations is calculated as the derivative of the modal gain g with respect to the *total carrier density*, $n = n_{\text{act}} + n_{\text{OCL}}$,

$$G^{\text{dif}} = \frac{\partial g}{\partial n} = \frac{\partial n_{\text{act}}}{\partial n}\frac{\partial g}{\partial n_{\text{act}}} = \frac{\partial n_{\text{act}}}{\partial n}G_{\text{act}}^{\text{dif}}, \tag{9}$$

where $G_{\text{act}}^{\text{dif}} = \partial g/\partial n_{\text{act}}$ is the differential gain calculated as the derivative with respect to the carrier density in the active region only. Due to the fact that $\partial n_{\text{act}}/\partial n << 1$, the effective differential gain is much lower than that of the active region,

$$G^{\text{dif}} << G_{\text{act}}^{\text{dif}} \tag{10}$$

and, as discussed below, the practically achievable modulation bandwidth of the laser can be significantly reduced.

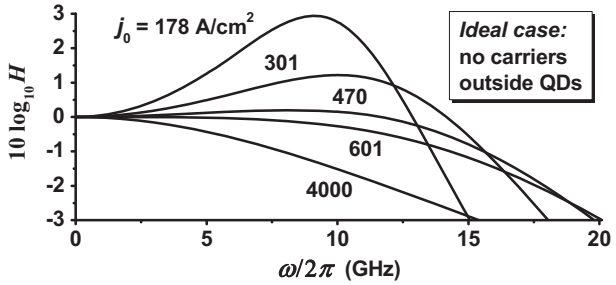

Fig. 1. Response function in the ideal case of no carriers outside QDs at different values of the dc component of the injection current density. In Figs. 1–4, a GaInAsP structure of [6] lasing at T = 300 K near 1.55 μm is considered: Z_L = 1, δ_{RMS} = 0.05 (10% QD-size fluctuations), N_S = 6.11×10^{10} cm^{-2}, and $I_{overlap}$ = 1; g^{max} = 29.52 cm^{-1} and G_{act}^{dif} = 1.36×10^{-14} cm^2. The cavity length L = 1.139 mm. At these parameters, $\omega_{-3dB}^{max}/2\pi$ = 20 GHz and j_{opt} = 601 A/cm^2 (see also Fig. 2).

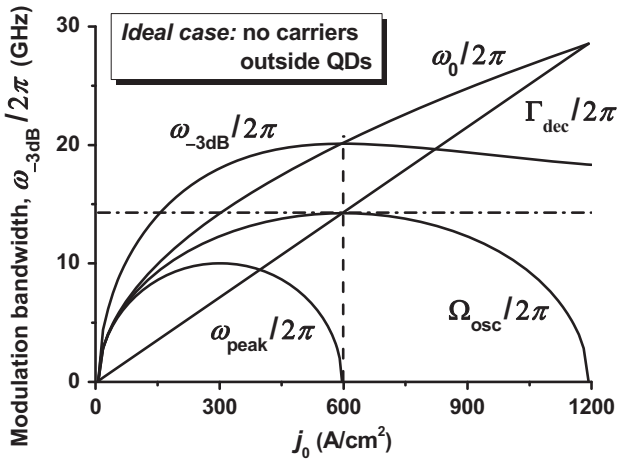

Fig. 2. Modulation bandwidth $\omega_{-3dB}/2\pi$, peak frequency of the response function $\omega_{peak}/2\pi$, relaxation oscillation frequency $\Omega_{osc}/2\pi$, $\Gamma_{dec}/2\pi$, and $\omega_0/2\pi$ versus dc component of the injection current density in the ideal case of no carriers outside QDs.

In (5), τ_{spon}^{dif} is the effective differential spontaneous recombination time, which is expressed in terms of the differential recombination times in the active region and OCL as follows:

$$\frac{1}{\tau_{spon}^{dif}} = \frac{\partial R_{spon}}{\partial n} = \frac{\partial n_{act}}{\partial n}\frac{1}{\tau_{spon,\,act}^{dif}} + \frac{\partial n_{OCL}}{\partial n}\frac{1}{\tau_{spon,\,OCL}^{dif}}, \tag{11}$$

where $1/\tau_{spon,\,act}^{dif} = \partial R_{spon}^{act}/\partial n_{act}$ and $1/\tau_{spon,\,OCL}^{dif} = \partial R_{spon}^{OCL}/\partial n_{OCL}$.

The most important dynamic characteristic is –3dB band-width (referred to as the modulation bandwidth $\omega_{-3dB}/2\pi$ here) – the frequency, at which the response function $H(\omega)$ is twice decreased compared to its dc (ω = 0) value. The equation for ω_{-3dB} is

$$\omega_{-3dB} = \sqrt{\omega_{peak}^2 + \sqrt{\omega_{peak}^4 + (r-1)\omega_0^4}}, \tag{12}$$

where $r = 10^{0.3} \approx 1.995$.

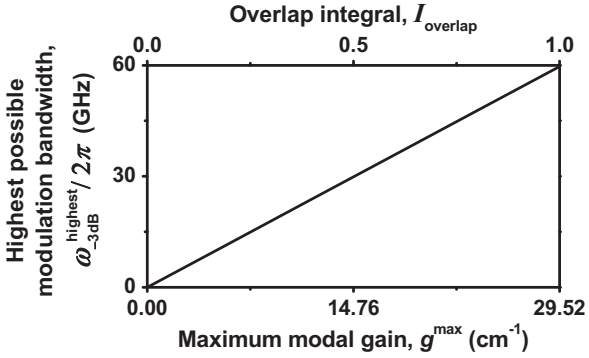

Fig. 3. Highest possible modulation bandwidth of a single QD-layer laser versus maximum modal gain (bottom axis) and overlap integral between the electron and hole wave functions in a QD (top axis).

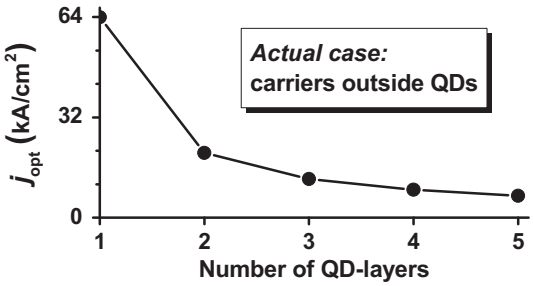

Fig. 4. Optimum dc injection current density maximizing the modulation bandwidth ($\omega_{-3dB}^{max}/2\pi$ = 20 GHz at L = 1.139 mm) versus number of QD-layers in the actual case of carriers outside QDs.

3. DISCUSSION

The relaxation oscillations are only possible [Ω_{osc} should be real – see (5)] within a certain range of values of N_0, i.e., of dc (steady-state) component j_0 of the injection current density. Within this range, Ω_{osc} increases from zero, approaches its maximum value, and then decreases to zero (Fig. 2). The peak of the response function also exists within its own range of j_0 [ω_{peak} should be real – see (4)]; ω_{peak} behaves similarly to Ω_{osc} with increasing j_0 (Fig. 2) — what this means is, at a certain j_0, the peak of $H(\omega)$ appears at $\omega_{peak} = 0$, then it moves to higher frequencies with increasing j_0, and then moves back to lower frequencies and finally disappears at $\omega_{peak} = 0$ (Fig. 2). At j_0 value, at which the peak of $H(\omega)$ disappears, Ω_{osc} becomes maximum (Fig. 2); although Ω_{osc} is maximum, the relaxation oscillations are strongly damped at this j_0: $\Gamma_{dec} = \Omega_{osc}^{max} = 1/\tau_{ph}$ and hence within one period $2\pi/\Omega_{osc}^{max}$ of oscillations the amplitude is decreased by a factor of $\exp[-\Gamma_{dec}(2\pi/\Omega_{osc}^{max})] = \exp(-2\pi)$, i.e., is practically vanishing.

As a function of j_0, the modulation bandwidth also has a maximum (Fig. 2). The maximum of ω_{-3dB} is obtained at approximately the same value j_{opt} of j_0, at which Ω_{osc} is maximum and the peak of the response function disappears (Fig. 2); at $j_0 = j_{opt}$, $H(\omega)$ is as flat as possible (Fig. 1). On further increase of j_0 beyond j_{opt}, ω_{-3dB} decreases and asymptotically approaches its saturation value.

The maximum values of ω_{peak}, Ω_{osc}, and ω_{-3dB} are controlled by the reciprocal photon lifetime in the cavity,

$$\omega_{\text{-3dB}}^{\max} \approx \sqrt{2}\,\Omega_{\text{osc}}^{\max} \approx \sqrt{2}\left(\sqrt{2}\,\omega_{\text{peak}}^{\max}\right) \approx \frac{\sqrt{2}}{\tau_{\text{ph}}} = \sqrt{2}\,\frac{\text{v}_\text{g}}{L}\ln\frac{1}{R}. \tag{13}$$

The saturation value of $\omega_{\text{-3dB}}$ is also controlled by $1/\tau_{\text{ph}}$,

$$\omega_{\text{-3dB}}\Big|_{j_0\to\infty} \approx \frac{1}{\tau_{\text{ph}}}. \tag{14}$$

The shorter the cavity, the higher $\omega_{\text{-3dB}}^{\max}$. The shortest cavity length $L^{\min}$ is controlled by the maximum modal gain $g^{\max}$ of the laser through the lasing condition (equality of the gain to the loss),

$$\frac{1}{L^{\min}}\ln\frac{1}{R} = g^{\max}. \tag{15}$$

Using $L^{\min}$ in (13), we find that *the highest possible bandwidth increases directly with* $g^{\max}$ *and is not affected by the differential gain*,

$$\omega_{\text{-3dB}}^{\text{highest}} = \sqrt{2}\,\text{v}_\text{g} g^{\max}. \tag{16}$$

While $\omega_{\text{-3dB}}^{\text{highest}}$ is controlled by merely $g^{\max}$, and $\omega_{\text{-3dB}}^{\max}$ by L, the current densities, at which they are obtained, are controlled by G^{dif} as well. Consequently, a practically achievable bandwidth can be significantly reduced compared to (16) and even (13).

The above analysis and equations apply to semiconductor lasers with any type of a quantum-confined active region assuming that the carrier transport to and exchange with the latter are instantaneous. Using the expression for $g^{\max}$ of a QD laser [6, 18], we obtain from (15) for the highest possible bandwidth

$$\omega_{\text{-3dB}}^{\text{highest}} = \sqrt{2}\,\text{v}_\text{g} g^{\max} \propto I_{\text{overlap}} Z_\text{L} N_\text{S} \frac{1}{\delta_{\text{RMS}}}, \tag{17}$$

where I_{overlap} is the overlap integral between the electron and hole wave functions in a QD, Z_L is the number of QD-layers, N_S is the surface density of QDs in one layer, and δ_{RMS} is the root mean square of QD-size fluctuations. Hence, $\omega_{\text{-3dB}}^{\text{highest}}$ is controlled by each of the four parameters controlling $g^{\max}$.

The absence of carriers in the OCL would be the ideal case of direct injection into a quantum-confined active region and would present the best-case scenario not only for the threshold and power characteristics of a laser but for the modulation characteristics as well. For such an ideal case of no carriers in the OCL, Fig. 1 shows the response function, and Fig. 2 shows the modulation bandwidth $\omega_{\text{-3dB}}/2\pi$ versus dc injection current density j_0. The parameters of the structure are presented in the caption to Fig. 1. As seen from the figures, $\omega_{\text{-3dB}}^{\max}$ [given by (13)] is easily attained at low j_{opt} (601 A/cm^2). This is because G^{dif} is high in this case: $G^{\text{dif}} = G_{\text{act}}^{\text{dif}} = 1.36\times10^{-14}$ cm^2.

Fig. 3 shows the highest possible modulation bandwidth $\omega_{\text{-3dB}}^{\text{highest}}/2\pi$ versus maximum modal gain $g^{\max}$ (bottom axis) in a single QD-layer laser. The top axis illustrates the situation when $g^{\max}$ is varied through changing I_{overlap}. At 10% QD-size fluctuations ($\delta_{\text{RMS}} = 0.05$), $N_\text{S} = 6.11\times10^{10}$ cm^{-2}, and ideal overlap between the electron and hole wave functions in a QD ($I_{\text{overlap}} = 1$), the maximum gain is $g^{\max} = 29.52$ cm^{-1}.[1)] As seen from the figure, at these parameters, *the highest possible modulation bandwidth in a single QD-layer laser* is

$$\omega_{\text{-3dB}}^{\text{highest}}/2\pi \approx 60\ \text{GHz}. \tag{18}$$

If the overlap between the electron and hole wave functions in a QD is poor or the QD-size dispersion is large, the maximum gain will be low and hence so will be even the highest possible bandwidth $\omega_{\text{-3dB}}^{\text{highest}}/2\pi$ — thus, $g^{\max} = 4.4$ cm^{-1} and $\omega_{\text{-3dB}}^{\text{highest}}/2\pi \approx 9$ GHz if $I_{\text{overlap}} = 0.15$. One way of increasing I_{overlap} is the use of more symmetrical (e.g., truncated or disk-shape) QDs [18].

[1)] At these parameters, the shortest cavity length is $L^{\min} = 386$ μm – see (15).

As seen from (17), the use of multiple layers with QDs can effectively enhance the modulation bandwidth thus compensating for a poor overlap between the electron and hole wave functions in a QD or for a large QD-size dispersion.

The use of submonolayer QDs allowing for a higher surface density N_S of QDs in a layer [19, 20] can also enhance the modulation bandwidth.

In the presence of carriers in the OCL, all the above expressions [including (13) and (17)] hold. At the same time, G^{dif} [see (9)] is considerably reduced as compared to G_{act}^{dif}. Due to this, ω_{-3dB}^{max} (and the more so $\omega_{-3dB}^{highest}$) becomes unattainable at practical values of the pump current density in a single QD-layer laser. Indeed, the condition for the maximum bandwidth ($\omega_{peak} = 0$) is obtained when $\omega_0^2 = 2\Gamma_{dec}^2$ – see (4). As seen from (6) and (7), both ω_0 and Γ_{dec} are controlled by the product of the photon number N_0 and G^{dif}. In a single QD-layer laser considered here, $\partial n_{act}/\partial n = 0.01$, i.e., G^{dif} is about two orders of magnitude lower than G_{act}^{dif} [see (9)]: $G^{dif} = 1.27\times10^{-16}$ cm^2. Hence, the photon number $N_0 = N_0^{opt}$, at which $\omega_0^2 = 2\Gamma_{dec}^2$, is two orders of magnitude higher than in the ideal case of no carriers in the OCL, and so is j_{opt} (64 kA/cm^2). Fig. 4 shows the optimum dc injection current density $j_0 = j_{opt}$ maximizing ω_{-3dB} versus number of QD-layers. While j_{opt} is very high even for $Z_L = 2$, the use of 4 or 5 layers makes ω_{-3dB}^{max} practically attainable thus compensating for the adverse effect of carriers in the OCL.

4. CONCLUSION

A general theory of the modulation characteristics of a semiconductor laser with a quantum-confined active region has been developed and discussed in the context of a QD laser. The modulation response of a QD laser has been calculated as a function of injection current density and parameters of the structure. The highest possible bandwidth has been shown to increase with increasing overlap integral between the electron and hole wave functions in a QD, number of QD-layers and surface density of QDs in a layer, and with reducing QD-size dispersion. At 10% QD-size fluctuations and ideal overlap between the electron and hole wave functions in a QD, the highest possible modulation bandwidth in a single QD-layer laser has been estimated to be 60 GHz.

ACKNOWLEDGMENTS

L.V.A. acknowledges the U.S. Army Research Office (Grant No. W911-NF-08-1-0462) and R.A.S. acknowledges the Russian Foundation for Basic Research for support of this work (Grant No. 08-02-01337).

REFERENCES

[1] Y. Arakawa and H. Sakaki, "Multidimensional quantum well laser and temperature dependence of its threshold current," *Appl. Phys. Lett.* **40**, 939 (1982).

[2] N. Kirstädter, N. N. Ledentsov, M. Grundmann, D. Bimberg, V. M. Ustinov, S. S. Ruvimov, M. V. Maximov, P. S. Kop'ev, Zh. I. Alferov, U. Richter, P. Werner, U. Gösele, and J. Heydenreich, "Low threshold, large T_0 injection laser emission from (InGa)As quantum dots," *Electron. Lett.* **30**, 1416 (1994).

[3] G. Park, O. B. Shchekin, D. L. Huffaker, and D. G. Deppe, "Low-threshold oxide-confined 1.3-μm quantum-dot laser," *IEEE Phot. Technol. Lett.* **13**, 230 (2000).

[4] S. Fathpour, Z. Mi, P. Bhattacharya, A. R. Kovsh, S. S. Mikhrin, I. L. Krestnikov, A. V. Kozhukhov, and N. N. Ledentsov, "The role of Auger recombination in the temperature-dependent output characteristics ($T_0 = \infty$) of p-doped 1.3 μm quantum dot lasers," *Appl. Phys. Lett.* **85**, 5164 (2004).

[5] S. Weisser, E. C. Larkins, K. Czotscher, W. Benz, J. Daleiden, I. Esquivias, J. Fleissner, J. D. Ralston, B. Romero, R. E. Sah, A. Schönfelder, and J. Rosenzweig, "Damping-limited modulation bandwidths up to 40 GHz in undoped short-cavity $In_{0.35}Ga_{0.65}As$–GaAs multiple-quantum-well lasers," *IEEE Phot. Technol. Lett.* **8**, 608 (1996).

[6] L. V. Asryan and R. A. Suris, "Inhomogeneous line broadening and the threshold current density of a semiconductor quantum dot laser," *Semicond. Sci. Technol.* **11**, 554 (1996).

[7] L. V. Asryan and R. A. Suris, "Characteristic temperature of quantum dot laser," *Electron. Lett.* **33**, 1871 (1997).

[8] L. V. Asryan and R. A. Suris, "Temperature dependence of the threshold current density of a quantum dot laser," *IEEE J. Quantum Electron.* **34**, 841 (1998).

[9] L. V. Asryan, S. Luryi, and R. A. Suris, "Intrinsic nonlinearity of the light-current characteristic of semiconductor lasers with a quantum-confined active region," *Appl. Phys. Lett.* **81**, 2154 (2002).

[10] L. V. Asryan, S. Luryi, and R. A. Suris, "Internal efficiency of semiconductor lasers with a quantum-confined active region," *IEEE J. Quantum Electron.* **39**, 404 (2003).

[11] T. Ikegami and Y. Suematsu, "Resonance-like characteristics of the direct modulation of a junction laser," *Proc. IEEE* **55**, 122 (1967).

[12] T. L. Paoli and J. E. Ripper, "Direct modulation of semiconductor lasers," *Proc. IEEE* **58**, 1457 (1970).

[13] M. J. Adams, "Rate equations and transient phenomena in semiconductor lasers," *Opto-electron.* **5**, 201 (1973).

[14] R. F. Kazarinov and R. A. Suris, "Heterodyne reception of light by an injection laser," *Sov. Phys.-JETP* **39**, 522 (1974).

[15] C. B. Su and V. A. Lanzisera, "Ultra-high-speed modulation of 1.3-μm InGaAsP diode lasers," *IEEE J. Quantum Electron.* **22**, 1568 (1986).

[16] R. Olshansky, P. Hill, V. Lanzisera, and W. Powazinik, "Frequency response of 1.3 μm InGaAsP high speed semiconductor lasers," *IEEE J. Quantum Electron.* **23**, 1410 (1987).

[17] R. Nagarajan, M. Ishikawa, T. Fukushima, R. S. Geels, and J. E. Bowers, "High speed quantum-well lasers and carrier transport effects," *IEEE J. Quantum Electron.* **28**, 1990 (1992).

[18] L. V. Asryan, M. Grundmann, N. N. Ledentsov, O. Stier, R. A. Suris, and D. Bimberg, "Maximum modal gain of a self-assembled InAs/GaAs quantum-dot laser," *J. Appl. Phys.* **90**, 1666 (2001).

[19] N. N. Ledentsov, D. Bimberg, F. Hopfer, A. Mutig, V. A. Shchukin, A. V. Savel'ev, G. Fiol, E. Stock, H. Eisele, M. Dähne, D. Gerthsen, U. Fischer, D. Litvinov, A. Rosenauer, S. S. Mikhrin, A. R. Kovsh, N. D. Zakharov, and P. Werner, "Submonolayer quantum dots for high speed surface emitting lasers," *Nanoscale Res. Lett.* **2**, 417 (2007).

[20] N. N. Ledentsov, F. Hopfer, and D. Bimberg, "High-speed quantum-dot vertical-cavity surface-emitting lasers," *Proc. IEEE* **95**, 1741 (2007).

Capture delay and modulation bandwidth in a quantum dot laser

Levon V. Asryan[*a)], Yuchang Wu[**a)] and Robert A. Suris[***b)]

[a)] Virginia Polytechnic Institute and State University, Blacksburg, VA 24061, USA

[b)] Ioffe Physico-Technical Institute, Saint Petersburg 194021, Russia

ABSTRACT

We show that the carrier capture from the optical confinement layer into quantum dots (QDs) can strongly limit the modulation bandwidth $\omega_{-3\,\mathrm{dB}}$ of a QD laser. Closed-form analytical expressions are obtained for $\omega_{-3\,\mathrm{dB}}$ in the limiting cases of fast and slow capture. $\omega_{-3\,\mathrm{dB}}$ is highest in the case of instantaneous capture into QDs, when the cross-section of carrier capture into a QD $\sigma_n = \infty$. With reducing σ_n, $\omega_{-3\,\mathrm{dB}}$ decreases and becomes zero at a certain non-vanishing value $\sigma_n^{\min}$. This $\sigma_n^{\min}$ presents the minimum tolerable capture cross-section for the lasing to occur at a given dc component j_0 of the injection current density. The higher is j_0, the smaller is $\sigma_n^{\min}$ and hence the direct modulation of the output power is possible at a slower capture. The use of multiple layers with QDs is shown to considerably improve the modulation response of the laser – the same $\omega_{-3\,\mathrm{dB}}$ is obtained in a multi-layer structure at a much lower j_0 than in a single-layer structure. At a plausible value of $\sigma_n = 10^{-11}$ cm^2, $\omega_{-3\,\mathrm{dB}}$ as high as 19 GHz is attainable in a 5-QD-layer structure.

Keywords: Carrier capture into a quantum dot, carrier escape from a quantum dot, modulation bandwidth, quantum dot lasers, semiconductor lasers

1. INTRODUCTION

Due to the quantum-size effect, reducing dimensionality of the active region has been a key to developing low-threshold semiconductor lasers [1, 2]. In commercial diode lasers, a two-dimensional active region (quantum well) is used [3, 4]. In quantum dot (QD) lasers, an ultimate case of a zero-dimensional active region is realized [5, 6]. The interesting physics involved in QD lasers and their potential for wide range of applications have motivated extensive experimental and theoretical studies of such lasers. However, in contrast to the steady-state threshold and power characteristics, the dynamic properties of QD lasers need to be further scrutinized. In particular, the potential of QD lasers for high-speed direct modulation of the output optical power by injection current should be clarified.

In [7], the highest modulation bandwidth attainable in QD lasers was estimated. For this purpose, an idealized situation of instantaneous carrier capture into QDs was assumed.

In actual semiconductor lasers, carriers are not directly injected into a quantum-confined active region – they are first injected into the reservoir [optical confinement layer (OCL)] and then captured into the active region (Fig. 1). Reservoir-mediated injection adversely affects the laser operating characteristics – the threshold current is increased [8] and more temperature-sensitive [9], and the output optical power is decreased [10, 11]. Due to a transport delay across the OCL and a capture delay from the OCL into the active region, the bandwidth of direct modulation of the output power by injection current is also reduced (see, e.g., [12, 13] for quantum well lasers).

* E-mail: asryan@mse.vt.edu; Web: http://www.mse.vt.edu/people/faculty/asryan.html; Telephone: 1 (540) 231-7033

** E-mail: yuchangw@vt.edu

*** E-mail: suris@theory.ioffe.ru; Web: http://www.ioffe.rssi.ru/Dep_TM/suris.html; Telephone: 7 (812) 292-7367

Quantum Dots and Nanostructures: Synthesis, Characterization, and Modeling VIII,
edited by Kurt G. Eyink, Frank Szmulowicz, Diana L. Huffaker, Proc. of SPIE Vol. 7947,
794708 · © 2011 SPIE · CCC code: 0277-786X/11/$18 · doi: 10.1117/12.874150

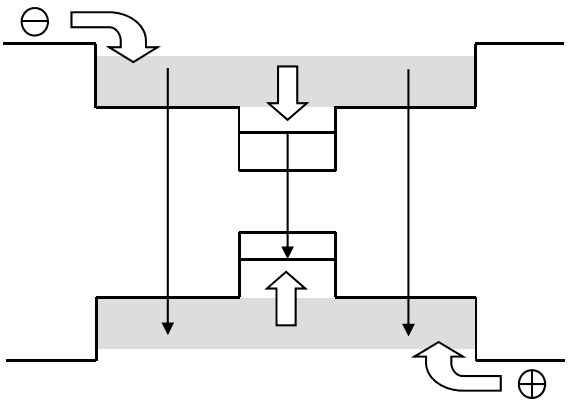

Fig. 1. Indirect injection into the quantum-confined active region of a semiconductor laser.

In this work, we study the effect of non-instantaneous capture of carriers from the OCL into QDs on the dynamic properties of a QD laser.

2. THEORETICAL MODEL

Our model is based on a set of three coupled rate equations – for free carriers in the OCL, carriers confined in the active region, and photons. These equations are

$$\frac{\partial n_{\mathrm{OCL}}}{\partial t} = \frac{j}{eb} - \sigma_{\mathrm{n}} \mathrm{v}_{\mathrm{n}} \frac{N_{\mathrm{S}}}{b}(1-f_{\mathrm{n}})\, n_{\mathrm{OCL}} + \sigma_{\mathrm{n}} \mathrm{v}_{\mathrm{n}} n_1 \frac{N_{\mathrm{S}}}{b} f_{\mathrm{n}} - B n_{\mathrm{OCL}}^2 , \tag{1}$$

$$\frac{\partial}{\partial t}\left(2\frac{N_{\mathrm{S}}}{b} f_{\mathrm{n}}\right) = \sigma_{\mathrm{n}} \mathrm{v}_{\mathrm{n}} \frac{N_{\mathrm{S}}}{b}(1-f_{\mathrm{n}})\, n_{\mathrm{OCL}} - \sigma_{\mathrm{n}} \mathrm{v}_{\mathrm{n}} n_1 \frac{N_{\mathrm{S}}}{b} f_{\mathrm{n}} - \frac{N_{\mathrm{S}}}{b}\frac{f_{\mathrm{n}}^2}{\tau_{\mathrm{QD}}} - \mathrm{v}_{\mathrm{g}} g^{\max}(2f_{\mathrm{n}}-1) n_{\mathrm{ph}} , \tag{2}$$

$$\frac{\partial n_{\mathrm{ph}}}{\partial t} = \mathrm{v}_{\mathrm{g}} g^{\max}(2f_{\mathrm{n}}-1) n_{\mathrm{ph}} - \mathrm{v}_{\mathrm{g}} \beta\, n_{\mathrm{ph}} , \tag{3}$$

where n_{OCL} is the free carrier density in the OCL, j is the injection current density, b is the OCL thickness, σ_{n} is the cross-section of carrier capture into a QD, v_{n} is the carrier thermal velocity, N_{S} is the surface density of QDs, f_{n} is the occupancy of the energy-level of a carrier in a QD, B is the spontaneous radiative recombination constant for the OCL (measured in units of cm^3/s), τ_{QD} is the spontaneous radiative lifetime in a QD, $\mathrm{v}_{\mathrm{g}} = c/\sqrt{\epsilon_{\mathrm{g}}}$ is the group velocity of light, c is the velocity of light in vacuum, $\sqrt{\epsilon_g}$ is the group index of the dispersive OCL material, and $g^{\max}$ is the maximum value of the modal gain [8].

The photon density n_{ph} presents the total number of photons in the lasing mode divided by the OCL volume, $\beta = (1/L)\ln(1/R)$ is the mirror loss, L is the cavity length, and R is the facet reflectivity.

The quantity n_1 in (1) and (2) characterizes the carrier thermal escape from a QD to the OCL and is given as

$$n_1 = N_{\mathrm{c}}^{\mathrm{3D}} \exp\left(-\frac{\Delta E_{\mathrm{c}} - \varepsilon_{\mathrm{n}}^{\mathrm{QD}}}{T}\right), \tag{4}$$

where $N_{\mathrm{c}}^{\mathrm{3D}} = 2\,[m_{\mathrm{c}}^{\mathrm{OCL}} T/(2\pi\hbar^2)]^{3/2}$ is the effective density of states in the OCL, $m_{\mathrm{c}}^{\mathrm{OCL}}$ is the carrier effective mass in the OCL, ΔE_{c} is the band offset between the OCL and a QD, $\varepsilon_{\mathrm{n}}^{\mathrm{QD}}$ is the quantized energy level in a QD, and T is the temperature measured in units of energy.

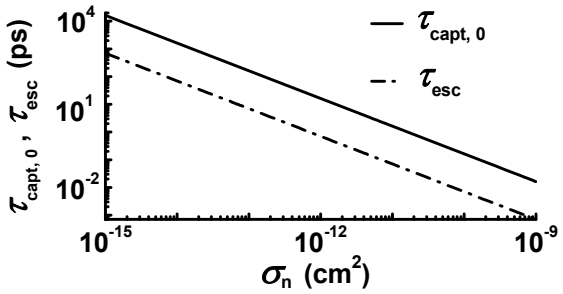

Fig. 2. Capture time into an unoccupied QD ensemble and escape time from a QD vs. capture cross-section.

Strictly speaking, σ_n is the only parameter, which adequately describes the capture/escape into/from a QD. Using σ_n, two distinct characteristic times can be introduced – the capture time $\tau_{capt,0}$ into an unoccupied QD ensemble [11] and the thermal escape time τ_{esc} from an individual QD [8],

$$\tau_{capt,0} = \frac{1}{\sigma_n v_n \frac{N_S}{b}}, \tag{5}$$

$$\tau_{esc} = \frac{1}{\sigma_n v_n n_1}. \tag{6}$$

The capture time into an unoccupied QD ensemble and the escape time from a QD are shown vs. σ_n in Fig. 2.

Within the framework of the small-signal analysis of rate equations, we consider the injection current density in (1) in the form of

$$j = j_0 + (\delta j_m) \exp(i\omega t), \tag{7}$$

where j_0 is the dc component and the amplitude δj_m of the time-harmonic ac component is small ($\delta j_m << j_0 - j_{th}$, where j_{th} is the threshold current density). We correspondingly look for n_{OCL}, f_n, and n_{ph} in (1)-(3) in the form of

$$n_{OCL} = n_{OCL,0} + (\delta n_{OCL-m}) \exp(i\omega t), \tag{8}$$

$$f_n = f_{n,0} + (\delta f_{n-m}) \exp(i\omega t), \tag{9}$$

$$n_{ph} = n_{ph,0} + (\delta n_{ph-m}) \exp(i\omega t), \tag{10}$$

where $n_{OCL,0}$, $f_{n,0}$, and $n_{ph,0}$ are the solutions of the steady-state rate equations at $j = j_0$ (see [10, 11]). They are given as follows:

$$f_{n,0} = \frac{1}{2}\left(1 + \frac{\beta}{g^{max}}\right) = \frac{1}{2}\left(1 + \frac{1}{\tau_{ph} v_g g^{max}}\right), \tag{11}$$

$$n_{OCL,0}(j_0) = \frac{1}{2B}\left[\sqrt{\left(\frac{1-f_{n,0}}{\tau_{capt,0}}\right)^2 + 4B\left(\frac{N_S}{b}\frac{f_{n,0}}{\tau_{esc}} + \frac{j_0}{eb}\right)} - \frac{1-f_{n,0}}{\tau_{capt,0}}\right], \tag{12}$$

$$n_{ph,0}(j_0) = \tau_{ph}\left\{\frac{1-f_{n,0}}{\tau_{capt,0}}\frac{1}{2B}\left[\sqrt{\left(\frac{1-f_{n,0}}{\tau_{capt,0}}\right)^2 + 4B\left(\frac{N_S}{b}\frac{f_{n,0}}{\tau_{esc}} + \frac{j_0}{eb}\right)} - \frac{1-f_{n,0}}{\tau_{capt,0}}\right] - \frac{N_S}{b}\frac{f_{n,0}}{\tau_{esc}} - \frac{N_S}{b}\frac{f_{n,0}^2}{\tau_{QD}}\right\}. \tag{13}$$

The photon lifetime in the cavity entering into eq. (11) is

$$\tau_{\rm ph} = \frac{1}{{\rm v}_{\rm g}\beta} = \frac{L}{{\rm v}_{\rm g} \ln\frac{1}{R}}. \tag{14}$$

Note that the confined-carrier level-occupancy $f_{\rm n,0}$ in a QD at the steady-state [eq. (11)] is pinned at its threshold value and does not change with dc injection current density j_0 above the lasing threshold. In contrast to $f_{\rm n,0}$, the steady-state free-carrier density $n_{\rm OCL,0}$ in the OCL [eq. (12)] is not pinned – it rises with j_0 above the lasing threshold. It should be emphasized that it is the non-instantaneous capture of carriers from the OCL into the quantum-confined active region that causes this rise in $n_{\rm OCL,0}$ above the lasing threshold [10, 11].

With (13), the steady-state light-current characteristic (the output optical power P_0 versus j_0) is

$$P_0(j_0) = \hbar\omega\frac{n_{\rm ph,\,0}}{\tau_{\rm ph}}WLb = \hbar\omega\, WLb\left\{\frac{1-f_{\rm n,0}}{\tau_{\rm capt,0}}\frac{1}{2B}\left[\sqrt{\left(\frac{1-f_{\rm n,0}}{\tau_{\rm capt,0}}\right)^2 + 4B\left(\frac{N_{\rm S}}{b}\frac{f_{\rm n,0}}{\tau_{\rm esc}} + \frac{j_0}{eb}\right)} - \frac{1-f_{\rm n,0}}{\tau_{\rm capt,0}}\right] - \frac{N_{\rm S}}{b}\frac{f_{\rm n,0}}{\tau_{\rm esc}} - \frac{N_{\rm S}}{b}\frac{f_{\rm n,0}^2}{\tau_{\rm QD}}\right\}, \tag{15}$$

where WLb is the OCL volume and W is the lateral size of the device.

Using (7)-(10) in (1)-(3), we obtain a set of algebraic equations in terms of the frequency-dependent amplitudes $\delta n_{\rm OCL-m}$, $\delta f_{\rm n-m}$, and $\delta n_{\rm ph-m}$, the solution of which for $\delta n_{\rm ph-m}$ allows us to calculate the modulation response function

$$H(\omega) = \left|\frac{\delta n_{\rm ph-m}(\omega)}{\delta n_{\rm ph-m}(0)}\right|^2. \tag{16}$$

Finally, we obtain a cubic equation for the square of the modulation bandwidth $\omega_{-3\ {\rm dB}}$ – the frequency, at which the response function $H(\omega)$ has fallen to half its dc ($\omega = 0$) value.

3. DISCUSSION

For an illustration of the results of our analysis, room-temperature operation of a GaInAsP heterostructure lasing near 1.55 μm [8] is considered here. We assume the following parameters: 10% QD-size fluctuations, the surface density of QDs in a single-layer $N_{\rm S} = 6.11\times10^{10}$ cm^{-2}, and an ideal overlap between the electron and hole wave functions in a QD. At these parameters, the maximum modal gain in a single-QD-layer structure is $g^{\rm max} = 29.52$ cm^{-1}. The OCL thickness $b = 0.28$ mm and the cavity length $L = 1.139$ mm.

The modulation bandwidth depends strongly on the capture cross-section $\sigma_{\rm n}$. At a fixed dc component j_0 of the injection current density, with making slower the capture into a QD (reducing $\sigma_{\rm n}$), $\omega_{-3\ {\rm dB}}$ decreases and finally becomes zero (Figs. 3 and 4). As seen from Fig. 4, $\omega_{-3\ {\rm dB}} = 0$ at a certain non-vanishing value $\sigma_{\rm n}^{\rm min}$. This is a consequence of the fact that, at a given j_0, no lasing is attainable in the structure if $\sigma_{\rm n} < \sigma_{\rm n}^{\rm min}$, where $\sigma_{\rm n}^{\rm min}$ is the minimum tolerable capture cross-section for the lasing to occur at such j_0. Indeed, while j_0 is fixed (the horizontal dash-dotted line in Fig. 4), the threshold current density increases with decreasing $\sigma_{\rm n}$ (the solid curve corresponding to the left axis in Fig. 4) [8],

$$j_{\rm th} = \frac{eN_{\rm S}}{\tau_{\rm QD}}f_{\rm n0}^2 + ebB\left(n_1\frac{f_{\rm n0}}{1-f_{\rm n0}} + \frac{1}{\sigma_{\rm n}{\rm v}_{\rm n}\tau_{\rm QD}}\frac{f_{\rm n0}^2}{1-f_{\rm n0}}\right)^2, \tag{17}$$

where $f_{\rm n,0}$ is given by eq. (11).

In order for the lasing to occur, j_0 should be higher than $j_{\rm th}$. At a certain $\sigma_{\rm n}^{\rm min}$, $j_{\rm th}$ becomes equal to j_0 (Fig. 4). At $\sigma_{\rm n} \le \sigma_{\rm n}^{\rm min}$, $j_{\rm th} \ge j_0$, which means that there can be no lasing and hence no direct modulation in the structure (the hatched region in Fig. 4).

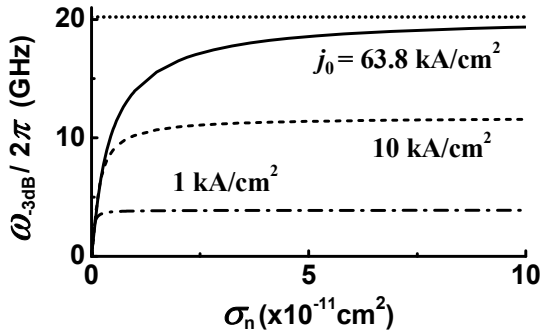

Fig. 3. Modulation bandwidth vs. capture cross-section into a QD at different values of the dc component of the injection current density in a single-layer structure. The horizontal dotted line shows $\omega_{-3\mathrm{dB}}^{\max}$ for the case of instantaneous capture into QDs [eq. (22)]. $T = 300$ K, $L = 1.139$ mm.

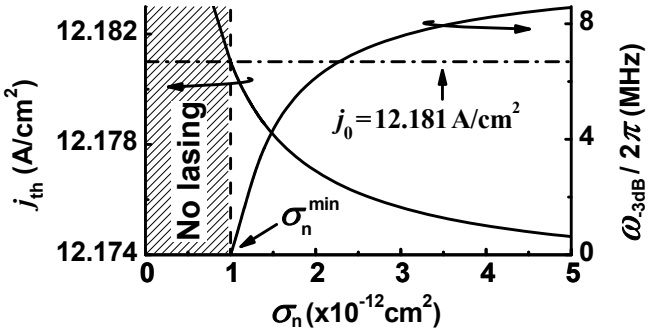

Fig. 4. Modulation bandwidth (at a very low dc component of the injection current density) and threshold current density vs. capture cross-section into a QD in a single-layer structure. No lasing is attainable in the structure if $\sigma_n < \sigma_n^{\min}$, where $\sigma_n^{\min}$ is given by (18).

$\sigma_n^{\min}$ is found from the condition $j_{th} = j_0$ and is given by

$$\sigma_n^{\min}(j_0) = \frac{\dfrac{1}{v_n \tau_{QD}} \dfrac{f_{n0}^2}{1-f_{n0}}}{\sqrt{\dfrac{1}{ebB}\left(j_0 - \dfrac{eN_S}{\tau_{QD}} f_{n0}^2\right)} - n_1 \dfrac{f_{n0}}{1-f_{n0}}} = \frac{1}{v_n \tau_{QD}} \frac{f_{n0}^2}{1-f_{n0}} \sqrt{ebB} \frac{\sqrt{j_0 - \dfrac{eN_S}{\tau_{QD}} f_{n0}^2} + \sqrt{j_{th}^{eq} - \dfrac{eN_S}{\tau_{QD}} f_{n0}^2}}{j_0 - j_{th}^{eq}}, \tag{18}$$

where j_{th}^{eq} is the threshold current density in the case of instantaneous capture into a QD [obtained using $\sigma_n = \infty$ in (17)],

$$j_{th}^{eq} = \frac{eN_S}{\tau_{QD}} f_{n0}^2 + ebB\left(n_1 \frac{f_{n0}}{1-f_{n0}}\right)^2. \tag{19}$$

The dependence of $\sigma_n^{\min}$ on j_0 is shown in Fig. 5. As seen from the figure and eq. (18), when j_0 decreases and approaches j_{th}^{eq}, $\sigma_n^{\min}$ increases infinitely, that is to say that no lasing is attainable at $j_0 \le j_{th}^{eq}$ even if the carrier capture into a QD is instantaneous.

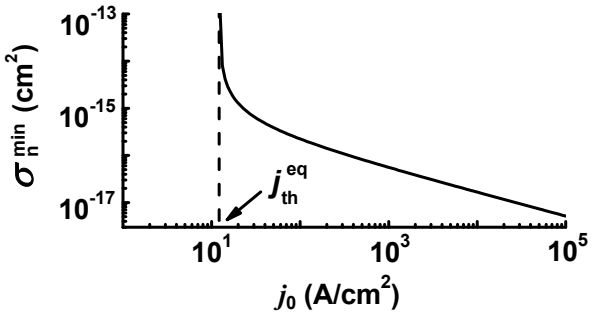

Fig. 5. Minimum tolerable cross-section of carrier capture into a QD vs. dc component of the injection current density. The vertical dashed line shows j_{th}^{eq} given by eq. (19).

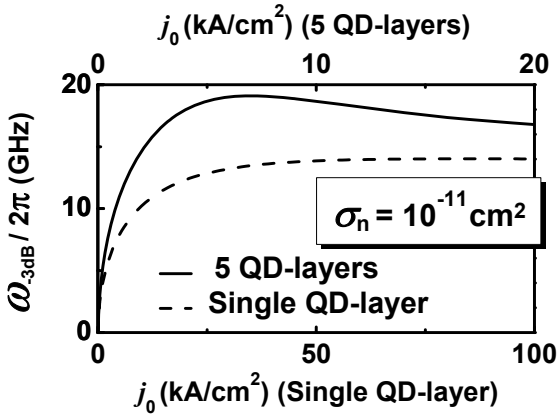

Fig. 6. Modulation bandwidth vs. dc component of the injection current density in a single-QD-layer structure (bottom axis) and a 5-QD-layer-structure (top axis). A plausible value of the capture cross-section $\sigma_n = 10^{-11}$ cm^2 is used [14, 15].

With increasing j_0, σ_n^{min} becomes smaller, i.e., the lasing can occur and hence the direct modulation of the output power is possible at a slower capture into a QD. At very high j_0, when $\sigma_n^{min} \to 0$ and when simultaneously σ_n is very small [so small that $(\sigma_n - \sigma_n^{min})/\sigma_n^{min} \to 0$],

$$\omega_{-3\,dB} \approx 2\sqrt{r-1}\; v_g g^{max} \frac{f_{n0}^2}{\frac{f_{n0}^2}{1-f_{n0}} + 2f_{n0}} \frac{\sigma_n - \sigma_n^{min}}{\sigma_n^{min}}, \tag{20}$$

where $r = 10^{0.3} \approx 1.995$.

At large σ_n, $\omega_{-3\,dB}$ increases and asymptotically approaches its saturation value $\omega_{-3\,dB}\big|_{\sigma_n=\infty}$ for the case of instantaneous capture into a QD: $\omega_{-3\,dB} - \omega_{-3\,dB}\big|_{\sigma_n=\infty} \propto 1/\sigma_n$. The expression for $\omega_{-3\,dB}\big|_{\sigma_n=\infty}$ was derived in [7].

As a function of the dc component j_0 of the injection current density, $\omega_{-3\,dB}$ has a maximum (Fig. 6). In a single-QD-layer structure (the dashed curve in Fig. 6), the optimum value j_{opt} of j_0, at which ω_{-3dB}^{max} is attained, is very high, i.e., ω_{-3dB}^{max} is unattainable. As seen from the figure, there are two advantages in a multiple-QD-layer structure (the solid curve in Fig. 6) as compared to a single-layer structure: (i) at the same value of j_0, $\omega_{-3\,dB}$ is considerably higher, and (ii) j_{opt} is considerably reduced, which means that ω_{-3dB}^{max} is practically attainable.

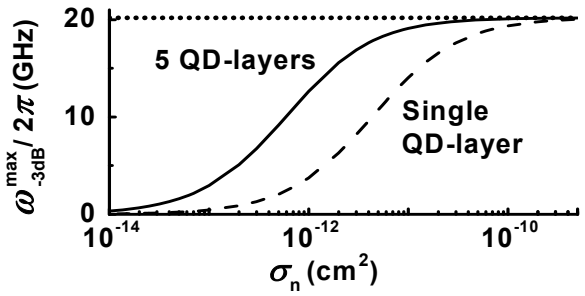

Fig. 7. Maximum modulation bandwidth vs. capture cross-section into a QD. The horizontal dotted line shows $\omega_{-3\mathrm{dB}}^{\max}$ for the case of instantaneous capture into QDs [eq. (22)].

The maximum value of $\omega_{-3\,\mathrm{dB}}$ increases with σ_n (Fig. 7). At large σ_n, when $\tau_{\mathrm{capt},0}/\tau_{\mathrm{ph}} \ll 1$ [$\tau_{\mathrm{capt},0}$ and τ_{ph} are given by (5) and (14), respectively],

$$\omega_{-3\mathrm{dB}}^{\max}\Big|_{\sigma_\mathrm{n}\to\infty} \approx \omega_{-3\mathrm{dB}}^{\max}\Big|_{\sigma_\mathrm{n}=\infty} - \frac{1}{\sigma_\mathrm{n} \mathrm{V}_\mathrm{n} \dfrac{N_\mathrm{S}}{b}} \frac{\sqrt{r}}{2(1-f_{\mathrm{n}0})^2} \frac{1}{\tau_{\mathrm{ph}}^2} \approx \frac{\sqrt{2}}{\tau_{\mathrm{ph}}} \left(1 - \frac{1}{2}\sqrt{\frac{r}{2}} \frac{1}{(1-f_{\mathrm{n}0})^2} \frac{\tau_{\mathrm{capt},0}}{\tau_{\mathrm{ph}}} \right), \tag{21}$$

where

$$\omega_{-3\mathrm{dB}}^{\max}\Big|_{\sigma_\mathrm{n}=\infty} \approx \frac{\sqrt{2}}{\tau_{\mathrm{ph}}} \tag{22}$$

is the maximum modulation bandwidth in the case of instantaneous capture into QDs [7]. As seen from Fig. 7, while the saturation value of $\omega_{-3\mathrm{dB}}^{\max}$ at $\sigma_\mathrm{n} \to \infty$ [eq. (22)] does not depend on the number of QD-layers, $\omega_{-3\mathrm{dB}}^{\max}$ at a given finite σ_n is higher in a multiple-QD-layer structure as compared to a single-QD-layer structure.

4. CONCLUSION

We have shown that the carrier capture from the optical confinement layer into quantum dots (QDs) can strongly limit the modulation bandwidth $\omega_{-3\,\mathrm{dB}}$ of a QD laser. Closed-form analytical expressions have been obtained for $\omega_{-3\,\mathrm{dB}}$ in the limiting cases of fast and slow capture. $\omega_{-3\,\mathrm{dB}}$ is highest in the case of instantaneous capture into QDs, when the cross-section of carrier capture into a QD $\sigma_\mathrm{n} = \infty$. With reducing σ_n, $\omega_{-3\,\mathrm{dB}}$ decreases and becomes zero at a certain non-vanishing value $\sigma_\mathrm{n}^{\min}$. This $\sigma_\mathrm{n}^{\min}$ presents the minimum tolerable capture cross-section for the lasing to occur at a given dc component j_0 of the injection current density. The higher is j_0, the smaller is $\sigma_\mathrm{n}^{\min}$ and hence the direct modulation of the output power is possible at a slower capture. The use of multiple layers with QDs has been shown to considerably improve the modulation response of the laser – the same $\omega_{-3\,\mathrm{dB}}$ is obtained in a multi-layer structure at a much lower j_0 than in a single-layer structure. At a plausible cross-section $\sigma_\mathrm{n} = 10^{-11}$ cm^2 [14, 15], $\omega_{-3\,\mathrm{dB}}$ as high as 19 GHz can be obtained in a 5-QD-layer structure with the cavity length $L = 1.139$ mm at a practical value of $j_0 = 7$ kA/cm^2.

Our analysis provides a basis for optimizing the QD laser design for high-speed operation.

ACKNOWLEDGEMENTS

L.V.A. and Y.W. acknowledge the U.S. Army Research Office (Grant No. W911-NF-08-1-0462), Y.W. also acknowledges the China Scholarship Council, and R.A.S. acknowledges the Russian Foundation for Basic Research (Grant No. 08-02-01337) for support of this work.

REFERENCES

[1] R. Dingle and C. H. Henry, "Quantum effects in heterostructure lasers," *U.S. Patent 3 982 207* (1976).

[2] Zh. I. Alferov, "Nobel Lecture: The double heterostructure concept and its applications in physics, electronics, and technology," *Rev. Mod. Phys.* **73**, 767 (2001).

[3] W. T. Tsang, "Extremely low threshold (AlGa)As graded-index waveguide separate-confinement heterostructure lasers grown by molecular beam epitaxy," *Appl. Phys. Lett.* **40**, 217 (1982).

[4] P. S. Zory, Jr, *Quantum Well Lasers*, Boston: Academic Press Inc., 1993, 504 p.

[5] Y. Arakawa and H. Sakaki, "Multidimensional quantum well laser and temperature dependence of its threshold current," *Appl. Phys. Lett.* **40**, 939 (1982).

[6] A. E. Zhukov, A. R. Kovsh, S. S. Mikhrin, A. P. Vasil'ev, E. S. Semenova, N. A. Maleev, V. M. Ustinov, M. M. Kulagina, E. V. Nikitina, I. P. Soshnikov, Yu. M. Shernyakov, D. A. Livshits, N. V. Kryjanovskaya, D. S. Sizov, M. V. Maximov, A. F. Tsatsul'nikov, N. N. Ledentsov, D. Bimberg, and Zh. I. Alferov, "High external differential efficiency and high optical gain of long-wavelength quantum dot diode laser" *Phys. E* **17**, 589 (2003).

[7] L. V. Asryan and R. A. Suris, "Upper limit for the modulation bandwidth of a quantum dot laser," *Appl. Phys. Lett.* **96**, Art. no. 221112 (2010).

[8] L. V. Asryan and R. A. Suris, "Inhomogeneous line broadening and the threshold current density of a semiconductor quantum dot laser," *Semicond. Sci. Technol.* **11**, 554 (1996).

[9] L. V. Asryan and R. A. Suris, "Temperature dependence of the threshold current density of a quantum dot laser," *IEEE J. Quantum Electron.* **34**, 841 (1998).

[10] L. V. Asryan, S. Luryi, and R. A. Suris, "Intrinsic nonlinearity of the light-current characteristic of semiconductor lasers with a quantum-confined active region," *Appl. Phys. Lett.* **81**, 2154 (2002).

[11] L. V. Asryan, S. Luryi, and R. A. Suris, "Internal efficiency of semiconductor lasers with a quantum-confined active region," *IEEE J. Quantum Electron.* **39**, 404 (2003).

[12] R. Nagarajan, M. Ishikawa, T. Fukushima, R. S. Geels, and J. E. Bowers, "High speed quantum-well lasers and carrier transport effects," *IEEE J. Quantum Electron.* **28**, 1990 (1992).

[13] L. A. Coldren and S. W. Corzine, *Diode Lasers and Photonic Integrated Circuits*, New York: Wiley, 1995, 594 p.

[14] O. Engström, M. Kaniewska, Y. Fu, J. Piscator, and M. Malmkvist, "Electron capture cross sections of InAs/GaAs quantum dots," *Appl. Phys. Lett.* **85**, 2908 (2004).

[15] S. K. Zhang, H. J. Zhu, F. Lu, Z. M. Jiang, and X. Wang, "Erratum: Coulomb charging effect in self-assembled Ge quantum dots studied by admittance spectroscopy," *Phys. Rev. Lett.* **82**, 2622 (1999).

Nanotechnology **21** (2010) 015201 (14pp) doi:10.1088/0957-4484/21/1/015201

Output power of a double tunneling-injection quantum dot laser

Dae-Seob Han and Levon V Asryan

Virginia Polytechnic Institute and State University, Blacksburg, VA 24061, USA

E-mail: asryan@mse.vt.edu

Received 31 July 2009, in final form 4 November 2009
Published 30 November 2009
Online at stacks.iop.org/Nano/21/015201

Abstract

We develop a comprehensive theoretical model for a double tunneling-injection (DTI) quantum dot (QD) laser. Both electrons and holes are injected into QDs by tunneling from two separate quantum wells (QWs). Ideally, out-tunneling of each type of carriers from QDs into the opposite-to-injection-side QW should be completely blocked; as a result, the parasitic electron–hole recombination outside QDs will be suppressed and the light–current characteristic (LCC) of a laser will be strictly linear. To scrutinize the potential of a DTI QD laser for high-power operation and the robustness of an actual device, our model includes out-tunneling leakage of carriers from QDs. We complement our calculations by an analytical model and derive closed-form expressions for the LCC and carrier population across the layered structure. We show that, even in the presence of out-tunneling leakage, the flux of parasitic recombination outside QDs remains restricted with increasing injection current. As a consequence, the LCC exhibits a remarkable feature distinguishing the DTI QD laser from other types of injection lasers—it becomes increasingly linear and the slope efficiency grows closer to unity at high injection currents. The linearity is due to the fact that the current paths connecting the opposite sides of the structure lie entirely within the QDs—in view of the three-dimensional confinement in QDs, the out-tunneling fluxes of carriers from dots are limited.

1. Introduction

A semiconductor quantum dot (QD) is a zero-dimensional (0D) heterostructure formed by growth of a nanometer-size island of a lower bandgap material within a wider bandgap matrix. Due to quantum confinement in all three directions, the energy spectrum of electrons and holes is discrete in a QD. There has been much effort to use QDs as an active region in diode lasers. In the 'conventional' design of QD lasers, the carriers are first injected from the cladding layers into a bulk reservoir (which also serves as the optical confinement layer (OCL) and includes a two-dimensional (2D) wetting layer (WL)) and then captured into QDs. Due to bipolar (i.e. both electron and hole) populations in the reservoir, a certain fraction of the injection current goes into electron–hole recombination there. The parasitic recombination outside QDs is a major source of the temperature dependence of the threshold current. In addition, the carrier capture from the reservoir into QDs is not instantaneous. For this reason, the carrier density in the reservoir, and hence the parasitic recombination rate, rise, even above the lasing threshold, with injection current. This leads to sublinearity of the light–current characteristic (LCC) and limits the output power, especially at high pump currents [1, 2]. Suppression of the parasitic recombination would thus be expected to significantly enhance the temperature stability and the output optical power of a laser.

Several approaches have been proposed to improve the QD laser characteristics. Among them is tunneling injection into QDs. In [3–5], to minimize hot carrier effects, tunneling injection of only electrons into QDs was proposed and realized from a single quantum well (QW) (previously, tunneling injection into a QW was utilized for the same purpose in a QW laser [6]). Laser structures exploiting tunneling injection of only electrons into QDs were also realized in [7–11]. In a recent work [11], high-temperature stability of the threshold current was reported—the characteristic temperature (a figure of merit of a diode laser from the viewpoint of temperature stability of the threshold current) was close to 200 K at and well above the room temperature. In the structures of [3–5] and [7–11], bipolar carrier density and hence parasitic recombination still remain on the hole-injecting side.

In [12, 13], tunneling injection of excitons into quantum dashes was reported.

In [14], resonant tunneling was proposed from the bulk region (OCL) into the QD excited state separated from the QD ground state by the energy of the longitudinal optical (LO) phonon.

In [15–17], to suppress the recombination outside QDs and thus to significantly improve the temperature stability of the laser, tunneling injection of both electrons and holes into QDs was proposed from two separate QWs. Here, by a certain analogy with the universally accepted term 'double-heterostructure laser', the structures of [15–17] are referred to as double tunneling-injection (DTI) QD lasers. The structures of [3–5] and [7–11] can be correspondingly referred to as single tunneling-injection (STI) QD lasers.

There have been experimental developments [18–21] related to the concept of DTI QD lasers. Tunneling injection can efficiently improve the uniformity of QDs by selecting the QDs of the 'right' size [15–18]; the carrier collection in QDs can also be improved [18]. A more symmetrical gain shape and a smaller refractive index change at the peak gain wavelength were reported for a DTI QD laser [21].

It is interesting to note the use of both terms 'tunnel-injection semiconductor laser' and 'double tunnel-injection', though in a different context, as early as 1963. In [22], to avoid some of the problems of junction formation of those days, tunneling injection of electrons (or holes) was proposed from a metal or semiconductor through a thin dielectric film into a suitable semiconductor to produce the population inversion necessary for laser action. In [23], double tunneling injection into a luminescent material was proposed from two metals (or semiconductors) through the insulating films. In [24], double tunneling injection was used to produce electroluminescence in metal–semiconductor tunnel diodes.

In this work, we develop a comprehensive theoretical model for the optical power of a DTI QD laser. We briefly reported on the LCC of such a laser in [25].

2. Theoretical model

The energy band diagram of the structure is shown in figure 1. A single layer with QDs, located in the central part of the OCL, is clad on each side by a thin barrier and a QW. Electrons (holes) are injected into QDs by tunneling from the left- (right-)hand side QW. The key idea of the device is that the QWs are not connected by a current path that bypasses QDs, which in particular assumes that (i) there is no thermal escape of carriers from the QWs over the barriers separating them from the QD layer, and (ii) there is no tunneling between the QWs through the material separating QDs in the QD layer. To realize this idea, certain conditions must be met, which were described in [15–17]. We discuss in this section the details of our extended model for a DTI QD laser.

2.1. Main assumptions

(1) Figure 1 shows the most optimum situation [15–17], when the lowest subband edge for majority carriers in the QW is in resonance with the energy level for the corresponding type of carriers in the average-sized QD, and hence the tunneling-injection rate is at its maximum. However, resonant injection is not the only possibility for tunneling into QDs. Thus, LO phonon-assisted [8, 9, 26, 27] or Auger-assisted [27] tunneling into QDs can be utilized. To also account for such possible situations, our model includes both direct and indirect tunneling—the effective tunneling rate from the entire QW subband into the QD ensemble is used (see below).

Tunneling-injection does not necessarily have to occur into the QD ground state. Carriers can efficiently tunnel from the QW to the QD excited state, and then relax rapidly to the QD ground state for stimulated recombination [28, 29]. In [19, 21], a lasing action from the QD excited state was reported.

In our model for tunneling, the QW and QD states are considered to be independent of each other. In a structure with thin barriers, the states of the combined QW–QD system should be self-consistently treated. The use of the effective rate of tunneling from the entire QW subband into QDs means that our model does not also distinguish between direct (coherent) [28] and indirect (incoherent) [8, 9, 26, 27] tunneling processes.

(2) Ideally, there should be no second tunneling step, i.e. out-tunneling from QDs into the 'foreign' QWs (electron-injecting QW for holes and hole-injecting QW for electrons). As a result, there will be no electrons (holes) in the hole- (electron-)injecting side of the structure. As shown below, the total suppression of bipolar population and, consequently, of recombination outside QDs leads to an ideal LCC (i.e. a linear LCC with the slope efficiency equal to unity).

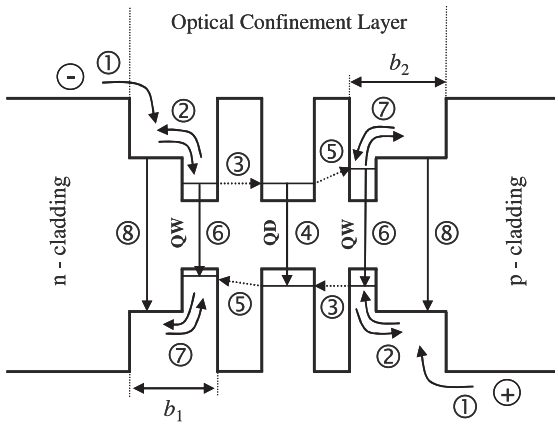

Figure 1. Energy band diagram of a double tunneling-injection QD laser and the main processes: ① injection from the cladding layers to the OCL, ② majority carrier capture from the OCL to the QW and thermal escape from the QW to the OCL, ③ tunneling injection from the QW into a QD, ④ spontaneous and stimulated recombination in a QD, ⑤ out-tunneling from a QD into the 'foreign' QW, ⑥ spontaneous recombination in the QWs, ⑦ minority carrier thermal escape from the QW to the OCL and capture from the OCL to the QW and ⑧ spontaneous recombination in the OCL.

Out-tunneling into the foreign QWs cannot be completely blocked in actual devices. Figure 1 shows an optimized structure, in which the lowest subband edge for minority carriers in the QW is misaligned from the energy level for the corresponding type of carriers in the average-sized QD. Even in such a structure, there will be an indirect out-tunneling (shown by the inclined arrows in figure 1)—electrons (holes) as minority carriers will appear in the hole- (electron-)injecting QW. Then they will thermally escape to the right- (left-)hand side of the OCL where holes (electrons) are the majority carriers. As a result, a bipolar population will be established outside QDs and parasitic recombination will occur. Our model includes these processes and addresses their effect on the device characteristics.

(3) We reasonably assume that the conduction (valence) band offset at the heteroboundary between the p- (n-)cladding and the OCL is large enough to block the further thermal escape of electrons (holes) to the p- (n-)cladding layer. In such a typical situation, the current in the p- (n-)cladding (including the boundary with the OCL) is purely the hole (electron) current. Hence, the total injection current density j will enter into the rate equation for free electrons (holes) in the left- (right-)hand side of the OCL (see equations (1) and (3) below).

(4) The internal optical loss, $\alpha_{\rm int}$, is set zero here.

(5) A structure without the WL is considered in this work. In self-assembled Stranski–Krastanow grown QD structures, such a layer is present and adjacent to QDs [30–32]. Due to coupling (through the capture and escape processes) between QDs and the WL, there will be a bipolar population and hence electron–hole recombination in the WL. A careful consideration of the effect of the WL on the temperature dependence of the threshold current and on the optical power of a DTI QD laser is hence required, which is the subject of a separate work.

2.2. Rate equations

Our model is based on rate equations, which include the main processes in the layered structure. With the above assumptions, we have the following set of equations:

for free electrons and holes on the left-hand side of the OCL:

$$b_1\frac{\partial n_{\rm L}}{\partial t}=\frac{j}{e}+\frac{n^{\rm L}_{\rm QW}}{\tau^{\rm L}_{\rm n,esc}}-v^{\rm L}_{\rm n,capt}n_{\rm L}-b_1Bn_{\rm L}p_{\rm L}, \quad (1)$$

$$b_1\frac{\partial p_{\rm L}}{\partial t}=\frac{p^{\rm L}_{\rm QW}}{\tau^{\rm L}_{\rm p,esc}}-v^{\rm L}_{\rm p,capt}p_{\rm L}-b_1Bn_{\rm L}p_{\rm L}, \quad (2)$$

for free holes and electrons on the right-hand side of the OCL:

$$b_2\frac{\partial p_{\rm R}}{\partial t}=\frac{j}{e}+\frac{p^{\rm R}_{\rm QW}}{\tau^{\rm R}_{\rm p,esc}}-v^{\rm R}_{\rm p,capt}p_{\rm R}-b_2Bn_{\rm R}p_{\rm R}, \quad (3)$$

$$b_2\frac{\partial n_{\rm R}}{\partial t}=\frac{n^{\rm R}_{\rm QW}}{\tau^{\rm R}_{\rm n,esc}}-v^{\rm R}_{\rm n,capt}n_{\rm R}-b_2Bn_{\rm R}p_{\rm R}, \quad (4)$$

for electrons and holes in the electron-injecting (left-hand side) QW:

$$\frac{\partial n^{\rm L}_{\rm QW}}{\partial t}=v^{\rm L}_{\rm n,capt}n_{\rm L}-\frac{n^{\rm L}_{\rm QW}}{\tau^{\rm L}_{\rm n,esc}}-w^{\rm L}_{\rm n,tunn}N_{\rm S}(1-f_{\rm n})n^{\rm L}_{\rm QW}+w^{\rm L}_{\rm n,tunn}n_1^{\rm L,QW}N_{\rm S}f_{\rm n}-B_{\rm 2D}n^{\rm L}_{\rm QW}p^{\rm L}_{\rm QW}, \quad (5)$$

$$\frac{\partial p^{\rm L}_{\rm QW}}{\partial t}=v^{\rm L}_{\rm p,capt}p_{\rm L}-\frac{p^{\rm L}_{\rm QW}}{\tau^{\rm L}_{\rm p,esc}}-w^{\rm L}_{\rm p,tunn}N_{\rm S}(1-f_{\rm p})p^{\rm L}_{\rm QW}+w^{\rm L}_{\rm p,tunn}p_1^{\rm L,QW}N_{\rm S}f_{\rm p}-B_{\rm 2D}n^{\rm L}_{\rm QW}p^{\rm L}_{\rm QW}, \quad (6)$$

for holes and electrons in the hole-injecting (right-hand side) QW:

$$\frac{\partial p^{\rm R}_{\rm QW}}{\partial t}=v^{\rm R}_{\rm p,capt}p_{\rm R}-\frac{p^{\rm R}_{\rm QW}}{\tau^{\rm R}_{\rm p,esc}}-w^{\rm R}_{\rm p,tunn}N_{\rm S}(1-f_{\rm p})p^{\rm R}_{\rm QW}+w^{\rm R}_{\rm p,tunn}p_1^{\rm R,QW}N_{\rm S}f_{\rm p}-B_{\rm 2D}n^{\rm R}_{\rm QW}p^{\rm R}_{\rm QW}, \quad (7)$$

$$\frac{\partial n^{\rm R}_{\rm QW}}{\partial t}=v^{\rm R}_{\rm n,capt}n_{\rm R}-\frac{n^{\rm R}_{\rm QW}}{\tau^{\rm R}_{\rm n,esc}}-w^{\rm R}_{\rm n,tunn}N_{\rm S}(1-f_{\rm n})n^{\rm R}_{\rm QW}+w^{\rm R}_{\rm n,tunn}n_1^{\rm R,QW}N_{\rm S}f_{\rm n}-B_{\rm 2D}n^{\rm R}_{\rm QW}p^{\rm R}_{\rm QW}, \quad (8)$$

for electrons and holes confined in QDs:

$$N_{\rm S}\frac{\partial f_{\rm n}}{\partial t}=w^{\rm L}_{\rm n,tunn}N_{\rm S}(1-f_{\rm n})n^{\rm L}_{\rm QW}-w^{\rm L}_{\rm n,tunn}n_1^{\rm L,QW}N_{\rm S}f_{\rm n}+w^{\rm R}_{\rm n,tunn}N_{\rm S}(1-f_{\rm n})n^{\rm R}_{\rm QW}-w^{\rm R}_{\rm n,tunn}n_1^{\rm R,QW}N_{\rm S}f_{\rm n}-N_{\rm S}\frac{f_{\rm n}f_{\rm p}}{\tau_{\rm QD}}-\frac{c}{\sqrt{\epsilon_{\rm g}}}\frac{g^{\max}}{S}(f_{\rm n}+f_{\rm p}-1)N, \quad (9)$$

$$N_{\rm S}\frac{\partial f_{\rm p}}{\partial t}=w^{\rm R}_{\rm p,tunn}N_{\rm S}(1-f_{\rm p})p^{\rm R}_{\rm QW}-w^{\rm R}_{\rm p,tunn}p_1^{\rm R,QW}N_{\rm S}f_{\rm p}+w^{\rm L}_{\rm p,tunn}N_{\rm S}(1-f_{\rm p})p^{\rm L}_{\rm QW}-w^{\rm L}_{\rm p,tunn}p_1^{\rm L,QW}N_{\rm S}f_{\rm p}-N_{\rm S}\frac{f_{\rm n}f_{\rm p}}{\tau_{\rm QD}}-\frac{c}{\sqrt{\epsilon_{\rm g}}}\frac{g^{\max}}{S}(f_{\rm n}+f_{\rm p}-1)N, \quad (10)$$

and for photons,

$$\frac{\partial N}{\partial t}=\frac{c}{\sqrt{\epsilon_{\rm g}}}g^{\max}(f_{\rm n}+f_{\rm p}-1)N-\frac{c}{\sqrt{\epsilon_{\rm g}}}\beta N. \quad (11)$$

In equations (1)–(11), b_1 (b_2) is the thickness of the left- (right-)hand side of the OCL (the separation between the n- (p-)cladding layer and the left- (right-)hand side barrier—figure 1) and $n_{\rm L}$ ($n_{\rm R}$) and $p_{\rm L}$ ($p_{\rm R}$) are the free-electron and -hole densities there, j is the injection current density, e is the electron charge, $n^{\rm L}_{\rm QW}$ ($n^{\rm R}_{\rm QW}$) and $p^{\rm L}_{\rm QW}$ ($p^{\rm R}_{\rm QW}$) are the 2D electron and hole densities in the left- (right-)hand side QW (figure 1), B and $B_{\rm 2D}$ are the spontaneous radiative recombination constants for the bulk (OCL) and 2D regions (QWs) measured in units of $\rm cm^3\ s^{-1}$ and $\rm cm^2\ s^{-1}$, respectively, $N_{\rm S}$ is the surface density of QDs, $f_{\rm n,p}$ are the electron- and hole-level occupancies in QDs, $\tau_{\rm QD}$ is the spontaneous radiative lifetime in QDs, c is the velocity of light in vacuum, $\sqrt{\epsilon_{\rm g}}$ is the group index of the dispersive OCL material, $g^{\max}$ is the maximum value of the modal gain [33], $S=WL$ is the cross section of the junction, W is the lateral size of the device, L is the cavity length, $\beta=(1/L)\ln(1/R)$ is the mirror loss, R is the facet reflectivity and N is the number of photons in the lasing mode.

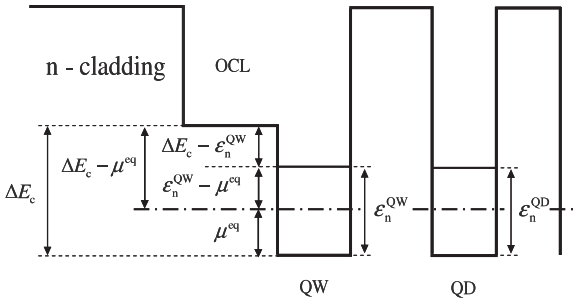

Figure 2. Conduction band diagram on the left-hand (electron-injecting) side of the structure. The Fermi level μ^{eq} (dash–dotted line) is shown solely as an illustration of the derivations of appendixes A and B for the equilibrium case. No equilibrium is assumed under lasing conditions.

We denoted the thermal escape times of electrons and holes from the QWs to the OCL by $\tau_{n,p,esc}^{L,R}$ and the capture velocities from the OCL to the QWs by $v_{n,p,capt}^{L,R}$. These quantities are related to each other. It is the capture velocity that describes the carrier capture to a QW [34, 35]. The general expression relating $\tau_{n,p,esc}$ and $v_{n,p,capt}$ is derived in appendix A using the detailed balance condition. For undoped OCL and QW, the relation is as follows:

$$\tau_{n,esc} = \frac{1}{v_{n,capt}} \frac{N_c^{2D}}{n_1}, \qquad \tau_{p,esc} = \frac{1}{v_{p,capt}} \frac{N_v^{2D}}{p_1}, \tag{12}$$

where $N_{c,v}^{2D} = m_{c,v}^{QW} T/(\pi\hbar^2)$ are the 2D effective densities of states in the conduction and valence bands in the QWs, $m_{c,v}^{QW}$ are the electron and hole effective masses in the QWs and the temperature T is measured in units of energy.

The quantities n_1 and p_1 are

$$n_1 = N_c^{3D} \exp\left(-\frac{\Delta E_c - \varepsilon_n^{QW}}{T}\right),$$
$$p_1 = N_v^{3D} \exp\left(-\frac{\Delta E_v - \varepsilon_p^{QW}}{T}\right), \tag{13}$$

where $N_{c,v}^{3D} = 2[m_{c,v}^{OCL} T/(2\pi\hbar^2)]^{3/2}$ are the three-dimensional (3D) effective densities of states in the conduction and valence bands in the OCL, $m_{c,v}^{OCL}$ are the electron and hole effective masses in the OCL, $\Delta E_{c,v}$ are the conduction and valence band offsets between the OCL and the QW (figure 2), and $\varepsilon_{n,p}^{QW}$ are the energies of the lowest electron- and hole-subband edges in the QW (figure 2).

We exploit four tunneling coefficients, $w_{n,p,tunn}^{L,R}$ (measured in units of cm^2 s^{-1}), for electron and hole tunneling between the QD ensemble and the QWs. These tunneling coefficients are primarily controlled by the thicknesses and material parameters of the barriers, and by the QD and QW parameters as well. In a properly designed structure, $w_{n,tunn}^{L}$ and $w_{p,tunn}^{R}$ should be large, and $w_{p,tunn}^{L}$ and $w_{n,tunn}^{R}$ small.

The quantities $n_1^{L,R,QW}$ and $p_1^{L,R,QW}$ entering into the electron and hole tunneling fluxes from the QD ensemble to the QWs (see (5)–(10)) are measured in units of cm^{-2}. The general expressions for n_1^{QW} and p_1^{QW} are derived in appendix B. In the case of an undoped QW and a resonance between the energy level in a QD and the lowest subband edge in a QW:

$$n_1^{L,QW} = N_c^{2D}, \qquad p_1^{R,QW} = N_v^{2D}. \tag{14}$$

As seen from (1)–(8), the equations for the carrier densities on the right-hand side QW and OCL are similar to those on the left-hand side. For this reason, we will analyze the rate equations and their solutions for the carrier densities on the left-hand side only. The solutions on the right-hand side are easily obtained from those on the left-hand side by an exchange between the electron and hole densities n and p and the left- and right-hand side indices 'L' and 'R'.

The first term on the right-hand side in (1) is the electron injection flux (in units of cm^{-2} s^{-1}) from the n-cladding layer to the OCL—see assumption 3 above.

The terms containing the escape times and capture velocities in the rate equations are respectively the fluxes of thermal escape from the QW to the OCL and capture from the OCL to the QW.

The last term on the right-hand side in (1) and (2) is the spontaneous radiative recombination flux in the OCL. The last term on the right-hand side in (5) and (6) is the spontaneous radiative recombination flux in the QW.

In (5) and (9), $w_{n,tunn}^{L} N_S (1-f_n) n_{QW}^{L}$ and $w_{n,tunn}^{L} n_1^{L,QW} N_S f_n$ are the fluxes of electron tunneling from the electron-injecting QW into the QD ensemble and back from the QD ensemble to the QW. The difference $w_{n,tunn}^{L} N_S (1 - f_n) n_{QW}^{L} - w_{n,tunn}^{L} n_1^{L,QW} N_S f_n$ is the net in-tunneling flux of electrons from the electron-injecting QW into QDs.

In (6) and (10), $w_{p,tunn}^{L} p_1^{L,QW} N_S f_p$ and $w_{p,tunn}^{L} N_S (1 - f_p) p_{QW}^{L}$ are the fluxes of hole tunneling from the QD ensemble to the electron-injecting (i.e. foreign) QW and back from the QW into the QD ensemble. The difference $w_{p,tunn}^{L} p_1^{L,QW} N_S f_p - w_{p,tunn}^{L} N_S (1 - f_p) p_{QW}^{L}$ is the net out-tunneling flux of holes from QDs to the electron-injecting QW.

In (9) and (10), $N_S f_n f_p/\tau_{QD}$ is the spontaneous radiative recombination flux in QDs and $(c/\sqrt{\epsilon_g})(g^{max}/S)(f_n + f_p - 1)N$ is the stimulated radiative recombination flux.

The first term on the right-hand side in (11) is the rate (in units of s^{-1}) of stimulated emission of photons and the second term is the rate of escape of photons from the cavity through the mirrors.

To optimize the device, it is desirable to maximize the net in-tunneling flux of electrons from the electron-injecting QW into QDs and minimize the net out-tunneling flux of holes from QDs to the electron-injecting QW.

The flux of electron (and similarly hole) tunneling from a QD ensemble to a QW can be written as

$$w_{n,tunn} n_1^{QW} N_S f_n = N_S \frac{f_n}{\tau_{n,tunn}^{QD \to QW}}, \tag{15}$$

where

$$\tau_{n,tunn}^{QD \to QW} = \frac{1}{w_{n,tunn} n_1^{QW}} \tag{16}$$

can be viewed as the tunneling time from a QD to a QW.

The flux of electron tunneling from a QW to a QD ensemble can be written as

$$w_{\mathrm{n,tunn}} N_{\mathrm{S}} (1 - f_{\mathrm{n}}) n_{\mathrm{QW}} = \frac{n_{\mathrm{QW}}}{\tau_{\mathrm{n,tunn}}^{\mathrm{QW}\to\mathrm{QDs}}}, \tag{17}$$

where

$$\tau_{\mathrm{n,tunn}}^{\mathrm{QW}\to\mathrm{QDs}} = \frac{\tau_{\mathrm{n,tunn},0}^{\mathrm{QW}\to\mathrm{QDs}}}{1 - f_{\mathrm{n}}} \tag{18}$$

can be considered as the tunneling time from a QW to a QD ensemble, and

$$\tau_{\mathrm{n,tunn},0}^{\mathrm{QW}\to\mathrm{QDs}} = \frac{1}{w_{\mathrm{n,tunn}} N_{\mathrm{S}}} \tag{19}$$

can be correspondingly considered as the tunneling time into an unoccupied QD ensemble (when $f_{\mathrm{n}} = 0$).

As seen from (16) and (19), the tunneling times $\tau_{\mathrm{n,tunn}}^{\mathrm{QD}\to\mathrm{QW}}$ and $\tau_{\mathrm{n,tunn},0}^{\mathrm{QW}\to\mathrm{QDs}}$ are not the same. In contrast to $\tau_{\mathrm{n,tunn}}^{\mathrm{QD}\to\mathrm{QW}}$, which describes tunneling from *an individual* QD to a QW, $\tau_{\mathrm{n,tunn},0}^{\mathrm{QW}\to\mathrm{QDs}}$ describes tunneling from a QW to *the entire QD ensemble*—the surface density of QDs, N_S, i.e. a characteristic of the entire QD ensemble, enters into equation (19) for $\tau_{\mathrm{n,tunn}}^{\mathrm{QW}\to\mathrm{QDs}}$. Both $\tau_{\mathrm{n,tunn}}^{\mathrm{QD}\to\mathrm{QW}}$ and $\tau_{\mathrm{n,tunn},0}^{\mathrm{QW}\to\mathrm{QDs}}$ are expressed in terms of a single coefficient $w_{\mathrm{n,tunn}}$. For these reasons, and to avoid possible confusion, we will not use here two separate times $\tau_{\mathrm{n,tunn}}^{\mathrm{QD}\to\mathrm{QW}}$ and $\tau_{\mathrm{n,tunn}}^{\mathrm{QW}\to\mathrm{QDs}}$ for tunneling between a QD ensemble and a QW. Instead, we use a single parameter—the tunneling coefficient $w_{\mathrm{n,tunn}}$.

3. Results and discussion

We consider a continuous-wave operation of the laser and correspondingly use the steady-state rate equations:

$$\frac{\partial}{\partial t}(b_1 n_{\mathrm{L}}, b_1 p_{\mathrm{L}}, b_2 n_{\mathrm{R}}, b_2 p_{\mathrm{R}}, n_{\mathrm{QW}}^{\mathrm{L}}, p_{\mathrm{QW}}^{\mathrm{L}}, n_{\mathrm{QW}}^{\mathrm{R}}, p_{\mathrm{QW}}^{\mathrm{R}}, N_{\mathrm{S}} f_{\mathrm{n}}, N_{\mathrm{S}} f_{\mathrm{p}}, N) = 0, \tag{20}$$

which are eleven equations in total. These equations do not, however, constitute a complete set for finding eleven unknowns (n_{L}, p_{L}, n_{R}, p_{R}, $n_{\mathrm{QW}}^{\mathrm{L}}$, $p_{\mathrm{QW}}^{\mathrm{L}}$, $n_{\mathrm{QW}}^{\mathrm{R}}$, $p_{\mathrm{QW}}^{\mathrm{R}}$, f_{n}, f_{p} and N). It is easily shown that only nine out of ten equations (1)–(10) are independent at the steady state, which is to say that the set should be complemented by one more equation. The equation is provided by the condition of charge neutrality in QDs (see below).

Above the lasing threshold, the number of stimulated photons is nonvanishing ($N \neq 0$). To satisfy equation (11) at the steady state at nonvanishing N, the following lasing condition should hold:

$$g^{\max}(f_{\mathrm{n}} + f_{\mathrm{p}} - 1) = \beta, \tag{21}$$

which is the condition of equality of the modal gain to the mirror loss at and above the lasing threshold (the internal optical loss is not considered here—see assumption 4).

Using the steady-state rate equations and introducing the photon lifetime in the cavity,

$$\tau_{\mathrm{ph}} = \frac{\sqrt{\epsilon_{\mathrm{g}}}}{c}\frac{1}{\beta}, \tag{22}$$

the following expression is obtained for the number of photons N and output power P:

$$P = \hbar\omega \frac{N}{\tau_{\mathrm{ph}}} = \frac{\hbar\omega}{e} S \Bigg(j - eN_{\mathrm{S}} \frac{f_{\mathrm{n}} f_{\mathrm{p}}}{\tau_{\mathrm{QD}}} - eB_{\mathrm{2D}} n_{\mathrm{QW}}^{\mathrm{L}} p_{\mathrm{QW}}^{\mathrm{L}} - eB_{\mathrm{2D}} n_{\mathrm{QW}}^{\mathrm{R}} p_{\mathrm{QW}}^{\mathrm{R}} - eb_1 B n_{\mathrm{L}} p_{\mathrm{L}} - eb_2 B n_{\mathrm{R}} p_{\mathrm{R}} \Bigg), \tag{23}$$

where $\hbar\omega$ is the photon energy. Expression (23) is general and holds no matter what a specific model is for the carrier capture from the OCL to QWs, escape from QWs to the OCL and tunneling between QWs and QDs. What it means is that the stimulated emission is produced by an excess of the injection current density j over the current densities of spontaneous recombination in QDs (second term in the brackets), QWs (third and fourth terms) and OCL (last two terms).

The confined-carrier level occupancies in QDs, 2D-carrier densities in the QWs and free-carrier densities in the OCL depend on the pump current density j. To calculate the LCC (i.e. P versus j given by (23)), these dependences should be found from the solution of the rate equations. We start with an ideal structure and next consider a structure with out-tunneling leakage from QDs.

3.1. Ideal structure: no out-tunneling from QDs, no recombination outside QDs

If out-tunneling from QDs into the foreign QWs is completely blocked ($w_{\mathrm{p,tunn}}^{\mathrm{L}}$ and $w_{\mathrm{n,tunn}}^{\mathrm{R}}$ are set to zero in the above rate equations), there will be no minority carriers outside QDs (p_{L}, $p_{\mathrm{QW}}^{\mathrm{L}}$, $n_{\mathrm{QW}}^{\mathrm{R}}$, $n_{\mathrm{R}} = 0$). The injection current will entirely go into the spontaneous and stimulated recombination in QDs. Equation (23) will be

$$P = \frac{\hbar\omega}{e} S \left(j - eN_{\mathrm{S}} \frac{f_{\mathrm{n}} f_{\mathrm{p}}}{\tau_{\mathrm{QD}}} \right). \tag{24}$$

In general, the level occupancies $f_{\mathrm{n,p}}$, and hence the spontaneous recombination current density in QDs, $eN_{\mathrm{S}}(f_{\mathrm{n}} f_{\mathrm{p}}/\tau_{\mathrm{QD}})$, can depend on the injection current density j. Whatever the dependence is, $f_{\mathrm{n,p}}$ cannot exceed unity; consequently, $eN_{\mathrm{S}}(f_{\mathrm{n}} f_{\mathrm{p}}/\tau_{\mathrm{QD}})$ cannot exceed $eN_{\mathrm{S}}/\tau_{\mathrm{QD}}$. For typical values of the surface density of QDs N_S (below 10^{11} cm^{-2}) and spontaneous radiative recombination time in QDs τ_{QD} (around 1 ns), $eN_{\mathrm{S}}/\tau_{\mathrm{QD}}$ is less than 20 A cm^{-2}. This means that, for $j > 100$ A cm^{-2}, the spontaneous recombination term can be safely neglected compared to j in (24). Hence, the LCC of an ideal DTI QD laser, in which out-tunneling from QDs is completely blocked, is virtually linear and the slope efficiency is unity. The reason is that the only remaining channel of nonstimulated recombination in this case is the spontaneous recombination in QDs, which is weak.

Let us show that the initial portion of the LCC (for which the term $eN_{\mathrm{S}}(f_{\mathrm{n}} f_{\mathrm{p}}/\tau_{\mathrm{QD}})$ cannot be neglected in (24)) is also linear. If charge neutrality holds in QDs ($f_{\mathrm{n}} = f_{\mathrm{p}}$), we immediately obtain from (21) that the level occupancies are pinned at their threshold value and do not depend on the injection current:

$$f_{\mathrm{n}} = f_{\mathrm{p}} = \frac{1}{2}\left(1 + \frac{\beta}{g^{\max}}\right) = \mathrm{const}(j). \tag{25}$$

In this case, $eN_S(f_n f_p/\tau_{QD}) = \text{const}(j)$. As discussed in [2] in the context of conventional QD lasers, violation of charge neutrality ($f_n \neq f_p$) can disrupt pinning the level occupancies and lead to their dependence on the pump current (just as it leads to the temperature dependence [36, 37]). Denoting $\Delta = f_p - f_n$, we have from (21)

$$f_{n,p}(j) = \frac{1}{2}\left(1 + \frac{\beta}{g^{max}}\right) \mp \frac{1}{2}\Delta(j), \tag{26}$$

where '−' and '+' correspond to 'n' and 'p' subscripts, respectively. With (24) and (26), the output power can be written as

$$P(j) = \frac{\hbar\omega}{e} S\left\{j - \frac{1}{4}\frac{eN_S}{\tau_{QD}}\left[\left(1 + \frac{\beta}{g^{max}}\right)^2 - \Delta^2(j)\right]\right\}. \tag{27}$$

Since f_p and f_n are less than unity, so is their difference Δ. As seen from (27), violation of charge neutrality in QDs appears as a second-order effect (Δ^2) in the expression for the LCC. Hence, in both cases of neutral and charged QDs, the LCC of an ideal DTI QD laser is also linear at low j.

3.2. Structure with out-tunneling leakage from QDs and recombination outside QDs

In an actual structure, there can be out-tunneling into the foreign QWs (figure 1). For this reason, the electron–hole recombination outside QDs cannot be completely suppressed. Hence, the rate equations (1)–(11) should be solved in the general case of nonvanishing tunneling coefficients $w^L_{p,tunn}$ and $w^R_{n,tunn}$.

We assume charge neutrality in QDs and use (25) for the level occupancies. The derivations lead to a quartic equation in n^L_{QW}, the solution of which provides us with n^L_{QW} as a function of j. The other carrier densities on the left-hand side of the structure (p^L_{QW}, n_L and p_L) are expressed in terms of n^L_{QW}. Similarly, the carrier densities on the right-hand side are expressed in terms of p^R_{QW}. Finally, the number of photons and output power are found from (23) as functions of j.

Under the conditions of negligible recombination in the OCL (up to high injection current densities—see appendix C), solving the rate equations simplifies considerably—closed-form expressions are obtained for the carrier densities and output power as functions of j (appendix D).

Several general conclusions can be easily made from the analysis of the rate equations.

At the steady state, equation (2) for free holes on the left-hand side of the OCL can be written as follows:

$$\frac{p^L_{QW}}{\tau_{p,esc}} = v^L_{p,capt} p_L + b_1 B n_L p_L. \tag{28}$$

Substituting $p^L_{QW}/\tau_{p,esc} - v^L_{p,capt} p_L = b_1 B n_L p_L$ in (6), we have

$$B_{2D} n^L_{QW} p^L_{QW} + b_1 B n_L p_L = w^L_{p,tunn} p_1^{L,QW} N_S f_p - w^L_{p,tunn} N_S (1 - f_p) p^L_{QW}. \tag{29}$$

As seen from (29), bimolecular recombination on the left-hand side QW and OCL is entirely due to the net out-tunneling of holes from QDs to the QW.

Substituting $v^L_{n,capt} n_L - n^L_{QW}/\tau_{n,esc} = j/e - b_1 B n_L p_L$ (see (1)) in (5), we have

$$B_{2D} n^L_{QW} p^L_{QW} + b_1 B n_L p_L = \frac{j}{e} - [w^L_{n,tunn} N_S (1 - f_n) n^L_{QW} - w^L_{n,tunn} n_1^{L,QW} N_S f_n]. \tag{30}$$

As seen from (30), the flux of bimolecular recombination on the left-hand side QW and OCL can alternatively be presented as the difference of the electron injection flux j/e and the net in-tunneling flux of electrons from the QW to QDs. In other words, the electron flux, which does not enter QDs, can only be consumed via recombination with holes outside QDs.

By dropping in (29) the flux $w^L_{p,tunn} N_S (1 - f_p) p^L_{QW}$ of backward tunneling of holes from the electron-injecting QW to QDs, we get an upper limit for the parasitic recombination flux on the left-hand side of the structure. Since $f_{n,p} \leqslant 1$, this limit, which presents the out-tunneling flux $w^L_{p,tunn} p_1^{L,QW} N_S f_p$ of holes from QDs to the foreign (electron-injecting) QW, is itself restricted and cannot exceed $w^L_{p,tunn} p_1^{L,QW} N_S$ at any j (under the condition of charge neutrality (see (25)), $w^L_{p,tunn} p_1^{L,QW} N_S f_p$ is pinned and does not change with j). Consequently, the recombination flux in the left-hand side QW and OCL is limited by $w^L_{p,tunn} p_1^{L,QW} N_S$:

$$B_{2D} n^L_{QW} p^L_{QW} + b_1 B n_L p_L < w^L_{p,tunn} p_1^{L,QW} N_S f_p < w^L_{p,tunn} p_1^{L,QW} N_S = \text{const}. \tag{31}$$

The parasitic recombination current density (the sum of the last four terms in the brackets in (23)) and the out-tunneling current density

$$j_{out-tunn} = e w^L_{p,tunn} p_1^{L,QW} N_S f_p + e w^R_{n,tunn} n_1^{R,QW} N_S f_n, \tag{32}$$

are shown in figure 3 versus the excess injection current density $j - j_{th}$ (solid curve and horizontal dashed line, respectively).

The fact that the parasitic recombination flux outside QDs remains limited with increasing j is due to a 0D nature of QDs—QDs constrain the carrier transfer between the opposite sides of the structure. If a QW or quantum wires would be used instead of QDs, the out-tunneling fluxes would be controlled by the 2D or 1D carrier densities, which, unlike $f_{n,p}$, would not be limited; accordingly, the parasitic recombination flux would not be limited.

With (29) and a similar equation for the right-hand side of the structure, equation (23) can be rewritten as follows:

$$P = \frac{\hbar\omega}{e} S\left[j - eN_S \frac{f_n f_p}{\tau_{QD}} - e w^L_{p,tunn} p_1^{L,QW} N_S f_p - e w^R_{n,tunn} n_1^{R,QW} N_S f_n + e w^L_{p,tunn} N_S (1 - f_p) p^L_{QW} + e w^R_{n,tunn} N_S (1 - f_n) n^R_{QW}\right]. \tag{33}$$

Whatever the dependences of p^L_{QW} and n^R_{QW} on j, it is clear from (33) that by dropping the last two terms in the brackets (the current densities of backward tunneling of

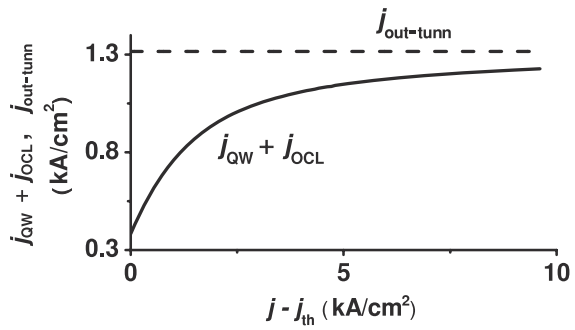

Figure 3. Parasitic recombination current density in the QWs and OCL (solid curve) and current density of out-tunneling from QDs to the foreign QWs (horizontal dashed line) against excess injection current density. A GaInAsP heterostructure lasing at room-temperature ($T = 300$ K) near the telecommunication wavelength 1.55 μm is considered here. 10% QD size fluctuations are assumed. The parameters of the structure are as follows: $N_S = 6.11 \times 10^{10}$ cm^{-2}, $L = 1.139$ mm, $R = 0.32$, $\beta = 10$ cm^{-1}, $W = 2$ μm, $\tau_{QD} = 0.71 \times 10^{-9}$ s, $g^{max} = 29.52$ cm^{-1}, $b_1 = b_2 = 0.14$ μm, $v^{L,R}_{n,p,capt} = 3 \times 10^5$ cm s^{-1}, $\lambda = 1.58$ μm, $B = 1.27 \times 10^{-10}$ cm^3 s^{-1} and $B_{2D} = 2.8 \times 10^{-4}$ cm^2 s^{-1}. In figures 3–10, the tunneling coefficients are as follows unless otherwise specified: $w^L_{n,tunn} = 0.073$ cm^2 s^{-1}, $w^L_{p,tunn} = 0.04$ cm^2 s^{-1}, $w^R_{n,tunn} = 0.013$ cm^2 s^{-1} and $w^R_{p,tunn} = 0.058$ cm^2 s^{-1}. The threshold current density is $j_{th} = 389$ A cm^{-2}.

minority carriers from the foreign QWs to QDs) we will obtain the lower limit for the output power:

$$P^{lowest} = \frac{\hbar\omega}{e} S\left(j - eN_S \frac{f_n f_p}{\tau_{QD}} - ew^L_{p,tunn} p_1^{L,QW} N_S f_p - ew^R_{n,tunn} n_1^{R,QW} N_S f_n \right). \quad (34)$$

Since $f_{n,p} \leqslant 1$, the last three terms in the brackets in (34) remain restricted with increasing j. Under the condition of charge neutrality in QDs, they are constant and, as is clear from (33) and (34), their sum presents the upper limit for the threshold current density:

$$j_{th}^{highest} = eN_S \frac{f_n f_p}{\tau_{QD}} + ew^L_{p,tunn} p_1^{L,QW} N_S f_p + ew^R_{n,tunn} n_1^{R,QW} N_S f_n. \quad (35)$$

With (35), equation (34) is

$$P^{lowest} = \frac{\hbar\omega}{e} S(j - j_{th}^{highest}). \quad (36)$$

The upper limit for the output power is obtained in an ideal structure discussed above and is given by (24), which we rewrite as follows:

$$P^{highest} = \frac{\hbar\omega}{e} S(j - j_{th}^{lowest}), \quad (37)$$

where

$$j_{th}^{lowest} = eN_S \frac{f_n f_p}{\tau_{QD}} \quad (38)$$

is the lower limit for the threshold current density.

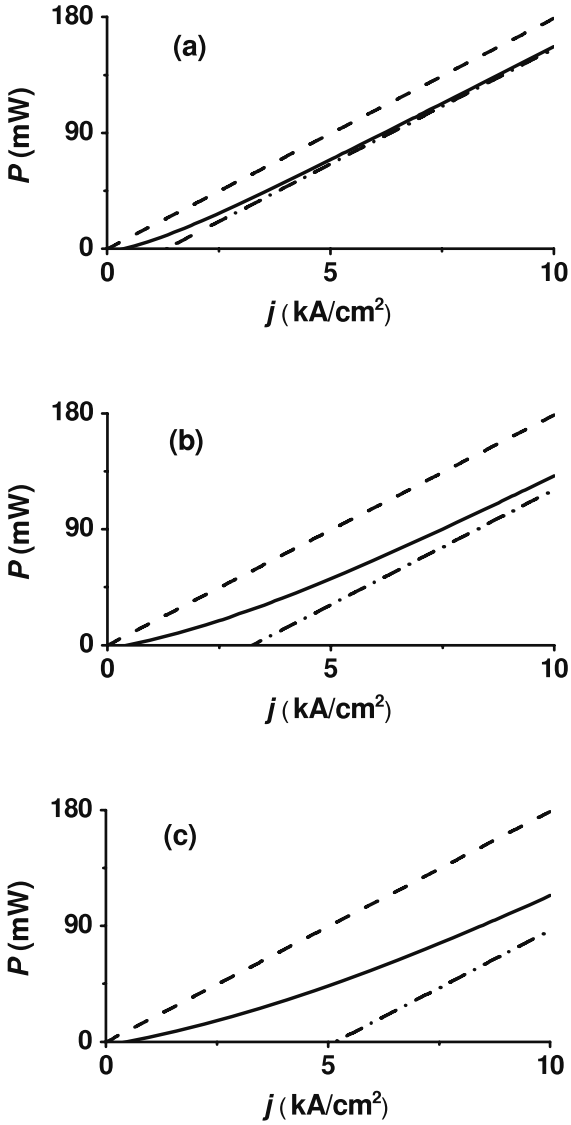

Figure 4. Light–current characteristic of a double tunneling-injection QD laser (solid curve) at different values of the out-tunneling coefficient $w^L_{p,tunn}$: (a) 0.04, (b) 0.1 and (c) 0.16 cm^2 s^{-1}. The threshold current density is $j_{th} = 389$, 457 and 479 A cm^{-2} in (a), (b) and (c), respectively. The dashed line is the LCC of an ideal structure given by (37); $j_{th}^{lowest} = 6.21$ A cm^{-2} (see (38)). The dash–dotted line is the asymptote given by (36); $j_{th}^{highest}$ (see (35)) is 1323, 3242 and 5161 A cm^{-2} in (a)–(c), respectively.

As seen from (36), the lower limit for the LCC is linear (dash–dotted line in figure 4) and its slope efficiency is unity. It is parallel to the upper limit (given by (37) and shown by the dashed line in figure 4) and shifted from the latter by the amount of the out-tunneling current density, $j_{out-tunn}$.

Hence, the actual LCC (obtained from the solution of the rate equations and shown by the solid curve in figure 4) is confined between the two parallel lines given by (36) and (37) (dash–dotted and dashed lines in figure 4). As seen from the figure and the analysis below, the lower limit (36) presents the asymptote of the actual LCC at high injection currents.

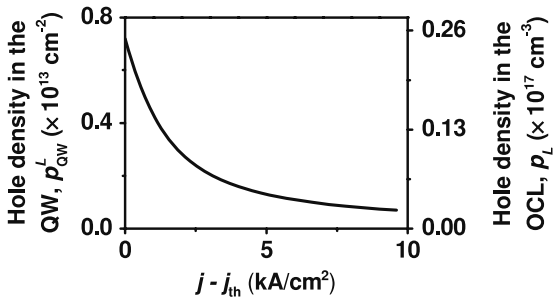

Figure 5. Minority carrier density on the left-hand side QW (left axis) and OCL (right axis) against excess injection current density. In view of a linear-proportionality relationship (D.3), the same curve depicts p_{QW}^L and p_L.

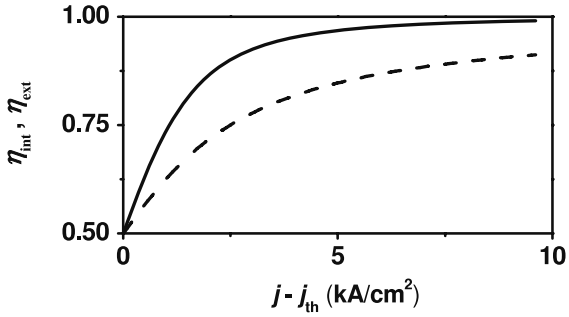

Figure 6. Internal quantum efficiency (dashed curve) and slope efficiency (solid curve) against excess injection current density.

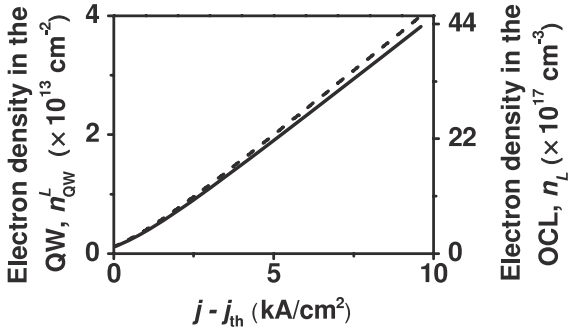

Figure 7. Majority carrier density on the left-hand side QW (solid curve, left axis) and OCL (dashed curve, right axis) against excess injection current density.

From (33), we have for the slope efficiency (external differential efficiency)

$$\eta_{ext} = \frac{1}{\frac{\hbar\omega}{e} S} \frac{\partial P}{\partial j} = 1 + e w_{p,tunn}^{L} N_S (1 - f_p) \frac{\partial p_{QW}^{L}}{\partial j} + e w_{n,tunn}^{R} N_S (1 - f_n) \frac{\partial n_{QW}^{R}}{\partial j}. \quad (39)$$

Since η_{ext} should not be higher than unity, the derivatives of p_{QW}^L and n_{QW}^R with respect to j should be negative—the minority carrier density in each of the two QWs decreases with j (figure 5). Hence, the last two terms in the brackets in equation (33) decrease with increasing j and the LCC asymptotically approaches the straight line given by (36) (figure 4).

The output power can be written as

$$P(j) = \frac{\hbar\omega}{e} S j_{stim}(j) = \frac{\hbar\omega}{e} S (j - j_{th}) \eta_{int}(j), \quad (40)$$

where

$$j_{stim} = \frac{e}{S} \frac{N}{\tau_{ph}} \quad (41)$$

is the stimulated recombination current density and

$$\eta_{int} = \frac{j_{stim}}{j - j_{th}} \quad (42)$$

is the internal differential quantum efficiency. Since the parasitic recombination current density remains restricted (see (31) and figure 3), η_{int}, which presents the fraction of the excess injection current density j–j_{th} that goes into the stimulated emission, should increase with j (dashed curve in figure 6). As a result, the LCC should become increasingly linear (figure 4).

With (40), the slope efficiency η_{ext} is expressed in terms of η_{int}:

$$\eta_{ext} = \eta_{int} + (j - j_{th}) \frac{\partial \eta_{int}}{\partial j}. \quad (43)$$

Since η_{int} increases with j, η_{ext} (solid curve in figure 6) also increases and is higher than η_{int} as is clear from (43). We did not consider the internal optical loss α_{int}; the inclusion of α_{int} will reduce the optical efficiency of the cavity, $\beta/(\beta + \alpha_{int})$, and hence η_{ext}.

The density of minority carriers on the left-hand side QW and OCL is shown in figure 5. As discussed above, the minority carrier density in the QW (holes on the left-hand side) decreases with j. The minority carrier density in the OCL is directly related to that in the QW (see equation (D.3) in appendix D), and hence also decreases.

The density of majority carriers on the left-hand side QW and OCL is shown in figure 7. Since majority carriers (electrons on the left-hand side) are supplied by injection, their density in the OCL and QW increases with pump current.

Auger recombination of electrons with holes in the OCL and QWs can be easily included in our model. In that case, the total parasitic recombination flux (the sum of the fluxes of bimolecular radiative recombination and trimolecular nonradiative Auger recombination) will enter into the left-hand side in (29) and will be equal to the net out-tunneling flux of minority carriers from QDs. Hence, the total parasitic recombination flux will remain limited with increasing j and all our conclusions about the LCC of a DTI QD laser will hold in the presence of Auger recombination. In particular, the lower limit for the LCC and the upper limit for the threshold current density will be given by equations (34) and (35), respectively.

In figure 1, we assumed that the QWs and QDs are of the same material, which does not need to be the case in general. Since the out-tunneling leakage of carriers from QDs to the foreign QWs is limited and hence so is the minority carrier

supply to the QWs, attaining the population inversion between the electron and hole states in the QWs, which could otherwise lead to lasing from the QWs, is effectively hampered in a DTI QD structure. Nevertheless, since the maximum gain of a QD ensemble is decreased due to inhomogeneous line broadening caused by the QD size distribution [33], the QDs should be made uniform enough to avoid a situation when the lasing action will be driven by the QW rather than QD transitions. In an STI QD laser of [38], a lasing action simultaneously driven by the QD and QW transitions was observed.

When discussing a DTI QD laser versus a conventional QD laser, we focused on the parasitic recombination outside QDs as a factor limiting the linearity of the LCC. Other factors, such as the gain saturation [39, 40] and heating [40, 41], which are known to limit the optical power in diode lasers, were not considered here. The expected better linearity of the LCC of a DTI QD laser was shown to be due to the fact that the parasitic recombination outside QDs is restricted in such a laser. Like in other diode lasers, both the gain saturation and heating would adversely affect the output power of a DTI QD laser. Quantitative analysis of these effects in a DTI QD laser is required to reveal their relative importance. All other factors being the same, elimination of even one source of sublinearity of the LCC (namely, parasitic recombination outside QDs) makes DTI QD lasers attractive for high-power operation.

3.2.1. Laser characteristics versus tunneling coefficients. As discussed above, due to the fact that QDs are 0D regions with a limited population ($f_{n,p} \leqslant 1$), the out-tunneling fluxes of minority carriers from QDs into the foreign QWs ($w^{L}_{p,tunn} p_1^{L,QW} N_S f_p$ and $w^{R}_{n,tunn} n_1^{R,QW} N_S f_n$) are also limited (see (31)). Although the level occupancies $f_{n,p}$ depend on the cavity length and other parameters of the structure, they can only change from 1/2 to 1 in the case of neutral QDs (see (25)). The surface density of QDs can also be varied within a limited range (typically, from several 10^{10} to 10^{11} cm^{-2}). In contrast to $f_{n,p}$ and N_S, the tunneling coefficients $w^{L}_{p,tunn}$ and $w^{R}_{n,tunn}$ depend strongly on the barrier thicknesses and can be easily varied within a wide range. Hence, for a given choice of materials for QDs, barriers and QWs, the out-tunneling fluxes of minority carriers are mainly controlled by $w^{L}_{p,tunn}$ and $w^{R}_{n,tunn}$.

As shown in appendix C, up to high injection current densities, the recombination in the OCL is negligible. What this means is that the out-tunneling fluxes of minority carriers from QDs are mainly consumed by the recombination in the QWs. Figure 8 shows n^{L}_{QW} and p^{L}_{QW} and the recombination current density in the QW, $j^{L}_{QW} = eB_{2D} n^{L}_{QW} p^{L}_{QW}$, versus the tunneling coefficient $w^{L}_{p,tunn}$. The hole density on the left-hand side QW, which is entirely due to out-tunneling, increases considerably with $w^{L}_{p,tunn}$ (figure 8(b)). The recombination in the QW should become more intense with increasing $w^{L}_{p,tunn}$. For this reason, the electron density decreases with increasing $w^{L}_{p,tunn}$ (figure 8(a)); the decrease is, however, negligible since electrons are majority carriers on the left-hand side QW. Both n^{L}_{QW} and p^{L}_{QW} saturate as $w^{L}_{p,tunn} \to \infty$. The barriers separating the QD layer from the QWs should block out-tunneling of

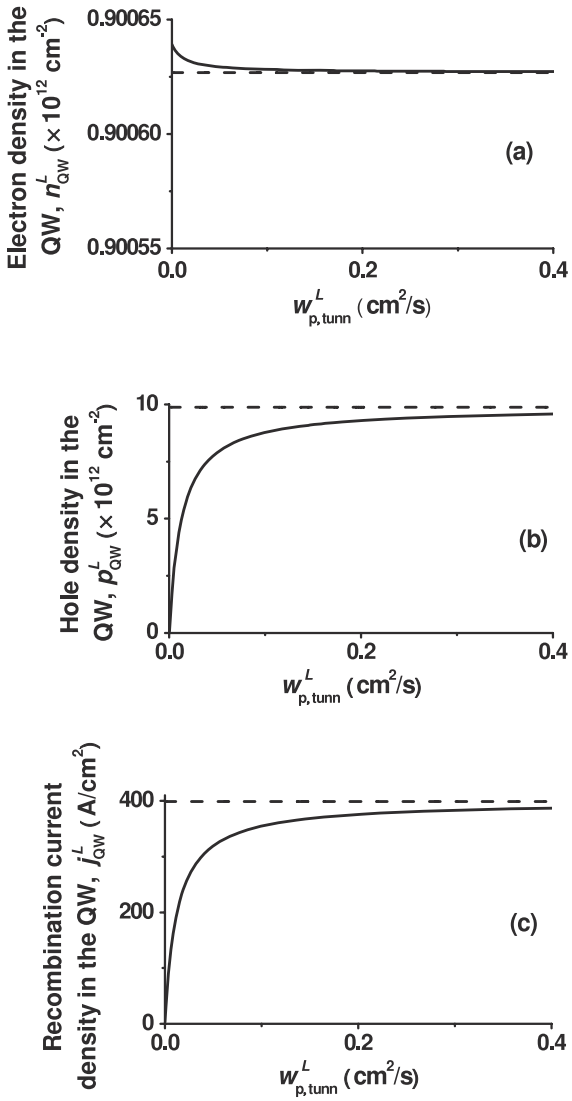

Figure 8. 2D density of electrons (a) and holes (b) and recombination current density (c) on the left-hand side QW against out-tunneling coefficient at an infinitely large in-tunneling coefficient ($w^{L}_{n,tunn} \to \infty$). The injection current density is $j = 10$ kA cm^{-2}. The horizontal dashed lines in (a) and (b) show the saturation values of n^{L}_{QW} and p^{L}_{QW} given by (44) and (45), respectively. The horizontal dashed line in (c) shows the saturation value of $j^{L}_{QW} = eB_{2D} n^{L}_{QW} p^{L}_{QW}$.

minority carriers from QDs, and yet allow for in-tunneling of majority carriers into QDs. It is therefore clear that, in the limiting case of infinitely large tunneling coefficients $w^{L}_{p,tunn}$ and $w^{R}_{n,tunn}$ for minority carriers, the tunneling coefficients $w^{L}_{n,tunn}$ and $w^{R}_{p,tunn}$ for majority carriers will also be infinitely large. The expressions for the saturation values of n^{L}_{QW} and p^{L}_{QW} (obtained from (D.7) and (D.8)) are as follows:

$$n^{L}_{QW}|_{w^{L}_{n,p,tunn}\to\infty} = n_1^{L,QW} \frac{f_n}{1 - f_n}, \tag{44}$$

$$p^{L}_{QW}|_{w^{L}_{n,p,tunn}\to\infty} = p_1^{L,QW} \frac{f_p}{1 - f_p}. \tag{45}$$

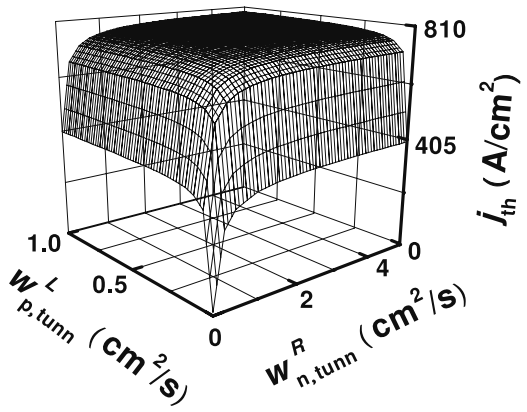

Figure 9. Threshold current density against out-tunneling coefficients at infinitely large in-tunneling coefficients ($w^{L}_{n,tunn}$, $w^{R}_{p,tunn} \to \infty$). The j_{th} value at $w^{L}_{p,tunn}$, $w^{R}_{n,tunn} = 0$ (the ideal case) is given by (38) and is 6.21 A cm^{-2}. The saturation value of j_{th} is given by (48).

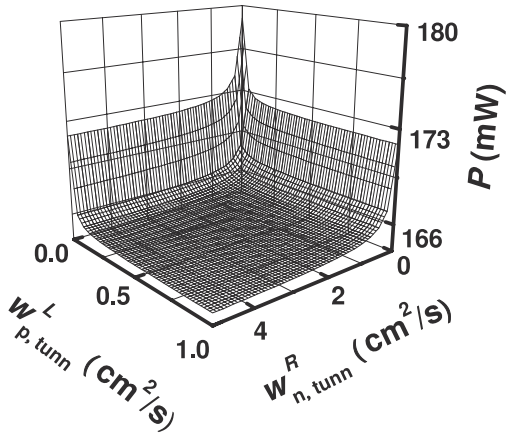

Figure 10. Optical power against out-tunneling coefficients at infinitely large in-tunneling coefficients ($w^{L}_{n,tunn}$, $w^{R}_{p,tunn} \to \infty$). The injection current density is $j = 10$ kA cm^{-2}. The P value at $w^{L}_{p,tunn}$, $w^{R}_{n,tunn} = 0$ (the ideal case) is given by (37) and is 179 mW. The saturation value of P is given by (49).

The horizontal dashed lines in figures 8(a) and (b) show these saturation values.

Due to the saturation of n^{L}_{QW} and p^{L}_{QW}, the recombination current density in the QW, $j^{L}_{QW} = eB_{2D}n^{L}_{QW}p^{L}_{QW}$, also saturates with increasing $w^{L}_{p,tunn}$ (figure 8(c)).

With the equilibrium level occupancies in a QD

$$f_{n,p} = \frac{1}{\exp\left(\frac{\varepsilon^{QD}_{n,p} - \mu_{n,p}}{T}\right) + 1}, \tag{46}$$

where $\varepsilon^{QD}_{n,p}$ are the energy levels of an electron and a hole in a QD and $\mu_{n,p}$ are the quasi-Fermi levels of electrons and holes, we would obtain from (44) and (45) the equilibrium densities in the QW:

$$\begin{aligned} n^{L}_{QW} &= N^{2D}_{c}\exp\left(-\frac{\varepsilon^{QW}_{n} - \mu_{n}}{T}\right), \\ p^{L}_{QW} &= N^{2D}_{v}\exp\left(-\frac{\varepsilon^{QW}_{p} - \mu_{p}}{T}\right), \end{aligned} \tag{47}$$

where $\varepsilon^{QW}_{n,p}$ are the energies of the electron- and hole-subband edges in the QW (the quantities for electrons, ε^{QD}_{n}, ε^{QW}_{n} and μ_{n}, are shown in figure 2). Hence, expressions (44) and (45) present the quasi-equilibrium relation between the carrier densities in the QW and level occupancies in a QD; this is easily understood—the limiting case of $w^{L,R}_{n,p,tunn} \to \infty$ describes an instant carrier exchange between the QWs and QDs.

Equation (45) can also be readily obtained from (D.9) by neglecting at large $w^{L}_{p,tunn}$ the recombination flux in the QW, $B_{2D}n^{L}_{QW}p^{L}_{QW}$, compared to the fluxes of out-tunneling from QDs, $w^{L}_{p,tunn}p^{L,QW}_{1}N_{S}f_{p}$, and backward tunneling into QDs, $w^{L}_{p,tunn}N_{S}(1-f_{p})p^{L}_{QW}$. The balance between the two tunneling fluxes yields the quasi-equilibrium relation (45).

Since the recombination current density outside QDs (the sum of the last four terms in the brackets in (23)) increases and saturates with increasing $w^{L}_{p,tunn}$ and $w^{R}_{n,tunn}$, so does the threshold current density (figure 9). As a result, the output power (at a given injection current) decreases and also saturates (figure 10). The expression for the saturation value of j_{th} can be obtained by assuming that, in addition to instant exchange between the QWs and QDs, the carrier exchange between the OCL and QWs is also instantaneous ($v^{L,R}_{n,p,capt} \to \infty$ or, equivalently, $\tau^{L,R}_{n,p,esc} \to 0$). In such a case, quasi-equilibrium distributions will establish for electrons and holes throughout the structure and the threshold current density will be given by

$$\begin{aligned} j_{th}|_{w^{L,R}_{n,p,tunn},\,v^{L,R}_{n,p,capt}\to\infty} &= eN_{S}\frac{f_{n}f_{p}}{\tau_{QD}} \\ &+ eB_{2D}\left(n^{L,QW}_{1}\frac{f_{n}}{1-f_{n}}\right)\left(p^{L,QW}_{1}\frac{f_{p}}{1-f_{p}}\right) \\ &+ eB_{2D}\left(n^{R,QW}_{1}\frac{f_{n}}{1-f_{n}}\right)\left(p^{R,QW}_{1}\frac{f_{p}}{1-f_{p}}\right) \\ &+ eb_{1}B\left(n^{L}_{1}\frac{f_{n}}{1-f_{n}}\right)\left(p^{L}_{1}\frac{f_{p}}{1-f_{p}}\right) \\ &+ eb_{2}B\left(n^{R}_{1}\frac{f_{n}}{1-f_{n}}\right)\left(p^{R}_{1}\frac{f_{p}}{1-f_{p}}\right), \end{aligned} \tag{48}$$

where the terms in the brackets are the equilibrium carrier densities in the corresponding parts of the structure. In figure 9, $j_{th}|_{w^{L,R}_{n,p,tunn},\,v^{L,R}_{n,p,capt}\to\infty} = 806$ A cm^{-2}.

The equilibrium carrier densities will not change with increasing injection current above the lasing threshold. Hence, the spontaneous recombination fluxes will be pinned and the excess of the injection current over the threshold current will entirely go into the stimulated recombination—the internal quantum efficiency will be unity. The output power will be given by

$$P|_{w^{L,R}_{n,p,tunn},\,v^{L,R}_{n,p,capt}\to\infty} = \frac{\hbar\omega}{e}S(j - j_{th}|_{w^{L,R}_{n,p,tunn},\,v^{L,R}_{n,p,capt}\to\infty}). \tag{49}$$

In figure 10, $P|_{w^{L,R}_{n,p,tunn},\,v^{L,R}_{n,p,capt}\to\infty} = 165$ mW at $j = 10$ kA cm^{-2}.

It should be emphasized that the carrier exchange between the QWs and QDs and between the OCL and QWs cannot be instantaneous in an actual structure—the conditions $w^{\mathrm{L,R}}_{\mathrm{n,p,tunn}} \to \infty$ and $v^{\mathrm{L,R}}_{\mathrm{n,p,capt}} \to \infty$ were just used to derive expressions (48) and (49) for the saturation values of j_{th} and P. For the same reason, the limiting case of $w^{\mathrm{L,R}}_{\mathrm{n,p,tunn}} \to \infty$ does not describe a structure without the barriers—as discussed in the Introduction and in [1, 2], the carrier capture from the reservoir (be it OCL or QW) into QDs cannot be instantaneous.

4. Conclusions

The theory of optical power of a double tunneling-injection (DTI) QD laser has been developed. We have shown that tunneling injection of electrons and holes into QDs from two separate QWs practically eliminates the adverse effect of the recombination outside QDs on the output power of such a laser. In an ideal device, out-tunneling of each type of carrier from QDs into the opposite-to-injection-side QW should be completely blocked; as a result, the parasitic recombination outside QDs will be suppressed and the LCC will be strictly linear. To scrutinize the potential of a DTI QD laser for high-power operation and the robustness of an actual device, we allowed for out-tunneling leakage of carriers from QDs. We have complemented our calculations by an analytical model and derived closed-form expressions for the LCC and carrier population in the OCL, QWs and QDs. We have shown that, even in the presence of out-tunneling leakage in an actual device, the intensity of parasitic recombination outside QDs remains restricted with increasing injection current. Consequently, the LCC becomes increasingly linear and the slope efficiency grows closer to unity at high injection currents—a remarkable feature distinguishing the DTI QD laser from other types of injection lasers. The linearity is due to the fact that the current paths connecting the opposite sides of the structure lie entirely within QDs—in view of the 3D confinement in QDs, the out-tunneling fluxes of carriers from dots are limited.

Acknowledgment

This work was supported by the US Army Research Office under grant no. W911-NF-08-1-0462.

Appendix A. Relationship between the carrier escape time from a QW to a bulk region and the capture velocity from a bulk region to a QW

For definiteness, we consider here electrons. The derivation and expressions for holes are similar. Under thermal equilibrium (no external voltage is applied to the structure and hence no current is injected), the flux $v_{\mathrm{n,capt}} n^{\mathrm{eq}}$ of electron capture from a bulk region (OCL) to a QW is equal to the flux $n^{\mathrm{eq}}_{\mathrm{QW}}/\tau_{\mathrm{n,esc}}$ of the reverse process, i.e. of thermal escape from a QW to a bulk region, to give

$$\frac{1}{\tau_{\mathrm{n,esc}}} = \frac{n^{\mathrm{eq}}}{n^{\mathrm{eq}}_{\mathrm{QW}}} v_{\mathrm{n,capt}}. \tag{A.1}$$

The equilibrium carrier density in a bulk region is

$$n^{\mathrm{eq}} = N_{\mathrm{c}}^{\mathrm{3D}} F_{1/2}\left(\frac{\mu^{\mathrm{eq}} - \Delta E_{\mathrm{c}}}{T}\right), \tag{A.2}$$

where $N_{\mathrm{c}}^{\mathrm{3D}}$ is the 3D effective density of states in the conduction band (see the expression for $N_{\mathrm{c}}^{\mathrm{3D}}$ in the text after (13)), $F_{1/2}$ is the Fermi–Dirac integral of order one-half, μ^{eq} is the equilibrium Fermi level (measured from the conduction band edge in a QW) and ΔE_{c} is the conduction band offset between the OCL and a QW (figure 2).

The closed-form expression for the 2D equilibrium carrier density in a QW is (see, e.g., [42])

$$n^{\mathrm{eq}}_{\mathrm{QW}} = N_{\mathrm{c}}^{\mathrm{2D}} \ln\left[1 + \exp\left(\frac{\mu^{\mathrm{eq}} - \varepsilon_{\mathrm{n}}^{\mathrm{QW}}}{T}\right)\right], \tag{A.3}$$

where $N_{\mathrm{c}}^{\mathrm{2D}}$ is the 2D effective density of states in a QW (see the expression for $N_{\mathrm{c}}^{\mathrm{2D}}$ in the text after (12)) and $\varepsilon_{\mathrm{n}}^{\mathrm{QW}}$ is the energy of the lowest subband edge in a QW (figure 2).

With (A.2) and (A.3), (A.1) becomes

$$\frac{1}{\tau_{\mathrm{n,esc}}} = \frac{N_{\mathrm{c}}^{\mathrm{3D}}}{N_{\mathrm{c}}^{\mathrm{2D}}} \frac{F_{1/2}\left(\frac{\mu^{\mathrm{eq}} - \Delta E_{\mathrm{c}}}{T}\right)}{\ln\left[1 + \exp\left(\frac{\mu^{\mathrm{eq}} - \varepsilon_{\mathrm{n}}^{\mathrm{QW}}}{T}\right)\right]} v_{\mathrm{n,capt}}. \tag{A.4}$$

Neglecting the difference between the effective masses in a bulk region and a QW, the ratio of the 3D to 2D effective density of states can be written as

$$\frac{N_{\mathrm{c}}^{\mathrm{3D}}}{N_{\mathrm{c}}^{\mathrm{2D}}} = \frac{\sqrt{\pi}}{\lambda_{\mathrm{dB},T}}, \tag{A.5}$$

where

$$\lambda_{\mathrm{dB},T} = \frac{2\pi\hbar}{\sqrt{2m_{\mathrm{c}}T}} \tag{A.6}$$

is the thermal de Broglie wavelength, i.e. the de Broglie wavelength of an electron having an energy equal to the thermal energy T (alternatively, in an infinitely deep square QW of thickness $\lambda_{\mathrm{dB},T}/2$, the energy of the lowest quantized level is T).

We can now write (A.4) as

$$\frac{1}{\tau_{\mathrm{n,esc}}} = \frac{F_{1/2}\left(\frac{\mu^{\mathrm{eq}} - \Delta E_{\mathrm{c}}}{T}\right)}{\ln\left[1 + \exp\left(\frac{\mu^{\mathrm{eq}} - \varepsilon_{\mathrm{n}}^{\mathrm{QW}}}{T}\right)\right]} \sqrt{\pi} \frac{v_{\mathrm{n,capt}}}{\lambda_{\mathrm{dB},T}}. \tag{A.7}$$

Equation (A.4) (or (A.7)) presents the general relationship between the escape time and capture velocity. If both bulk and QW materials are nondegenerate (the Fermi level μ^{eq} is below $\varepsilon_{\mathrm{n}}^{\mathrm{QW}}$ by several T), which is the case of undoped OCL and QW considered here, then

$$F_{1/2}\left(\frac{\mu^{\mathrm{eq}} - \Delta E_{\mathrm{c}}}{T}\right) \approx \exp\left(-\frac{\Delta E_{\mathrm{c}} - \mu^{\mathrm{eq}}}{T}\right), \tag{A.8}$$

$$\ln\left[1 + \exp\left(\frac{\mu^{\mathrm{eq}} - \varepsilon_{\mathrm{n}}^{\mathrm{QW}}}{T}\right)\right] \approx \exp\left(-\frac{\varepsilon_{\mathrm{n}}^{\mathrm{QW}} - \mu^{\mathrm{eq}}}{T}\right). \tag{A.9}$$

With (A.8) and (A.9), equation (12) is obtained from (A.4), which can also be written in the form of equation (1.3) of [34].

Appendix B. Quantities n_1^{QW} and p_1^{QW} in the tunneling fluxes of electrons and holes from QDs to a QW

As in appendix A, we use the detailed balance condition under thermal equilibrium—here, for the fluxes of carrier tunneling from a QW to QDs, $w_{n,tunn}N_S(1-f_n^{eq})n_{QW}^{eq}$, and from QDs to a QW, $w_{n,tunn}n_1^{QW}N_S f_n^{eq}$. Thus we obtain

$$n_{QW}^{eq} = n_1^{QW}\frac{f_n^{eq}}{1-f_n^{eq}}, \tag{B.1}$$

where n_{QW}^{eq} is given by (A.3) and

$$f_n^{eq} = \frac{1}{\exp\left(\frac{\varepsilon_n^{QD}-\mu^{eq}}{T}\right)+1} \tag{B.2}$$

is the equilibrium occupancy of the energy level ε_n^{QD} in a QD (figure 2).

With (A.3), (B.1) and (B.2), we have for n_1^{QW}

$$n_1^{QW} = N_c^{2D}\exp\left(\frac{\varepsilon_n^{QD}-\mu^{eq}}{T}\right)\ln\left[1+\exp\left(\frac{\mu^{eq}-\varepsilon_n^{QW}}{T}\right)\right]. \tag{B.3}$$

If a QW material is nondegenerate (which is the case of an undoped QW considered here), we have from (A.9) and (B.3)

$$n_1^{QW} = N_c^{2D}\exp\left(-\frac{\varepsilon_n^{QW}-\varepsilon_n^{QD}}{T}\right). \tag{B.4}$$

The quantity n_1^{QW} (measured in units of cm^{-2}) is a 2D analog of n_1 (measured in units of cm^{-3})—while n_1 characterizes the electron excitation from a QW to a bulk region (and thus $\Delta E_c - \varepsilon_n^{QW}$ and N_c^{3D} enter into (13)), n_1^{QW} characterizes excitation from a QD to a QW (which is why $\varepsilon_n^{QW}-\varepsilon_n^{QD}$ and N_c^{2D} enter into (B.4)).

If the energy level in a QD is in resonance with the subband edge in a QW ($\varepsilon_n^{QD}=\varepsilon_n^{QW}$), equation (14) is obtained from (B.4).

Appendix C. Criterion for neglecting the recombination in the OCL

We derive here the criterion for neglecting the recombination flux on the left-hand side of the OCL compared to the hole capture flux from the OCL to the QW (in view of (28), also compared to the hole escape flux from the QW to the OCL, $p_{QW}^L/\tau_{p,esc}^L$), i.e. the criterion for holding the inequality

$$b_1 B n_L p_L \ll v_{p,capt}^L p_L, \tag{C.1}$$

or, equivalently,

$$b_1 B n_L \ll v_{p,capt}^L. \tag{C.2}$$

From (5) at the steady state, we have

$$n_L = \frac{1}{v_{n,capt}^L}\left[\frac{n_{QW}^L}{\tau_{n,esc}^L} + w_{n,tunn}^L N_s(1-f_n)n_{QW}^L - w_{n,tunn}^L n_1^{L,QW}N_s f_n + B_{2D}n_{QW}^L p_{QW}^L\right]. \tag{C.3}$$

Table C.1. Highest injection current densities (second and third columns) satisfying the criteria for neglecting recombination in, respectively, the left- and right-hand sides of the OCL (see (C.8) for the left-hand side) at different values of the capture velocity from the OCL to the QWs.

$v_{n,p,capt}^{L,R}$ (cm s^{-1})	j (A cm^{-2})	
3×10^5	7.3×10^6	7.8×10^6
3×10^4	7.9×10^4	8.0×10^4
1×10^4	8.3×10^3	8.9×10^3

Since the left-hand side in (30) is positive, the right-hand side should also be positive to give

$$n_{QW}^L \leqslant \frac{1}{w_{n,tunn}^L N_S(1-f_n)}\left(\frac{j}{e} + w_{n,tunn}^L n_1^{L,QW}N_S f_n\right). \tag{C.4}$$

Substituting the expression on the right-hand side of (C.4) for n_{QW}^L in the first two terms on the right-hand side in (C.3), we obtain the following inequality:

$$n_L < \frac{1}{v_{n,capt}^L}\left\{\left[1+\frac{1}{\tau_{n,esc}^L}\frac{1}{w_{n,tunn}^L N_S(1-f_n)}\right]\frac{j}{e} + \frac{1}{\tau_{n,esc}^L}n_1^{L,QW}\frac{f_n}{1-f_n} + B_{2D}n_{QW}^L p_{QW}^L\right\}. \tag{C.5}$$

Substituting $w_{p,tunn}^L p_1^{L,QW}N_S f_p$ for $B_{2D}n_{QW}^L p_{QW}^L$ (see (31)) in (C.5), a stronger inequality is obtained:

$$n_L < \frac{1}{v_{n,capt}^L}\left\{\left[1+\frac{1}{\tau_{n,esc}^L}\frac{1}{w_{n,tunn}^L N_S(1-f_n)}\right]\frac{j}{e} + \frac{1}{\tau_{n,esc}^L}n_1^{L,QW}\frac{f_n}{1-f_n} + w_{p,tunn}^L p_1^{L,QW}N_S f_p\right\}, \tag{C.6}$$

or, by multiplying both sides of (C.6) by $b_1 B$:

$$b_1 B n_L < \frac{b_1 B}{v_{n,capt}^L}\left\{\left[1+\frac{1}{\tau_{n,esc}^L}\frac{1}{w_{n,tunn}^L N_S(1-f_n)}\right]\frac{j}{e} + \frac{1}{\tau_{n,esc}^L}n_1^{L,QW}\frac{f_n}{1-f_n} + w_{p,tunn}^L p_1^{L,QW}N_S f_p\right\}. \tag{C.7}$$

As seen from (C.7), a sufficient condition for holding (C.2) is the condition that the right-hand side of (C.7) is less than $v_{p,capt}^L$. Thus we arrive at the following criterion:

$$j \ll e\frac{\frac{v_{p,capt}^L v_{n,capt}^L}{b_1 B} - \frac{1}{\tau_{n,esc}^L}n_1^{L,QW}\frac{f_n}{1-f_n} - w_{p,tunn}^L p_1^{L,QW}N_S f_p}{1+\frac{1}{\tau_{n,esc}^L}\frac{1}{w_{n,tunn}^L N_S(1-f_n)}}. \tag{C.8}$$

The capture velocities to QWs are typically of the order of 10^5 cm s^{-1} [34, 43, 44]. The second column in table C.1 shows the highest injection current density j satisfying (C.8) at different values of $v_{n,p,capt}^L$. Even for a low capture velocity of 10^4 cm s^{-1}, (C.8) satisfies up to $j = 8.3$ kA cm^{-2}. Hence, criterion (C.8) for neglecting the parasitic recombination on the left-hand side of the OCL holds up to very high j; that is to say, that the out-tunneling flux of minority carriers from QDs is mainly consumed by the recombination in the QW—this flux practically does not reach the OCL.

The criterion for neglecting the recombination throughout the OCL is given by the strongest of inequality (C.8) and a

similar inequality for the right-hand side of the structure (the highest j satisfying the inequality for the right-hand side is shown in the third column in table C.1).

Appendix D. Closed-form solutions of the rate equations

As shown in appendix C, the recombination in the OCL can be neglected up to very high j. Thus equations (1) and (2) are simplified as follows at the steady state:

$$0 = \frac{j}{e} + \frac{n_{\mathrm{QW}}^{\mathrm{L}}}{\tau_{\mathrm{n,esc}}^{\mathrm{L}}} - v_{\mathrm{n,capt}}^{\mathrm{L}} n_{\mathrm{L}}, \tag{D.1}$$

$$0 = \frac{p_{\mathrm{QW}}^{\mathrm{L}}}{\tau_{\mathrm{p,esc}}^{\mathrm{L}}} - v_{\mathrm{p,capt}}^{\mathrm{L}} p_{\mathrm{L}}. \tag{D.2}$$

From (D.2), the minority carrier density in the OCL is expressed in terms of the minority carrier density in the QW:

$$p_{\mathrm{L}} = \frac{1}{v_{\mathrm{p,capt}}^{\mathrm{L}} \tau_{\mathrm{p,esc}}^{\mathrm{L}}} p_{\mathrm{QW}}^{\mathrm{L}}. \tag{D.3}$$

From (D.1), the majority carrier density in the OCL is expressed in terms of the majority carrier density in the QW:

$$n_{\mathrm{L}} = \frac{1}{v_{\mathrm{n,capt}}^{\mathrm{L}} \tau_{\mathrm{n,esc}}^{\mathrm{L}}} n_{\mathrm{QW}}^{\mathrm{L}} + \frac{j}{e v_{\mathrm{n,capt}}^{\mathrm{L}}}. \tag{D.4}$$

Substituting $v_{\mathrm{n,capt}}^{\mathrm{L}} n_{\mathrm{L}} - n_{\mathrm{QW}}^{\mathrm{L}}/\tau_{\mathrm{n,esc}}^{\mathrm{L}} = j/e$ (see (D.1)) in equation (5) at the steady state, we obtain the following equation relating the 2D electron and hole densities in the QW:

$$n_{\mathrm{QW}}^{\mathrm{L}} = \frac{1}{1 + \frac{B_{\mathrm{2D}} p_{\mathrm{QW}}^{\mathrm{L}}}{w_{\mathrm{n,tunn}}^{\mathrm{L}} N_{\mathrm{S}}(1-f_{\mathrm{n}})}} \times \left[n_1^{\mathrm{L,QW}} \frac{f_{\mathrm{n}}}{1-f_{\mathrm{n}}} + \frac{j}{e w_{\mathrm{n,tunn}}^{\mathrm{L}} N_{\mathrm{S}}(1-f_{\mathrm{n}})} \right]. \tag{D.5}$$

By using (D.2) in equation (6) at the steady state, we obtain the second (in addition to (D.5)) equation relating $n_{\mathrm{QW}}^{\mathrm{L}}$ and $p_{\mathrm{QW}}^{\mathrm{L}}$:

$$p_{\mathrm{QW}}^{\mathrm{L}} = \frac{1}{1 + \frac{B_{\mathrm{2D}} n_{\mathrm{QW}}^{\mathrm{L}}}{w_{\mathrm{p,tunn}}^{\mathrm{L}} N_{\mathrm{S}}(1-f_{\mathrm{p}})}} p_1^{\mathrm{L,QW}} \frac{f_{\mathrm{p}}}{1-f_{\mathrm{p}}}. \tag{D.6}$$

From (D.5) and (D.6), a quadratic equation in $n_{\mathrm{QW}}^{\mathrm{L}}$ (or $p_{\mathrm{QW}}^{\mathrm{L}}$) is obtained, solution of which gives $n_{\mathrm{QW}}^{\mathrm{L}}$ and then $p_{\mathrm{QW}}^{\mathrm{L}}$ as functions of the injection current density j:

$$n_{\mathrm{QW}}^{\mathrm{L}}(j) = \frac{1}{2}\Bigg[\Bigg\{\Bigg[n_1^{\mathrm{L,QW}} \frac{f_{\mathrm{n}}}{1-f_{\mathrm{n}}} + \frac{j}{e w_{\mathrm{n,tunn}}^{\mathrm{L}} N_{\mathrm{S}}(1-f_{\mathrm{n}})} - \frac{w_{\mathrm{p,tunn}}^{\mathrm{L}}}{w_{\mathrm{n,tunn}}^{\mathrm{L}}} p_1^{\mathrm{L,QW}} \frac{f_{\mathrm{p}}}{1-f_{\mathrm{n}}} - \frac{1}{B_{\mathrm{2D}}} w_{\mathrm{p,tunn}}^{\mathrm{L}} N_{\mathrm{S}}(1-f_{\mathrm{p}})\Bigg]^2 + 4\frac{1}{B_{\mathrm{2D}}} w_{\mathrm{p,tunn}}^{\mathrm{L}} N_{\mathrm{S}}(1-f_{\mathrm{p}})\Bigg[n_1^{\mathrm{L,QW}} \frac{f_{\mathrm{n}}}{1-f_{\mathrm{n}}} + \frac{j}{e w_{\mathrm{n,tunn}}^{\mathrm{L}} N_{\mathrm{S}}(1-f_{\mathrm{n}})}\Bigg]\Bigg\}^{\frac{1}{2}} + n_1^{\mathrm{L,QW}} \frac{f_{\mathrm{n}}}{1-f_{\mathrm{n}}} + \frac{j}{e w_{\mathrm{n,tunn}}^{\mathrm{L}} N_{\mathrm{S}}(1-f_{\mathrm{n}})} - \frac{w_{\mathrm{p,tunn}}^{\mathrm{L}}}{w_{\mathrm{n,tunn}}^{\mathrm{L}}} p_1^{\mathrm{L,QW}} \frac{f_{\mathrm{p}}}{1-f_{\mathrm{n}}} - \frac{1}{B_{\mathrm{2D}}} w_{\mathrm{p,tunn}}^{\mathrm{L}} N_{\mathrm{S}}(1-f_{\mathrm{p}})\Bigg], \tag{D.7}$$

$$p_{\mathrm{QW}}^{\mathrm{L}}(j) = \frac{1}{2}\Bigg[\Bigg\{\Bigg[p_1^{\mathrm{L,QW}} \frac{f_{\mathrm{p}}}{1-f_{\mathrm{p}}} - \frac{j}{e w_{\mathrm{p,tunn}}^{\mathrm{L}} N_{\mathrm{S}}(1-f_p)} - \frac{w_{\mathrm{n,tunn}}^{\mathrm{L}}}{w_{\mathrm{p,tunn}}^{\mathrm{L}}} n_1^{\mathrm{L,QW}} \frac{f_{\mathrm{n}}}{1-f_{\mathrm{p}}} - \frac{1}{B_{\mathrm{2D}}} w_{\mathrm{n,tunn}}^{\mathrm{L}} N_{\mathrm{S}}(1-f_{\mathrm{n}})\Bigg]^2 + 4\frac{1}{B_{\mathrm{2D}}} w_{\mathrm{n,tunn}}^{\mathrm{L}} N_{\mathrm{S}}(1-f_{\mathrm{n}}) p_1^{\mathrm{L,QW}} \frac{f_{\mathrm{p}}}{1-f_{\mathrm{p}}}\Bigg\}^{\frac{1}{2}} + p_1^{\mathrm{L,QW}} \frac{f_{\mathrm{p}}}{1-f_{\mathrm{p}}} - \frac{j}{e w_{\mathrm{p,tunn}}^{\mathrm{L}} N_{\mathrm{S}}(1-f_{\mathrm{p}})} - \frac{w_{\mathrm{n,tunn}}^{\mathrm{L}}}{w_{\mathrm{p,tunn}}^{\mathrm{L}}} n_1^{\mathrm{L,QW}} \frac{f_{\mathrm{n}}}{1-f_{\mathrm{p}}} - \frac{1}{B_{\mathrm{2D}}} w_{\mathrm{n,tunn}}^{\mathrm{L}} N_{\mathrm{S}}(1-f_{\mathrm{n}})\Bigg]. \tag{D.8}$$

By using (D.3), (D.4), (D.7), (D.8) and similar expressions for the carrier densities on the right-hand side of the structure, a closed-form expression for the LCC is obtained from (23).

By analyzing equation (39) in the general case, we already showed that the minority carrier density in the QW decreases with increasing j (figure 5). This result can also be easily obtained from (29). Neglecting the recombination flux in the OCL in (29), we get

$$w_{\mathrm{p,tunn}}^{\mathrm{L}} N_{\mathrm{S}}(1-f_{\mathrm{p}}) p_{\mathrm{QW}}^{\mathrm{L}} + B_{\mathrm{2D}} n_{\mathrm{QW}}^{\mathrm{L}} p_{\mathrm{QW}}^{\mathrm{L}} = w_{\mathrm{p,tunn}}^{\mathrm{L}} p_1^{\mathrm{L,QW}} N_{\mathrm{S}} f_{\mathrm{p}}. \tag{D.9}$$

The right-hand side of (D.9) remains limited (constant if charge neutrality holds in QDs) with j. Since the majority carrier density ($n_{\mathrm{QW}}^{\mathrm{L}}$) should increase with j (figure 7), keeping limited the left-hand side of (D.9) requires decreasing $p_{\mathrm{QW}}^{\mathrm{L}}$. The decrease of $p_{\mathrm{QW}}^{\mathrm{L}}$ with j can also be seen from the analytical expression (D.8).

References

[1] Asryan L V, Luryi S and Suris R A 2002 Intrinsic nonlinearity of light-current characteristic of semiconductor lasers with a quantum-confined active region *Appl. Phys. Lett.* **81** 2154–6

[2] Asryan L V, Luryi S and Suris R A 2003 Internal efficiency of semiconductor lasers with a quantum-confined active region *IEEE J. Quantum Electron.* **39** 404–18

[3] Kamath K, Klotzkin D and Bhattacharya P 1997 Small-signal modulation characteristics of self-organized quantum dot separate confinement heterostructure and tunneling injection lasers *Proc. IEEE LEOS 10th Annual Mtg.* vol 2, pp 498–9

[4] Bhattacharya P, Zhang X K, Yuan Y S, Kamath K, Klotzkin D, Caneau C and Bhat R 1998 High-speed tunnel injection quantum well and quantum dot lasers *Proc. SPIE* **3283** 702–9

[5] Bhattacharya P and Ghosh S 2002 Tunnel injection $In_{0.4}Ga_{0.6}As$/GaAs quantum dot lasers with 15 GHz modulation bandwidth at room temperature *Appl. Phys. Lett.* **80** 3482–4

[6] Sun H C, Davis L, Sethi S, Singh J and Bhattacharya P 1993 Properties of a tunneling injection quantum-well laser: recipe for a 'cold' device with a large modulation bandwidth *IEEE Photon. Technol. Lett.* **5** 870–2

[7] Qiu Y, Uhl D, Chacon R and Yang R Q 2003 Lasing characteristics of InAs quantum-dot lasers on (001) InP substrate *Appl. Phys. Lett.* **83** 1704–6

[8] Tokranov V, Yakimov M, van Eisden J and Oktyabrsky S 2006 Tunnel quantum well-on-dots InGaAs–InAs high-gain medium for laser diodes *Proc. SPIE* **6129** 612908

[9] George A A, Smowton P M, Mi Z and Bhattacharya P 2007 Long wavelength quantum-dot lasers selectively populated using tunnel injection *Semicond. Sci. Technol.* **22** 557–60

[10] Rudno-Rudzinski W, Sęk G, Ryczko K, Syperek M, Misiewicz J, Semenova E S, Lemaitre A and Ramdane A 2009 Room temperature free carrier tunneling in dilute nitride based quantum well—quantum dot tunnel injection system for 1.3 μm *Appl. Phys. Lett.* **94** 171906

[11] Pavelescu E-M, Gilfert C, Reithmaier J P, Martin-Minguez A and Esquivias I 2009 High-power tunnel-injection 1060-nm InGaAs-(Al)GaAs quantum-dot lasers *IEEE Photon. Technol. Lett.* **21** 999–1001

[12] Podemski P, Kudrawiec R, Misiewicz J, Somers A, Reithmaier J P and Forchel A 2006 On the tunnel injection of excitons and free carriers from $In_{0.53}Ga_{0.47}As/In_{0.53}Ga_{0.23}Al_{0.24}As$ quantum well to $InAs/In_{0.53}Ga_{0.23}Al_{0.24}As$ quantum dashes *Appl. Phys. Lett.* **89** 061902

[13] Sęk G, Poloczek P, Podemski P, Kudrawiec R, Misiewicz J, Somers A, Hein S, Höfling S and Forchel A 2007 Experimental evidence on quantum well–quantum dash energy transfer in tunnel injection structures for 1.55 μm emission *Appl. Phys. Lett.* **90** 081915

[14] Arakawa Y 1994 Fabrication of quantum wires and dots by MOCVD selective growth *Solid-State Electron.* **37** 523–8

[15] Asryan L V and Luryi S 2001 Tunneling-injection quantum-dot laser: ultrahigh temperature stability *IEEE J. Quantum Electron.* **37** 905–10

[16] Asryan L V and Luryi S 2003 Temperature-insensitive semiconductor quantum dot laser *Solid-State Electron.* **47** 205–12

[17] Asryan L V and Luryi S 2005 Semiconductor laser with reduced temperature sensitivity *US Patent* 6870178 B2

[18] Chung T, Walter G and Holonyak N 2001 Coupled strained-layer InGaAs quantum-well improvement of an InAs quantum dot AlGaAs–GaAs–InGaAs–InAs heterostructure laser *Appl. Phys. Lett.* **79** 4500–2

[19] Walter G, Chung T and Holonyak N 2002 High-gain coupled InGaAs quantum well InAs quantum dot AlGaAs–GaAs–InGaAs heterostructure diode laser operation *Appl. Phys. Lett.* **80** 1126–8

[20] Walter G, Chung T and Holonyak N 2002 Coupled-stripe quantum-well-assisted AlGaAs–GaAs–InGaAs–InAs quantum-dot laser *Appl. Phys. Lett.* **80** 3045–7

[21] Kondratko P K, Chuang S-L, Walter G, Chung T and Holonyak N 2003 Observations of near-zero linewidth enhancement factor in a quantum-well coupled quantum-dot laser *Appl. Phys. Lett.* **83** 4818–20

[22] Hanks R V and Unwin A M 1963 Tunnel-injection semiconductor laser *Proc. 7th IEEE National Convention on Military Electron.* pp 169–73

[23] Fischer A G and Moss H I 1963 Tunnel-injection electroluminescence *J. Appl. Phys.* **34** 2112–3

[24] Eastman P C, Haering R R and Barnes P A 1964 Injection electroluminescence in metal–semiconductor tunnel diodes *Solid-State Electron.* **7** 879–85

[25] Han D-S and Asryan L V 2008 Tunneling-injection of electrons and holes into quantum dots: a tool for high-power lasing *Appl. Phys. Lett.* **92** 251113

[26] Bhattacharya P, Ghosh S, Pradhan S, Singh J, Wu Z-K, Urayama J, Kim K and Norris T B 2003 Carrier dynamics and high-speed modulation properties of tunnel injection InGaAs–GaAs quantum-dot lasers *IEEE J. Quantum Electron.* **39** 952–62

[27] Chang S-W, Chuang S-L and Holonyak N 2004 Phonon- and Auger-assisted tunneling from a quantum well to a quantum dot *Phys. Rev.* B **70** 125312

[28] Chuang S L and Holonyak N 2002 Efficient quantum well to quantum dot tunneling: analytical solution *Appl. Phys. Lett.* **80** 1270–2

[29] Mi Z, Bhattacharya P and Fathpour S 2005 High-speed 1.3 μm tunnel injection quantum-dot lasers *Appl. Phys. Lett.* **86** 153109

[30] Bimberg D *et al* 2000 Quantum dot lasers: breakthrough in optoelectronics *Thin Solid Films* **367** 235–49

[31] Matthews D R, Summers H D, Smowton P M and Hopkinson M 2002 Experimental investigation of the effect of wetting-layer states on the gain-current characteristic of quantum-dot lasers *Appl. Phys. Lett.* **81** 4904–6

[32] Löffler A, Poloczek P, Sęk G, Misiewicz J, Reithmaier J P and Forchel A 2006 Optical characteristics of lowly strained GaInAs quantum dots *Phys. Status Solidi* c **3** 3815–8

[33] Asryan L V and Suris R A 1996 Inhomogeneous line broadening and the threshold current density of a semiconductor quantum dot laser *Semicond. Sci. Technol.* **11** 554–67

[34] Yassievich I N, Schmalz K and Beer M 1994 Capture and emission of carriers in semiconductor quantum wells *Semicond. Sci. Technol.* **9** 1763–74

[35] Tsai C-Y, Lo Y H, Spencer R M and Eastman L F 1995 Nonlinear gain coefficients in semiconductor quantum-well lasers: effects of carrier diffusion, capture, and escape *IEEE J. Sel. Top. Quantum Electron.* **1** 316–30

[36] Asryan L V and Suris R A 1997 Charge neutrality violation in quantum-dot lasers *IEEE J. Sel. Top. Quantum Electron.* **3** 148–57

[37] Asryan L V and Suris R A 1997 Characteristic temperature of quantum dot laser *Electron. Lett.* **33** 1871–2

[38] Kondratko P K, Chuang S-L, Walter G, Holonyak N, Heller R D, Zhang X and Dupuis R D 2005 Gain narrowing and output behavior of InP–InGaAlP tunneling injection quantum-dot-well laser *IEEE Photon. Technol. Lett.* **17** 938–40

[39] Agrawal G P and Dutta N K 1986 *Long-Wavelength Semiconductor Lasers* 2nd edn (New York: Van Nostrand-Reinhold)

[40] Zory P S Jr 1993 *Quantum Well Lasers* (New York: Academic)

[41] Karachinsky L Y *et al* 2006 Metamorphic 1.5 μm-range quantum dot lasers on a GaAs substrate *Semicond. Sci. Technol.* **21** 691–6

[42] Vahala K J and Zah C E 1988 Effect of doping on the optical gain and the spontaneous noise enhancement factor in quantum well amplifiers and lasers studied by simple analytical expressions *Appl. Phys. Lett.* **52** 1945–7

[43] Solov'ev S A, Yassievich I N and Chistyakov V M 1995 Capture of carriers in quantum-wells and thermal emission of carriers in III–V semiconductors *Semiconductors* **29** 654–60

[44] Dargys A and Kundrotas J 1998 Impact ionization of excitons by hot carriers in quantum wells *Semicond. Sci. Technol.* **13** 1258–61

Effect of the Wetting Layer on the Output Power of a Double Tunneling-Injection Quantum-Dot Laser

Dae-Seob Han and Levon V. Asryan, *Senior Member, IEEE*

***Abstract*—To suppress bipolar population and hence electron–hole recombination outside quantum dots (QDs), tunneling-injection of electrons and holes into QDs from two separate quantum wells was proposed earlier. Close-to-ideal operating characteristics were predicted for such a double tunneling-injection (DTI) laser. In the Stranski–Krastanow growth mode, a two-dimensional wetting layer (WL) is initially grown followed by the formation of QDs. Due to thermal escape of carriers from QDs, there will be bipolar population and hence electron–hole recombination in the WL, even in a DTI structure. In this work, the light–current characteristic (LCC) of a DTI QD laser is studied in the presence of the WL. Since the opposite sides of a DTI structure are only connected by the current paths through QDs and the WL is located in the n-side of the structure, the only source of holes for the WL is provided by QDs. It is shown that, due to the zero-dimensional nature of QDs, the rate of the hole supply to the WL remains limited with increasing injection current. For this reason, as in the other parts of the structure outside QDs (quantum wells and optical confinement layer), the parasitic electron–hole recombination remains restricted in the WL. As a result, even in the presence of the WL, the LCC of a DTI QD laser becomes increasingly linear at high injection currents, which is a further demonstration of the potential of such a laser for high-power operation.**

***Index Terms*—Quantum-dot laser, semiconductor laser.**

I. Introduction

SEMICONDUCTOR quantum dots (QDs) can be conveniently used as an active medium for stimulated emission in injection lasers [1]–[7]. Conventionally, QDs are grown by the strain-induced island formation method, which is called as the Stranski–Krastanow growth mode [8]. In the Stranski–Krastanow growth mode, several monolayers of one material are grown first on a crystal surface of another material (substrate) having a different lattice constant. Beyond a critical thickness of the deposited layer, three-dimensional (3-D) islands (QDs) start forming from two-dimensional (2-D) monolayers thus partially relaxing the strain and reducing the elastic energy. The initially grown monolayers are called as the wetting layer (WL). Hence, the 2-D WL is inherently present in self-assembled Stranski–Krastanow grown QD structures [9]–[12].

In the conventional design of QD lasers, the carriers are first injected from the cladding layers into the optical confinement layer (OCL), and then captured into the WL and QDs. A certain fraction of carriers thermally escapes back from QDs to the WL and OCL. Due to bipolar (both electron and hole) population in the OCL and WL, parasitic electron–hole recombination occurs there [13]–[15] in addition to recombination in QDs. The role of the WL in conventional QD lasers has been investigated both experimentally and theoretically (see, e.g., [15]–[19]).

To suppress the parasitic recombination outside QDs, tunneling-injection of both electrons and holes into QDs was proposed [20]–[22]. In such a double-tunneling injection (DTI) QD laser, the parasitic recombination rate remains restricted even if there is out-tunneling leakage of carriers from QDs [23]. As a result, the light–current characteristic (LCC) of a DTI QD laser is essentially linear. No WL was assumed in the structures of [20]–[22]. If the Stranski–Krastanow mode is used for the growth of QDs, the WL should be properly taken into account. As seen from Fig. 1, even if there is no tunneling between the electron-injecting quantum well (QW) and the WL, there will be bipolar population in the WL. This is because (i) there is such population in QDs (which is maintained to have stimulated emission) and (*ii*) the WL is coupled to QDs by the processes of thermal escape and capture. Besides, while QDs present the sole source for the hole supply to the WL, electrons can directly tunnel to the WL from the electron-injecting QW (Fig. 1). Hence, even in an ideal case of total suppression of parasitic recombination in the QWs and OCL, such recombination will occur in the WL.

In this work, we develop a theoretical model for the optical power of a DTI QD laser, which includes the WL and processes therein.

II. Theoretical Model

Fig. 1 shows the energy band diagram of a DTI QD laser with the WL, which follows the barrier separating the electron-injecting QW from QDs. As seen from the figure, the holes can only be supplied to the WL by thermal escapes from QDs. In contrast, in addition to thermal escapes from QDs, electrons can directly tunnel to the WL from the left-hand-side (electron-injecting) QW.

We assume that the material separating QDs in the QD layer (it may be the same as the material of barriers) has high enough bandgap to suppress all tunneling other than via QDs, in particular, tunneling between the QWs, and between the hole-injecting (right-hand side) QW and the WL. Hence, the opposite sides of the structure are only connected to each other by the current paths through QDs.

Manuscript received August 09, 2009; revised September 22, 2009. First published October 06, 2009; current version published November 30, 2009. This work was supported by the U.S. Army Research Office under Grant W911-NF-08-1-0462.

The authors are with the Virginia Polytechnic Institute and State University, Blacksburg, VA 24061 USA (e-mail: asryan@mse.vt.edu).

Digital Object Identifier 10.1109/JLT.2009.2033716

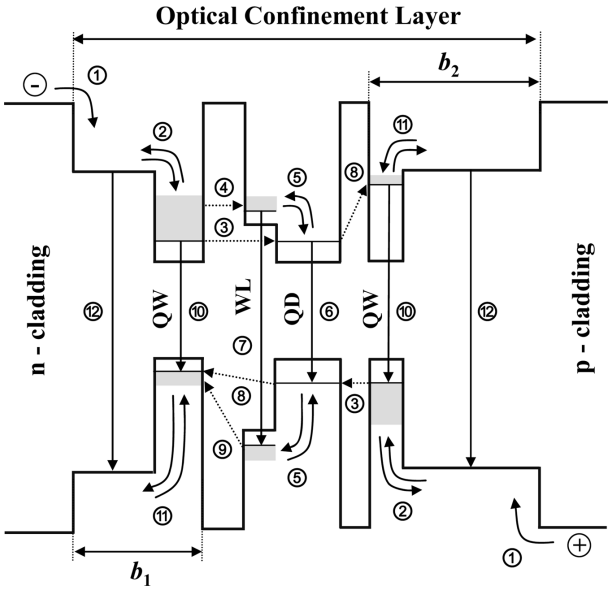

Fig. 1. Energy band diagram of a double tunneling-injection QD laser with the WL and the main processes: ① carrier injection from the cladding layers to the OCL, ② majority carrier capture from the OCL to the QW and thermal escape from the QW to the OCL, ③ majority carrier tunneling-injection from the QW into a QD, ④ electron tunneling from the QW to the WL, ⑤ thermal escape from a QD to the WL and capture from the WL into a QD, ⑥ spontaneous and stimulated recombination in a QD, ⑦ spontaneous recombination in the WL, ⑧ out-tunneling from a QD into the "foreign" QW, ⑨ hole tunneling from the WL into the electron-injecting QW, ⑩ spontaneous recombination in the QWs, ⑪ minority carrier thermal escape from the QW to the OCL and capture from the OCL to the QW, and ⑫ spontaneous recombination in the OCL.

We use the following set of rate equations. For free electrons and holes in the left-hand side of the OCL

$$b_1\frac{\partial n_L}{\partial t}=\frac{j}{e}+\frac{n^L_{\rm QW}}{\tau^L_{\rm n,esc}}-v^L_{\rm n,capt}n_L-b_1Bn_Lp_L \tag{1}$$

$$b_1\frac{\partial p_L}{\partial t}=\frac{p^L_{\rm QW}}{\tau^L_{\rm p,esc}}-v^L_{\rm p,capt}p_L-b_1Bn_Lp_L \tag{2}$$

for free holes and electrons in the right-hand side of the OCL

$$b_2\frac{\partial p_R}{\partial t}=\frac{j}{e}+\frac{p^R_{\rm QW}}{\tau^R_{\rm p,esc}}-v^R_{\rm p,capt}p_R-b_2Bn_Rp_R \tag{3}$$

$$b_2\frac{\partial n_R}{\partial t}=\frac{n^R_{\rm QW}}{\tau^R_{\rm n,esc}}-v^R_{\rm n,capt}n_R-b_2Bn_Rp_R \tag{4}$$

for electrons and holes in the electron-injecting (left-hand-side) QW

$$\begin{aligned}\frac{\partial n^L_{\rm QW}}{\partial t}&=v^L_{\rm n,capt}n_L-\frac{n^L_{\rm QW}}{\tau^L_{\rm n,esc}}-w^L_{\rm n,tunn}N_S(1-f_{\rm n})n^L_{\rm QW}\\&\quad+w^L_{\rm n,tunn}n_1^{L,\rm QW}N_Sf_{\rm n}-w^{\rm QW\leftrightarrow WL}_{\rm n,tunn}\tilde{n}_1^{\rm WL}n^L_{\rm QW}\\&\quad+w^{\rm QW\leftrightarrow WL}_{\rm n,tunn}N^{\rm QW}_{\rm c,2D}n_{\rm WL}-B_{\rm 2D}n^L_{\rm QW}p^L_{\rm QW}\end{aligned} \tag{5}$$

$$\begin{aligned}\frac{\partial p^L_{\rm QW}}{\partial t}&=v^L_{\rm p,capt}p_L-\frac{p^L_{\rm QW}}{\tau^L_{\rm p,esc}}-w^L_{\rm p,tunn}N_S(1-f_{\rm p})p^L_{\rm QW}\\&\quad+w^L_{\rm p,tunn}p_1^{L,\rm QW}N_Sf_{\rm p}-w^{\rm QW\leftrightarrow WL}_{\rm p,tunn}\tilde{p}_1^{\rm WL}p^L_{\rm QW}\\&\quad+w^{\rm QW\leftrightarrow WL}_{\rm p,tunn}N^{\rm QW}_{\rm v,2D}p_{\rm WL}-B_{\rm 2D}n^L_{\rm QW}p^L_{\rm QW}\end{aligned} \tag{6}$$

for holes and electrons in the hole-injecting (right-hand-side) QW

$$\begin{aligned}\frac{\partial p^R_{\rm QW}}{\partial t}&=v^R_{\rm p,capt}p_R-\frac{p^R_{\rm QW}}{\tau^R_{\rm p,esc}}-w^R_{\rm p,tunn}N_S(1-f_{\rm p})p^R_{\rm QW}\\&\quad+w^R_{\rm p,tunn}p_1^{R,\rm QW}N_Sf_{\rm p}-B_{\rm 2D}n^R_{\rm QW}p^R_{\rm QW}\end{aligned} \tag{7}$$

$$\begin{aligned}\frac{\partial n^R_{\rm QW}}{\partial t}&=v^R_{\rm n,capt}n_R-\frac{n^R_{\rm QW}}{\tau^R_{\rm n,esc}}-w^R_{\rm n,tunn}N_S(1-f_{\rm n})n^R_{\rm QW}\\&\quad+w^R_{\rm n,tunn}n_1^{R,\rm QW}N_Sf_{\rm n}-B_{\rm 2D}n^R_{\rm QW}p^R_{\rm QW}\end{aligned} \tag{8}$$

for electrons and holes confined in QDs

$$\begin{aligned}N_S\frac{\partial f_{\rm n}}{\partial t}&=w^L_{\rm n,tunn}N_S(1-f_{\rm n})n^L_{\rm QW}-w^L_{\rm n,tunn}n_1^{L,\rm QW}N_Sf_{\rm n}\\&\quad+w^R_{\rm n,tunn}N_S(1-f_{\rm n})n^R_{\rm QW}-w^R_{\rm n,tunn}n_1^{R,\rm QW}N_Sf_{\rm n}\\&\quad+w_{\rm n,capt}N_S(1-f_{\rm n})n_{\rm WL}-w_{\rm n,capt}n_1^{\rm WL}N_Sf_{\rm n}\\&\quad-N_S\frac{f_{\rm n}f_{\rm p}}{\tau_{\rm QD}}-\frac{c}{\sqrt{\epsilon_{\rm g}}}\frac{g^{\max}}{S}(f_{\rm n}+f_{\rm p}-1)N\end{aligned} \tag{9}$$

$$\begin{aligned}N_S\frac{\partial f_{\rm p}}{\partial t}&=w^R_{\rm p,tunn}N_S(1-f_{\rm p})p^R_{\rm QW}-w^R_{\rm p,tunn}p_1^{R,\rm QW}N_Sf_{\rm p}\\&\quad+w^L_{\rm p,tunn}N_S(1-f_{\rm p})p^L_{\rm QW}-w^L_{\rm p,tunn}p_1^{L,\rm QW}N_Sf_{\rm p}\\&\quad+w_{\rm p,capt}N_S(1-f_{\rm p})p_{\rm WL}-w_{\rm p,capt}p_1^{\rm WL}N_Sf_{\rm p}\\&\quad-N_S\frac{f_{\rm n}f_{\rm p}}{\tau_{\rm QD}}-\frac{c}{\sqrt{\epsilon_g}}\frac{g^{\max}}{S}(f_{\rm n}+f_{\rm p}-1)N\end{aligned} \tag{10}$$

for electrons and holes in the WL,

$$\begin{aligned}\frac{\partial n_{\rm WL}}{\partial t}&=w_{\rm n,capt}n_1^{\rm WL}N_Sf_{\rm n}-w_{\rm n,capt}N_S(1-f_{\rm n})n_{\rm WL}\\&\quad+w^{\rm QW\leftrightarrow WL}_{\rm n,tunn}\tilde{n}_1^{\rm WL}n^L_{\rm QW}-w^{\rm QW\leftrightarrow WL}_{\rm n,tunn}N^{\rm QW}_{\rm c,2D}n_{\rm WL}\\&\quad-B_{\rm 2D}n_{\rm WL}p_{\rm WL}\end{aligned} \tag{11}$$

$$\begin{aligned}\frac{\partial p_{\rm WL}}{\partial t}&=w_{\rm p,capt}p_1^{\rm WL}N_Sf_{\rm p}-w_{\rm p,capt}N_S\left(1-f_{\rm p}\right)p_{\rm WL}\\&\quad+w^{\rm QW\leftrightarrow WL}_{\rm p,tunn}\tilde{p}_1^{\rm WL}p^L_{\rm QW}-w^{\rm QW\leftrightarrow WL}_{\rm p,tunn}N^{\rm QW}_{\rm v,2D}p_{\rm WL}\\&\quad-B_{\rm 2D}n_{\rm WL}p_{\rm WL}\end{aligned} \tag{12}$$

and for photons

$$\frac{\partial N}{\partial t}=\frac{c}{\sqrt{\epsilon_g}}g^{\max}(f_{\rm n}+f_{\rm p}-1)N-\frac{c}{\sqrt{\epsilon_g}}\beta N. \tag{13}$$

In (1)–(13), b_1 (b_2) is the thickness of the left- (right-) hand side of the OCL [the separation between the n- (p-) cladding layer and the left- (right-) hand-side barrier—Fig. 1] and n_L (n_R) and p_L (p_R) are the free-electron and -hole densities there, j is the injection current density, e is the electron charge, $n^L_{\rm QW}$ ($n^R_{\rm QW}$) and $p^L_{\rm QW}$ ($p^R_{\rm QW}$) are the 2-D electron and hole densities in the left- (right-) hand-side QW (Fig. 1), $n_{\rm WL}$ and $p_{\rm WL}$ are the 2-D electron and hole densities in the WL, B and $B_{\rm 2D}$ are the spontaneous radiative recombination constants for the bulk (OCL) and 2-D regions (QWs and WL) measured in units of cm^3/s and cm^2/s, respectively, N_S is the surface density of QDs, $f_{\rm n,p}$ are the electron- and hole-level occupancies in QDs, $\tau_{\rm QD}$ is the spontaneous radiative lifetime in QDs, c is the velocity of light in vacuum, $\sqrt{\epsilon_g}$ is the group index of the dispersive OCL material, $g^{\max}$ is the maximum value of the modal gain [13], [24], $S=WL$ is the cross section of the junction, W is the lateral size of the device, L is the cavity length, $\beta=(1/L)\ln(1/R)$ is the mirror loss, R is the facet reflectivity, and N is the number of photons in the lasing mode;

$\tau^{L,R}_{\mathrm{n,p,esc}}$ are the thermal escape times of electrons and holes from the QWs to the OCL and $v^{L,R}_{\mathrm{n,p,capt}}$ are the capture velocities from the OCL to the QWs.

We exploit six tunneling coefficients (measured in units of cm^2/s)—these are four coefficients $w^{L,R}_{\mathrm{n,p,tunn}}$ for electron and hole tunneling between the QD ensemble and the QWs, and two coefficients $w^{\mathrm{QW}\leftrightarrow\mathrm{WL}}_{\mathrm{n,p,tunn}}$ for electron and hole tunneling between the WL and the electron-injecting QW. These tunneling coefficients are primarily controlled by the thicknesses and material parameters of the barriers, and by the QD, QW, and WL parameters as well.

The quantities $n_1^{L,R,\mathrm{QW}}$ and $p_1^{L,R,\mathrm{QW}}$ entering into the electron and hole tunneling fluxes from the QD ensemble to the QWs [see (5)–(10)] are measured in units of cm^{-2}. In the case of an undoped QW and a resonance between the energy level in a QD and the lowest subband edge in a QW

$$n_1^{L,\mathrm{QW}} = N^{\mathrm{QW}}_{\mathrm{c,2D}}, \quad p_1^{R,\mathrm{QW}} = N^{\mathrm{QW}}_{\mathrm{v,2D}}, \tag{14}$$

where $N^{\mathrm{QW}}_{\mathrm{c,v,2D}} = m^{\mathrm{QW}}_{\mathrm{c,v}} T/(\pi\hbar^2)$ are the 2-D effective densities of states in the conduction and valence bands in the QWs, $m^{\mathrm{QW}}_{\mathrm{c,v}}$ are the electron and hole effective masses in the QWs, and the temperature T is measured in units of energy.

The terms $w^{\mathrm{QW}\leftrightarrow\mathrm{WL}}_{\mathrm{n,tunn}} \tilde{n}_1^{\mathrm{WL}} n^L_{\mathrm{QW}}$ and $w^{\mathrm{QW}\leftrightarrow\mathrm{WL}}_{\mathrm{n,tunn}} N^{\mathrm{QW}}_{\mathrm{c,2D}} n_{\mathrm{WL}}$ in the right-hand side in (5) and (11) are the fluxes of electron tunneling from the electron-injecting QW to the WL and backward tunneling from the WL to the electron-injecting QW, respectively. The difference $w^{\mathrm{QW}\leftrightarrow\mathrm{WL}}_{\mathrm{n,tunn}} \tilde{n}_1^{\mathrm{WL}} n^L_{\mathrm{QW}} - w^{\mathrm{QW}\leftrightarrow\mathrm{WL}}_{\mathrm{n,tunn}} N^{\mathrm{QW}}_{\mathrm{c,2D}} n_{\mathrm{WL}}$ is the net in-tunneling flux of electrons from the electron-injecting QW to the WL.

The quantities $\tilde{n}_1^{\mathrm{WL}}$ and $\tilde{p}_1^{\mathrm{WL}}$ entering into the electron and hole tunneling fluxes from the electron-injecting QW to the WL [see (5), (6), (11), and (12)] are measured in units of cm^{-2}. The general expressions for $\tilde{n}_1^{\mathrm{WL}}$ and $\tilde{p}_1^{\mathrm{WL}}$ are derived in Appendix I [see (A3)]. In the case of undoped QW and WL considered here

$$\tilde{n}_1^{\mathrm{WL}} = N^{\mathrm{WL}}_{\mathrm{c,2D}} \exp\left(-\frac{\varepsilon_{\mathrm{n}}^{\mathrm{WL}} - \varepsilon_{\mathrm{n}}^{\mathrm{QW}}}{T}\right) \tag{15}$$

where $\varepsilon_{\mathrm{n}}^{\mathrm{WL}}$ and $\varepsilon_{\mathrm{n}}^{\mathrm{QW}}$ are the energies of the lowest electron-subband edge in the WL and QW, respectively, $N^{\mathrm{WL}}_{\mathrm{c,2D}} = m_{\mathrm{c}}^{\mathrm{WL}} T/(\pi\hbar^2)$ is the 2-D effective density of states in the conduction band in the WL, and $m_{\mathrm{c}}^{\mathrm{WL}}$ is the electron effective mass in the WL. The expression for $\tilde{p}_1^{\mathrm{WL}}$ is similar to (15).

The terms $w_{\mathrm{n,capt}} n_1^{\mathrm{WL}} N_S f_{\mathrm{n}}$ and $w_{\mathrm{n,capt}} N_S (1-f_{\mathrm{n}}) n_{\mathrm{WL}}$ in the right-hand side in (9) and (11) are the fluxes of thermal escape of electrons from QDs to the WL and capture from the WL into QDs, respectively. The difference $w_{\mathrm{n,capt}} n_1^{\mathrm{WL}} N_S f_{\mathrm{n}} - w_{\mathrm{n,capt}} N_S (1-f_{\mathrm{n}}) n_{\mathrm{WL}}$ is the net electron escape flux from QDs to the WL. The coefficients $w_{\mathrm{n,p,capt}}$ in (9)–(12) describe the electron and hole capture from the WL into a QD and escape from a QD to the WL. They are measured in units of cm^2/s and were referred to as the temporal cross-sections in [25], [26].

The quantities n_1^{WL} and p_1^{WL} entering into the electron and hole thermal escape fluxes from QDs to the WL [see (9)–(12)] are measured in units of cm^{-2}. The general expressions for n_1^{WL} and p_1^{WL} are derived in Appendix II [see (A7)]. In the case of an undoped WL

$$n_1^{\mathrm{WL}} = N^{\mathrm{WL}}_{\mathrm{c,2D}} \exp\left(-\frac{\varepsilon_{\mathrm{n}}^{\mathrm{WL}} - \varepsilon_{\mathrm{n}}^{\mathrm{QD}}}{T}\right) \tag{16}$$

where $\varepsilon_{\mathrm{n}}^{\mathrm{QD}}$ is the energy of the electron level in a QD. The expression for p_1^{WL} is similar to (16).

The last term in the right-hand side in (11) is the spontaneous radiative recombination flux in the WL.

The terms describing the processes related to the WL for holes in (6), (10), and (12) are similar to those for electrons in (5), (9), and (11).

Due to size-distribution in Stranski–Krastanow grown QDs, the gain spectrum of a QD laser is inhomogeneously broadened and the peak of the gain spectrum is lowered [13], [24]. The maximum value of the modal gain spectrum peak is proportional to the surface density of QDs, N_S, and is inversely proportional to the inhomogeneous line broadening, $(\Delta\varepsilon)_{\mathrm{inhom}}$, i.e., $g^{\max} \propto N_S/(\Delta\varepsilon)_{\mathrm{inhom}}$ [13], [24]. Resonant injection means that nonlasing QDs are not pumped either. On the one hand, this leads to an effective narrowing of the inhomogeneous linewidth $(\Delta\varepsilon)_{\mathrm{inhom}}$. On the other hand, the surface density of QDs, N_S, entering into the expression for $g^{\max}$ is reduced. To maximize the number of active (pumped) QDs, the energy of the lowest subband edge in the electron- (hole-) injecting QW should be in resonance with the energy of the electron (hole) level in the QDs of average size [20]. The fact whether $g^{\max}$ will be finally increased or decreased due to resonant injection will depend on a specific type of the QD size distribution.

III. Results and Discussion

We consider a continuous-wave operation of the laser and correspondingly use the set of rate equations (1)–(13) at the steady-state

$$\frac{\partial}{\partial t}\left(b_1 n_L, b_1 p_L, b_2 n_R, b_2 p_R, n^L_{\mathrm{QW}}, p^L_{\mathrm{QW}}, n^R_{\mathrm{QW}}, p^R_{\mathrm{QW}}, n_{\mathrm{WL}}, p_{\mathrm{WL}}, N_S f_{\mathrm{n}}, N_S f_{\mathrm{p}}, N\right) = 0. \tag{17}$$

It can be shown that only eleven out of twelve equations (1)–(12) are independent at the steady-state. Hence, to solve the set, we should complement it by one more equation. The equation is provided by the charge neutrality condition in QDs.

Above the lasing threshold, the number of stimulated photons is nonvanishing ($N \neq 0$). To satisfy (13) at the steady-state at nonvanishing N, the following lasing condition should hold:

$$g^{\max}(f_{\mathrm{n}} + f_{\mathrm{p}} - 1) = \beta \tag{18}$$

which is the condition of equality of the modal gain to the mirror loss at and above the lasing threshold (the internal optical loss is not considered here).

If charge neutrality holds in QDs ($f_{\mathrm{n}} = f_{\mathrm{p}}$), we immediately obtain from (18) that the level occupancies in QDs are pinned at their threshold value and do not depend on the injection current density j

$$f_{\mathrm{n}} = f_{\mathrm{p}} = \frac{1}{2}\left(1 + \frac{\beta}{g^{\max}}\right) = \mathrm{const}(j). \tag{19}$$

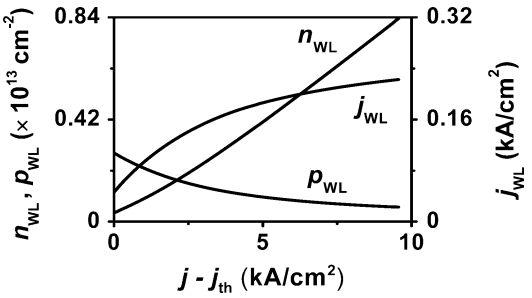

Fig. 2. 2-D densities of electrons and holes (left axis) and recombination current density (right axis) in the WL against excess injection current density. A GaInAsP heterostructure lasing at room-temperature ($T = 300$ K) near the telecommunication wavelength 1.55 μm is considered here. 10% QD size fluctuations are assumed. The parameters of the laser structure used in Figs. 2–6 are presented in Table I.

Since the opposite sides of the structure are only connected to each other by the current paths through QDs, the fact that $f_{n,p}$ do not change with j means that the steady-state rate equations for the left- and right-hand sides of the structure present two independent sets. Hence, the solutions of the rate equations (3), (4), (7), and (8) for the right-hand side of the structure are unaffected by the presence of the WL.

Using the steady-state rate equations, the following expression is obtained for the number of photons N and output power P from the rate equations

$$P = \hbar\omega \frac{c}{\sqrt{\epsilon_g}} \beta N = \frac{\hbar\omega}{e} S \left(j - eN_S \frac{f_n f_p}{\tau_{QD}} - eB_{2D} n_{WL} p_{WL} - eB_{2D} n^L_{QW} p^L_{QW} - eB_{2D} n^R_{QW} p^R_{QW} - eb_1 B n_L p_L - eb_2 B n_R p_R \right) \quad (20)$$

where $\hbar\omega$ is the photon energy. Equation (20) states that the stimulated emission is produced by an excess of the injection current density j over the current densities of spontaneous recombination in QDs (second term in the brackets), WL (third term), QWs (fourth and fifth terms), and OCL (last two terms).

To calculate the LCC [i.e., P versus j given by (20)], the dependences of the carrier densities on the injection current density j are found from the solution of the rate equations.

As seen from Fig. 2, the electron density n_{WL} in the WL increases with j, which is due to the increase of the electron density n^L_{QW} in the electron-injecting QW [Fig. 3(a)]. At the same time, the hole densities p_{WL} and p^L_{QW} decrease [Figs. 2 and 3(b)] [see also the text after (34)]. The electron densities increase faster than the hole densities decrease. For this reason, the recombination current densities increase with j [Figs. 2 and 3(b)].

Since the WL consumes a certain fraction of electrons from the electron-injecting QW, the electron density in the latter is reduced compared to the case of no WL [Fig. 3(a)]. At the same time, the hole density in the electron-injecting QW is increased [Fig. 3(b)]. This is because the holes from the WL tunnel to the electron-injecting QW in addition to the holes from QDs. At high injection currents, the increase of p^L_{QW} due to the presence of the WL outweighs the decrease of n^L_{QW}. As a result, the recombination current density j^L_{QW} in the electron-injecting QW is increased [Fig. 3(c)].

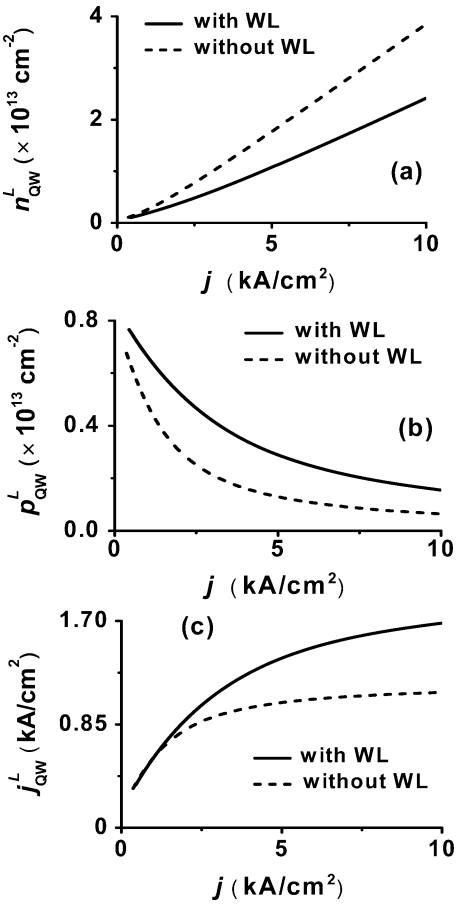

Fig. 3. 2-D densities of electrons (a) and holes (b) and recombination current density (c) in the electron-injecting QW against injection current density for the structures with (solid curve) and without (dashed curve) the WL.

Hence, not only an additional electron–hole recombination channel appears (Fig. 2), but the recombination in the electron-injecting QW becomes stronger as well in the presence of the WL [Fig. 3(c)]. Since the recombination in the right-hand side of the structure is unaffected, the total parasitic recombination current density outside QDs is increased. For this reason, the output power is reduced in a structure with the WL (solid curve in Fig. 4). The output power depends strongly on the temporal cross section $w_{p,capt}$ of hole capture from the WL into a QD [see (29)–(33)]. The larger $w_{p,capt}$, the lower is the power and the stronger is the deviation of the LCC from that for a structure without the WL (dashed curve in Fig. 4). Clearly the internal quantum efficiency [Fig. 5(a)] and the slope efficiency [Fig. 5(b)] are reduced in the presence of the WL. To have high internal efficiency not only at high but also at low injection current densities, the structure should be optimized to minimize out-tunneling of electrons and holes from QDs into the foreign QWs, and to minimize the hole thermal escape from QDs into the WL.

Despite the fact that the output power is reduced in the presence of the WL, it is clear from Fig. 4 that the LCC becomes increasingly linear with j. This remarkable feature can be understood and several general conclusions can be made from the analysis of the rate equations.

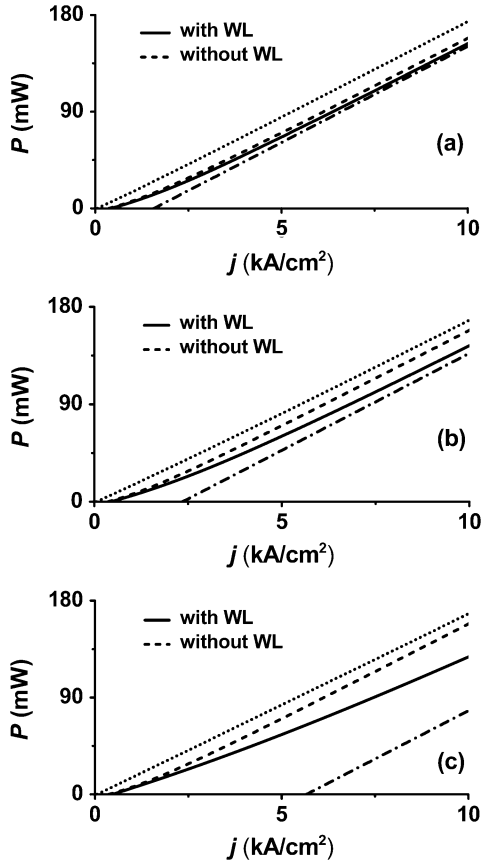

Fig. 4. Light-current characteristics of the double tunneling-injection QD lasers with (solid curve) and without (dashed curve) the WL. The temporal cross-sections of electron and hole capture from the WL into a QD are $w_{\mathrm{n,p,capt}} = 0.03, 0.1$, and 0.4 cm^2/s in (a), (b), and (c), respectively. The threshold current density is $j_{\mathrm{th}} = 417, 440$, and 467 A/cm^2; for the structure without the WL, $j_{\mathrm{th}} = 366.3$ A/cm^2. The dotted line given by (32) is the upper limit for the LCC. The dash-dotted line given by (30) is the asymptote and the lower limit for the LCC.

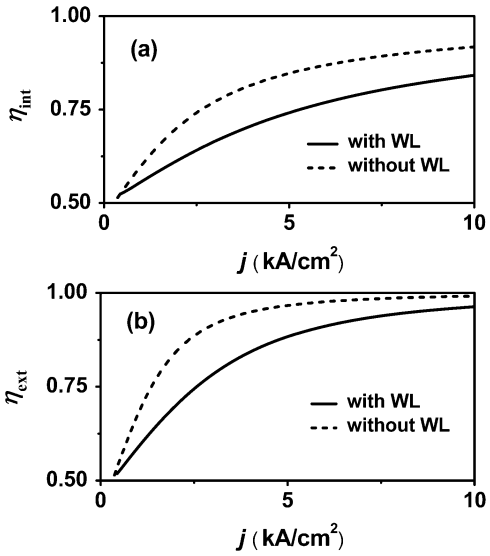

Fig. 5. Internal quantum efficiency (a) and slope efficiency (b) against injection current density for the DTI QD lasers with (solid curve) and without (dashed curve) the WL. Since η_{int} increases with j, η_{ext} is higher than η_{int} as is clear from (34).

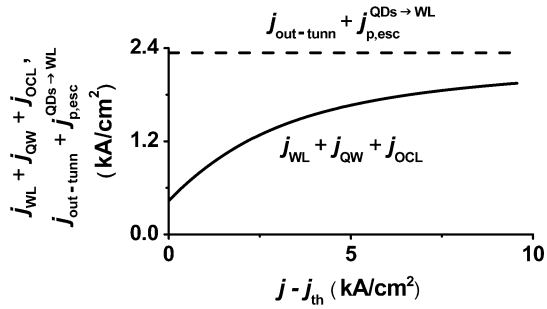

Fig. 6. Parasitic recombination current density outside QDs (solid curve). The horizontal dashed line is the sum of the current densities of electron and hole out-tunneling from QDs to the foreign QWs and hole thermal escape from QDs to the WL.

At the steady-state, equations (2) and (12) for holes in the left-hand side of the OCL and in the WL can be written as

$$\frac{p^L_{\mathrm{QW}}}{\tau^L_{\mathrm{p,esc}}} - v^L_{\mathrm{p,capt}} p_L = b_1 B n_L p_L \tag{21}$$

$$w^{\mathrm{QW}\leftrightarrow\mathrm{WL}}_{\mathrm{p,tunn}} N^{\mathrm{QW}}_{\mathrm{v,2D}} p_{\mathrm{WL}} - w^{\mathrm{QW}\leftrightarrow\mathrm{WL}}_{\mathrm{p,tunn}} \tilde{p}^{\mathrm{WL}}_1 p^L_{\mathrm{QW}} = w_{\mathrm{p,capt}} p^{\mathrm{WL}}_1 N_S f_{\mathrm{p}} - w_{\mathrm{p,capt}} N_S (1 - f_{\mathrm{p}}) p_{\mathrm{WL}} - B_{\mathrm{2D}} n_{\mathrm{WL}} p_{\mathrm{WL}}. \tag{22}$$

Using (21) and (22) in (6), we have

$$B_{\mathrm{2D}} n_{\mathrm{WL}} p_{\mathrm{WL}} + B_{\mathrm{2D}} n^L_{\mathrm{QW}} p^L_{\mathrm{QW}} + b_1 B n_L p_L = \left[w^L_{\mathrm{p,tunn}} p^{L,\mathrm{QW}}_1 N_S f_{\mathrm{p}} - w^L_{\mathrm{p,tunn}} N_S (1 - f_{\mathrm{p}}) p^L_{\mathrm{QW}} \right] + \left[w_{\mathrm{p,capt}} p^{\mathrm{WL}}_1 N_S f_{\mathrm{p}} - w_{\mathrm{p,capt}} N_S (1 - f_{\mathrm{p}}) p_{\mathrm{WL}} \right] \tag{23}$$

As seen from (23), bimolecular recombination in the WL and in the left-hand-side QW and OCL is entirely due to the net out-tunneling of holes from QDs to the electron-injecting QW [first brackets in (23)] and the net escape of holes from QDs to the WL (second brackets).

Bimolecular recombination in the right-hand-side QW and OCL is entirely due to the net out-tunneling of electrons from QDs to the hole-injecting QW and is not affected by the presence of the WL

$$B_{\mathrm{2D}} n^R_{\mathrm{QW}} p^R_{\mathrm{QW}} + b_1 B n_R p_R = w^R_{\mathrm{n,tunn}} n^{R,\mathrm{QW}}_1 N_S f_{\mathrm{n}} - w^R_{\mathrm{n,tunn}} N_S (1 - f_{\mathrm{n}}) n^R_{\mathrm{QW}}. \tag{24}$$

By dropping in (23) the flux $w^L_{\mathrm{p,tunn}} N_S (1 - f_{\mathrm{p}}) p^L_{\mathrm{QW}}$ of backward tunneling of holes from the electron-injecting QW to QDs and the flux $w_{\mathrm{p,capt}} N_S (1 - f_{\mathrm{p}}) p_{\mathrm{WL}}$ of hole capture from the WL into QDs, we obtain the upper limit for the parasitic recombination flux in the left-hand side of the structure. Since $f_{\mathrm{n,p}} \leq 1$, this limit, which presents the sum of the out-tunneling flux $w^L_{\mathrm{p,tunn}} p^{L,\mathrm{QW}}_1 N_S f_{\mathrm{p}}$ of holes from QDs to the electron-injecting QW and the thermal escape flux $w_{\mathrm{p,capt}} p^{\mathrm{WL}}_1 N_S f_{\mathrm{p}}$ of holes from QDs to the WL, is itself restricted and cannot exceed $w^L_{\mathrm{p,tunn}} p^{L,\mathrm{QW}}_1 N_S + w_{\mathrm{p,capt}} p^{\mathrm{WL}}_1 N_S$ at any j [under the condition of charge neutrality (19), $w^L_{\mathrm{p,tunn}} p^{L,\mathrm{QW}}_1 N_S f_{\mathrm{p}}$ and

TABLE I
PARAMETERS OF THE LASER STRUCTURE

Parameter	Value
N_S	6.11×10^{10} cm^{-2}
L	1.139 mm
R	0.32
β	10 cm^{-1}
W	2 μm
$\tau_{\rm QD}$	0.71×10^{-9} s
$g^{\max}$	29.52 cm^{-1}
b_1, b_2	0.14 μm
λ	1.58 μm
B	1.27×10^{-10} cm^3/s
$B_{\rm 2D}$	2.8×10^{-4} cm^2/s
$v^{L,R}_{\rm n,p,capt}$	3×10^5 cm/s
$w^{L}_{\rm n,tunn}$, $w^{\rm QW\leftrightarrow WL}_{\rm n,tunn}$	0.073 cm^2/s
$w^{L}_{\rm p,tunn}$, $w^{\rm QW\leftrightarrow WL}_{\rm p,tunn}$	0.04 cm^2/s
$w^{R}_{\rm n,tunn}$	0.013 cm^2/s
$w^{R}_{\rm p,tunn}$	0.058 cm^2/s
$w_{\rm n,p,capt}$	0.1 cm^2/s

$w_{\rm p,capt}p_1^{\rm WL}N_Sf_{\rm p}$ are pinned and do not change with j]. Consequently, we have for the recombination flux in the left-hand side of the structure

$$\begin{aligned} &b_1Bn_Lp_L+B_{\rm 2D}n^L_{\rm QW}p^L_{\rm QW}+B_{\rm 2D}n_{\rm WL}p_{\rm WL}\\ &\quad<w^L_{\rm p,tunn}p_1^{L,\rm QW}N_Sf_{\rm p}+w_{\rm p,capt}p_1^{\rm WL}N_Sf_{\rm p}\\ &\quad<w^L_{\rm p,tunn}p_1^{L,\rm QW}N_S+w_{\rm p,capt}p_1^{\rm WL}N_S=\text{const}. \end{aligned} \tag{25}$$

From (24), we have for the recombination flux in the right-hand side of the structure

$$\begin{aligned} &b_2Bn_Rp_R+B_{\rm 2D}n^R_{\rm QW}p^R_{\rm QW}\\ &\quad<w^R_{\rm n,tunn}n_1^{R,\rm QW}N_Sf_{\rm n}<w^R_{\rm n,tunn}n_1^{R,\rm QW}N_S=\text{const} \end{aligned} \tag{26}$$

Fig. 6 (solid curve) shows the recombination current density outside QDs [the sum of the last five terms in the brackets in (20)]. The horizontal dashed line is the sum of the current densities of electron and hole out-tunneling from QDs to the foreign QWs

$$j_{\rm out-tunn}=ew^L_{\rm p,tunn}p_1^{L,\rm QW}N_Sf_{\rm p}+ew^R_{\rm n,tunn}n_1^{R,\rm QW}N_Sf_{\rm n} \tag{27}$$

and hole thermal escape from QDs to the WL

$$j^{\rm QDs\to WL}_{\rm p,esc}=ew_{\rm p,capt}p_1^{\rm WL}N_Sf_{\rm p}. \tag{28}$$

As in a structure without the WL [23], in the presence of the WL too, the fact that the parasitic recombination flux outside QDs remains limited with increasing j is due to the zero-dimensional nature of QDs—the flux of escape from QDs (be it out-tunneling escape to the foreign QW or thermal escape to the WL) is controlled by the QD level occupancy $f_{\rm n,p}$ [see (27) and (28)], which cannot exceed unity with increasing j [$f_{\rm n}=f_{\rm p}=\text{const}$ in the case of charge neutrality—see (19)].

With (23) and (24), (20) can be rewritten as follows:

$$\begin{aligned} P=\frac{\hbar\omega}{e}S\Big[&j-eN_S\frac{f_{\rm n}f_{\rm p}}{\tau_{\rm QD}}-ew^L_{\rm p,tunn}p_1^{L,\rm QW}N_Sf_{\rm p}\\ &-ew^R_{\rm n,tunn}n_1^{R,\rm QW}N_Sf_{\rm n}-ew_{\rm p,capt}p_1^{\rm WL}N_Sf_{\rm p}\\ &+ew^L_{\rm p,tunn}N_S(1-f_{\rm p})p^L_{\rm QW}+ew^R_{\rm n,tunn}N_S(1-f_{\rm n})n^R_{\rm QW}\\ &+ew_{\rm p,capt}N_S(1-f_{\rm p})p_{\rm WL}\Big]. \end{aligned} \tag{29}$$

Whatever the dependences of $p^L_{\rm QW}, n^R_{\rm QW}$ and $p_{\rm WL}$ on j, it is clear from (29) that by dropping the last three terms in the brackets (the current densities of backward tunneling of minority carriers from the foreign QWs to QDs and of hole capture from the WL into QDs) we will obtain the lower limit for the output power

$$P^{\rm lowest}=\frac{\hbar\omega}{e}S\left(j-j^{\rm highest}_{\rm th}\right), \tag{30}$$

where

$$\begin{aligned} j^{\rm highest}_{\rm th}=&eN_S\frac{f_{\rm n}f_{\rm p}}{\tau_{\rm QD}}+ew^L_{\rm p,tunn}p_1^{L,\rm QW}N_Sf_{\rm p}\\ &+ew^R_{\rm n,tunn}n_1^{R,\rm QW}N_Sf_{\rm n}+ew_{\rm p,capt}p_1^{\rm WL}N_Sf_{\rm p} \end{aligned} \tag{31}$$

is the upper limit for the threshold current density.

As seen from (30), the lower limit for the LCC is linear (dash-dotted line in Fig. 4) and its slope efficiency is unity.

The upper limit for the LCC is obtained in an ideal structure wherein out-tunneling from QDs to the foreign QWs and hence recombination in the QWs and OCL are completely blocked. Since recombination in the WL will still occur in such a structure, we have from (20)

$$P^{\rm highest}=\frac{\hbar\omega}{e}S\left(j-eN_S\frac{f_{\rm n}f_{\rm p}}{\tau_{\rm QD}}-eB_{\rm WL}n_{\rm WL}p_{\rm WL}\right). \tag{32}$$

In this case, we obtain from (25) that the recombination current density $eB_{\rm WL}n_{\rm WL}p_{\rm WL}$ in the WL is limited by the current density $ew_{\rm p,capt}p_1^{\rm WL}N_Sf_{\rm p}$ of hole thermal escape from QDs to the WL,

$$B_{\rm 2D}n_{\rm WL}p_{\rm WL}<w_{\rm p,capt}p_1^{\rm WL}N_Sf_{\rm p}<w_{\rm p,capt}p_1^{\rm WL}N_S. \tag{33}$$

With increasing $j, eB_{\rm WL}n_{\rm WL}p_{\rm WL}$ asymptotically approaches $ew_{\rm p,capt}p_1^{\rm WL}N_Sf_{\rm p}$ and the upper limit (32) for the LCC becomes linear (dotted line in Fig. 4).

Hence, the actual LCC (obtained from the solution of the rate equations and shown by the solid curve in Fig. 4) in a structure with the WL is confined between the two parallel lines given by (30) and (32) (dash-dotted and dotted lines). Since the parasitic recombination current density remains restricted [see (25), (26) and Fig. 6], the fraction of the excess injection current density $j-j_{\rm th}$ that goes into the stimulated emission [the internal differential quantum efficiency, $\eta_{\rm int}=e(c/\sqrt{\epsilon_{\rm g}})\beta(N/S)/(j-j_{\rm th})$] should rise with j

[Fig. 5(a)]. As a result, the LCC should become increasingly linear (Fig. 4).

From (29), we have for the slope efficiency (external differential quantum efficiency)

$$\eta_{\rm ext} = \frac{1}{\frac{\hbar\omega}{e}S}\frac{\partial P}{\partial j} = \eta_{\rm int} + (j - j_{\rm th})\frac{\partial \eta_{\rm int}}{\partial j}$$
$$= 1 + ew^{L}_{\rm p,tunn}N_S(1-f_{\rm p})\frac{\partial p^{L}_{\rm QW}}{\partial j}$$
$$+ ew^{R}_{\rm n,tunn}N_S(1-f_{\rm n})\frac{\partial n^{R}_{\rm QW}}{\partial j} + ew_{\rm p,capt}N_S(1-f_{\rm p})\frac{\partial p_{\rm WL}}{\partial j}. \quad (34)$$

Since $\eta_{\rm ext}$ should not be higher than unity, the derivatives of $p^{L}_{\rm QW}, n^{R}_{\rm QW}$, and $p_{\rm WL}$ with respect to j should be negative—the minority carrier density in each of the two QWs and the hole density in the WL decrease with j [Figs. 2 and 3(b)]. Hence, the last three terms in the brackets in (29) decrease with increasing j and the LCC asymptotically approaches the straight line given by (30) (Fig. 4).

We did not discuss in this paper the effect of the WL on the temperature dependences of the operating characteristics of a DTI QD laser. Also not considered here is the above-threshold alpha-parameter as a function of the injection current density. In the presence of the WL states in a laser exploiting tunneling-injection of only electrons into QDs, the alpha-parameter was predicted to remain constant over a wide range of the pump current [27]. In the context of a DTI QD laser, these issues are matters of separate studies.

IV. Conclusion

The effect of the WL, which is inherently present in self-assembled Stranski–Krastanow grown structures, on the optical power of a DTI QD laser has been studied. Due to thermal escape of carriers from QDs, bipolar population establishes and hence electron–hole recombination occurs in the WL. Since the opposite sides of a DTI structure are only connected by the current paths through QDs, and the WL is located in the n-side of the structure, the only source of holes for the WL is provided by QDs. It has been shown that, due to the zero-dimensional nature of QDs, the rate of the hole supply to the WL remains limited with increasing injection current. For this reason, as in the other parts of the structure outside QDs (QWs and OCL), the parasitic electron–hole recombination remains restricted in the WL. As a result, even in the presence of the WL, the LCC of a DTI QD laser becomes increasingly linear at high injection currents, which is a further demonstration of robustness of such a laser and its potential for high-power operation.

Appendix I
Quantities $\tilde{n}_1^{\rm WL}$ and $\tilde{p}_1^{\rm WL}$ in the Tunneling Fluxes of Electrons and Holes From the Electron-Injecting QW to the WL

For definiteness, we consider in Appendixes I and II electrons. The derivation and expressions for holes are similar. Under thermal equilibrium, the flux $w^{\rm QW\leftrightarrow WL}_{\rm n,tunn}\tilde{n}_1^{\rm WL}n^{\rm eq}_{\rm QW}$ of electron tunneling from the electron-injecting QW to the WL is equal to the flux $w^{\rm QW\leftrightarrow WL}_{\rm n,tunn}N^{\rm QW}_{\rm c,2D}n^{\rm eq}_{\rm WL}$ of backward tunneling of electrons from the WL to the QW, to give

$$\tilde{n}_1^{\rm WL} = N^{\rm QW}_{\rm c,2D}\frac{n^{\rm eq}_{\rm WL}}{n^{\rm eq}_{\rm QW}}. \quad (A1)$$

Using the closed-form expression for the 2-D equilibrium carrier density (see, e.g., [28]), we have for $n^{\rm eq}_{\rm WL}$ and $n^{\rm eq}_{\rm QW}$

$$n^{\rm eq}_{\rm WL,QW} = N^{\rm WL,QW}_{\rm c,2D}\ln\left[1+\exp\left(\frac{\mu^{\rm eq}-\varepsilon^{\rm WL,QW}_{\rm n}}{T}\right)\right], \quad (A2)$$

where $N^{\rm WL,QW}_{\rm c,2D} = m^{\rm WL,QW}_{\rm c}T/(\pi\hbar^2)$ are the 2-D effective densities of states in the conduction band in the WL and QW, respectively, $m^{\rm WL,QW}_{\rm c}$ are the electron effective masses there, T is the temperature (measured in units of energy), $\varepsilon^{\rm WL,QW}_{\rm n}$ are the energies of the lowest electron-subband edge in the WL and QW, respectively, and $\mu^{\rm eq}$ is the equilibrium Fermi level.

With (A2), (A1) becomes

$$\tilde{n}_1^{\rm WL} = N^{\rm WL}_{\rm c,2D}\frac{\ln\left[1+\exp\left(\frac{\mu^{\rm eq}-\varepsilon^{\rm WL}_{\rm n}}{T}\right)\right]}{\ln\left[1+\exp\left(\frac{\mu^{\rm eq}-\varepsilon^{\rm QW}_{\rm n}}{T}\right)\right]}. \quad (A3)$$

If both QW and WL materials are nondegenerate (the Fermi level $\mu^{\rm eq}$ is below $\varepsilon^{\rm QW}_{\rm n}$ by several T), which is the case of undoped QW and WL considered here, then

$$\ln\left[1+\exp\left(\frac{\mu^{\rm eq}-\varepsilon^{\rm WL,QW}_{\rm n}}{T}\right)\right] \approx \exp\left(-\frac{\varepsilon^{\rm WL,QW}_{\rm n}-\mu^{\rm eq}}{T}\right). \quad (A4)$$

With (A4), (15) is obtained from (A3).

Appendix II
Quantities $n_1^{\rm WL}$ and $p_1^{\rm WL}$ in the Thermal Escape Fluxes of Electrons and Holes from QDs to the WL

We now use the detailed balance condition under thermal equilibrium for the flux $w_{\rm n,capt}n_1^{\rm WL}N_S f^{\rm eq}_{\rm n}$ of carrier thermal escape from QDs to the WL and the flux $w_{\rm n,capt}N_S(1-f^{\rm eq}_{\rm n})n^{\rm eq}_{\rm WL}$ of capture from the WL to QDs to obtain

$$n_1^{\rm WL} = \frac{1-f^{\rm eq}_{\rm n}}{f^{\rm eq}_{\rm n}}n^{\rm eq}_{\rm WL} \quad (A5)$$

where

$$f^{\rm eq}_{\rm n} = \frac{1}{\exp\left(\frac{\varepsilon^{\rm QD}_{\rm n}-\mu^{\rm eq}}{T}\right)+1} \quad (A6)$$

is the equilibrium occupancy of the energy level $\varepsilon^{\rm QD}_{\rm n}$ in a QD.

With (A2) for $n^{\rm eq}_{\rm WL}$, (A5) becomes

$$n_1^{\rm WL} = N^{\rm WL}_{\rm c,2D}\exp\left(\frac{\varepsilon^{\rm QD}_{\rm n}-\mu^{\rm eq}}{T}\right)\ln\left[1+\exp\left(\frac{\mu^{\rm eq}-\varepsilon^{\rm WL}_{\rm n}}{T}\right)\right]. \quad (A7)$$

If a WL material is nondegenerate ($\mu^{\rm eq}$ is below $\varepsilon_{\rm n}^{\rm WL}$ by several T), which is the case of an undoped WL considered here, the use of (A4) in (A7) yields (16). In (16), the separation $\varepsilon_{\rm n}^{\rm WL} - \varepsilon_{\rm n}^{\rm QD}$ between the energies of the lowest subband edge in the WL and the level in a QD can be controlled by post-growth annealing [11] or changing the growth temperature [12].

REFERENCES

[1] Y. Arakawa and H. Sakaki, "Multidimensional quantum well laser and temperature dependence of its threshold current," *Appl. Phys. Lett.*, vol. 40, no. 3, pp. 217–219, Jun. 1982.

[2] N. Kirstädter, N. N. Ledentsov, M. Grundmann, D. Bimberg, V. M. Ustinov, S. S. Ruvimov, M. V. Maximov, P. S. Kop'ev, Z. I. Alferov, U. Richter, P. Werner, U. Gösele, and J. Heydenreich, "Low threshold, large T_0 injection laser emission from (InGa)As quantum dots," *Electron. Lett.*, vol. 30, no. 17, pp. 1416–1417, Aug. 1994.

[3] R. Mirin, A. Gossard, and J. Bowers, "Room temperature lasing from InGaAs quantum dots," *Electron. Lett.*, vol. 32, no. 18, pp. 1732–1734, Aug. 1996.

[4] G. Park, O. B. Shchekin, D. L. Huffaker, and D. G. Deppe, "Low-threshold oxide-confined 1.3-μm quantum-dot laser," *IEEE Photon. Technol. Lett.*, vol. 13, no. 3, pp. 230–232, Mar. 2000.

[5] Y. Qiu, P. Gogna, S. Forouhar, A. Stintz, and L. F. Lester, "High-performance InAs quantum-dot lasers near 1.3 μm," *Appl. Phys. Lett.*, vol. 79, no. 22, pp. 3570–3572, Nov. 2001.

[6] P. Bhattacharya and S. Ghosh, "Tunnel injection $In_{0.4}Ga_{0.6}As/GaAs$ quantum dot lasers with 15 GHz modulation bandwidth at room temperature," *Appl. Phys. Lett.*, vol. 80, no. 19, pp. 3482–3484, May 2002.

[7] D. Zhou, R. Piron, F. Grillot, O. Dehaese, E. Homeyer, M. Dontabactouny, T. Batte, K. Tavernier, J. Even, and S. Loualiche, "Study of the characteristics of 1.55 μm quantum dash/dot semiconductor lasers on InP substrate," *Appl. Phys. Lett.*, vol. 93, no. 16, pp. 161104-1–161104-3, Oct. 2008.

[8] V. A. Shchukin, N. N. Ledentsov, and D. Bimberg, *Epitaxy of Nanostructures*. Berlin, Germany: Springer, 2003, p. 400.

[9] K. Nishi, R. Mirin, D. Leonard, G. Medeiros-Ribeiro, P. M. Petroff, and A. C. Gossard, "Structural and optical characterization of InAs/InGaAs self-assembled quantum dots grown on (311)B GaAs," *J. Appl. Phys.*, vol. 80, no. 6, pp. 3466–3470, Sep. 1996.

[10] R. Leon, Y. Kim, C. Jagadish, M. Gal, J. Zou, and D. J. H. Cockayne, "Effects of interdiffusion on the luminescence of InGaAs/GaAs quantum dots," *Appl. Phys. Lett.*, vol. 69, no. 13, pp. 1888–1890, Sep. 1996.

[11] A. Patanè, A. Polimeni, P. C. Main, M. Henini, and L. Eaves, "High-temperature light emission from InAs quantum dots," *Appl. Phys. Lett.*, vol. 75, no. 6, pp. 814–816, Aug. 1999.

[12] J. S. Kim and I.-H. Bae, "Optical properties of wetting layer in InAs quantum dots at different growth temperatures," *J. Korean Phys. Soc.*, vol. 42, no. 92, pp. S483–S486, Feb. 2003.

[13] L. V. Asryan and R. A. Suris, "Inhomogeneous line broadening and the threshold current density of a semiconductor quantum dot laser," *Semicond. Sci. Technol.*, vol. 11, no. 4, pp. 554–567, Apr. 1996.

[14] L. V. Asryan and R. A. Suris, "Temperature dependence of the threshold current density of a quantum dot laser," *IEEE J. Quantum Electron.*, vol. 34, no. 5, pp. 841–850, May 1998.

[15] M. V. Maximov, L. V. Asryan, Y. M. Shernyakov, A. F. Tsatsul'nikov, I. N. Kaiander, V. V. Nikolaev, A. R. Kovsh, S. S. Mikhrin, V. M. Ustinov, A. E. Zhukov, Z. I. Alferov, N. N. Ledentsov, and D. Bimberg, "Gain and threshold characteristics of long wavelength lasers based on InAs/GaAs quantum dots formed by activated alloy phase separation," *IEEE J. Quantum Electron.*, vol. 37, no. 5, pp. 676–683, May 2001.

[16] D. R. Matthews, H. D. Summers, P. M. Smowton, and M. Hopkinson, "Experimental investigation of the effect of wetting-layer states on the gain-current characteristic of quantum-dot lasers," *Appl. Phys. Lett.*, vol. 81, no. 26, pp. 4904–4906, Dec. 2002.

[17] G. Agnello, V. Tokranov, M. Yakimov, M. Lamberti, Y. G. Zheng, and S. Oktyabrsky, "Structural and optical effects of capping layer material and growth rate on the properties of self-assembled InAs quantum dot structures," in *Proc. MRS Symp.*, 2005, vol. 829, pp. 63–68.

[18] K. Veselinov, F. Grillot, P. Miska, E. Homeyer, P. Caroff, C. Platz, J. Even, X. Marie, O. Dehaese, S. Loualiche, and A. Ramdane, "Carrier dynamics and saturation effect in (113)B InAs/InP quantum dot lasers," *Opt. Quantum Electron.*, vol. 38, no. 4–6, pp. 369–379, Mar. 2006.

[19] K. Veselinov, F. Grillot, C. Cornet, J. Even, A. Bekiarski, M. Gioannini, and S. Loualiche, "Analysis of the double laser emission occurring in 1.55-μm InAs-InP (113)B quantum-dot lasers," *IEEE J. Quantum Electron.*, vol. 43, no. 9, pp. 810–816, Sep. 2007.

[20] L. V. Asryan and S. Luryi, "Tunneling-injection quantum-dot laser: Ultrahigh temperature stability," *IEEE J. Quantum Electron.*, vol. 37, no. 7, pp. 905–910, Jul. 2001.

[21] L. V. Asryan and S. Luryi, "Temperature-insensitive semiconductor quantum dot laser," *Solid-State Electron.*, vol. 47, no. 2, pp. 205–212, Feb. 2003.

[22] L. V. Asryan and S. Luryi, "Semiconductor Laser With Reduced Temperature Sensitivity," U.S. Patent 6 870 178 B2, Mar. 22, 2005.

[23] D.-S. Han and L. V. Asryan, "Tunneling-injection of electrons and holes into quantum dots: A tool for high-power lasing," *Appl. Phys. Lett.*, vol. 92, no. 25, pp. 251113-1–251113-3, Jun. 2008.

[24] L. V. Asryan and R. A. Suris, "Charge neutrality violation in quantum dot lasers," *IEEE J. Sel. Topics Quantum Electron.*, vol. 3, no. 2, pp. 148–157, Apr. 1997.

[25] S. Raymond, S. Fafard, K. Hinzer, S. Charbonneau, and J. I. Merz, "Temporal cross section for carrier capture by self-assembled quantum dots," *Microelectron. Eng.*, vol. 53, no. 1, pp. 241–244, Jun. 2000.

[26] S. Raymond, K. Hinzer, S. Fafard, and J. L. Merz, "Experimental determination of Auger capture coefficients in self-assembled quantum dots," *Phys. Rev. B*, vol. 61, no. 24, pp. R16 331–R16 334, Jun. 2000.

[27] Z. Mi and P. Bhattacharya, "Analysis of the linewidth-enhancement factor of long-wavelength tunnel-injection quantum-dot lasers," *IEEE J. Quantum Electron.*, vol. 43, no. 5, pp. 363–369, May 2007.

[28] K. J. Vahala and C. E. Zah, "Effect of doping on the optical gain and the spontaneous noise enhancement factor in quantum well amplifiers and lasers studied by simple analytical expressions," *Appl. Phys. Lett.*, vol. 52, no. 23, pp. 1945–1947, Jun. 1988.

Dae-Seob Han received the B.S. and M.S. degrees, both in materials science and engineering, from Chungnam National University, Daejeon, Korea, and Gwangju Institute of Science and Technology, Gwangju, South Korea, in 2000 and 2005, respectively. He is currently pursuing the Ph.D. degree in materials science and engineering at Virginia Polytechnic Institute and State University, focusing on the theory of quantum dot lasers.

He worked in ACIB Circuit R&D Center at Samsung for three years and in information electronic materials group at LG for two years.

Levon V. Asryan (M'04–SM'05) received the Ph.D. degree in physics and mathematics and the Doctor of Physical and Mathematical Sciences degree, both from the Ioffe Physico-Technical Institute, St. Petersburg, Russia, in 1988 and 2003, respectively.

From 1992 to 2004, he was a Member of Scientific Staff with the Ioffe Institute (since 1999 as a Senior Member). During 2000–2004, he was a Research Associate Professor with the Department of Electrical and Computer Engineering, State University of New York at Stony Brook, on leave from the Ioffe Institute. In 2004, he joined Virginia Polytechnic Institute and State University, where he is currently an Associate Professor of Materials Science and Engineering. His research interests include the theory of semiconductors and semiconductor devices, opto- and nanoelectronics, and photonics.

Dr. Asryan was awarded the State Prize of the Russian Federation in Science and Technology (Russia's highest scientific award) for the year 2001 and the first IEEE JOURNAL OF QUANTUM ELECTRONICS Best Paper Award for his work on quantum dot lasers.

ISSN 1063-7826, Semiconductors, 2011, Vol. 45, No. 11, pp. 1494–1500. © Pleiades Publishing, Ltd., 2011.
Original Russian Text © Z.N. Sokolova, I.S. Tarasov, L.V. Asryan, 2011, published in Fizika i Tekhnika Poluprovodnikov, 2011, Vol. 45, No. 11, pp. 1553–1559.

PHYSICS OF SEMICONDUCTOR DEVICES

Capture of Charge Carriers and Output Power of a Quantum Well Laser

Z. N. Sokolova[a]^, I. S. Tarasov[a], and L. V. Asryan[b]

[a] *Ioffe Physical Technical Institute, Russian Academy of Sciences, ul. Polytekhnicheskaya 26, St. Petersburg, 194021 Russia*
^e-mail: Zina.Sokolova@mail.ioffe.ru
[b] *Virginia Polytechnic Institute and State University, Blacksburg, Virginia 24061, USA*

Submitted April 20, 2011; accepted for publication April 29, 2011

Abstract—The effect of noninstantaneous carrier capture by a nanoscale active region on the power characteristics of a semiconductor laser is studied. A laser structure based on a single quantum well is considered. It is shown that delayed carrier capture by the quantum well results in a decrease in the internal differential quantum efficiency and sublinearity of the light–current characteristic of the laser. The main parameter of the developed theoretical model is the velocity of carrier capture from the bulk (waveguide) region to the two-dimensional region (quantum well). The effect of the capture velocity on the dependence of the following laser characteristics on the pump current density is studied: the output optical power, internal quantum efficiency of stimulated emission, current of stimulated recombination in the quantum well, current of spontaneous recombination in the optical confinement layer, and carrier concentration in the optical confinement layer. A decrease in the carrier capture velocity results in a larger sublinearity of the light–current characteristic, which results from an increase in the injection current fraction expended to parasitic spontaneous recombination in the optical confinement layer and, hence, a decrease in the injection current fraction expended to stimulated recombination in the quantum well. A comparison of calculated and experimental light–current characteristics for a structure considered as an example shows that good agreement between them (up to a very high injection current density of 45 kA/cm^2) is attained at a capture velocity of 2×10^6 cm/s. The results of this study can be used to optimize quantum well lasers for generating high optical powers.

DOI: 10.1134/S1063782611110261

1. INTRODUCTION

Our objective is to theoretically study the effect of charge-carrier capture by a nanoscale active region (quantum well, QW) on the optical power of semiconductor lasers. In the most commonly used laser separate-confinement heterostructures, the nanoscale active region is "built into" the waveguide region (optical confinement layer, OCL) based on a wide-gap semiconductor material. The optical confinement layer in such a structure performs two main functions: first, optical emission is confined mostly within this layer; second, the OCL is a reservoir from which carriers are "delivered" to the active region (the fact is that carriers are first injected from emitters to the OCL and only after this are they captured from it by the active region).

Carrier capture from the OCL by the active region occurs not instantaneously, but at a finite rate. This results in accumulation of carriers and an increase in their concentration in the waveguide region as the pump current increases under conditions of stimulated emission. The increase in the carrier concentration in the OCL, in turn, leads to amplification of parasitic spontaneous recombination in the OCL [1–9]. As a result, the internal quantum efficiency of stimulated emission decreases with the injection current; therefore, the light–current (L–I) characteristic of the laser with a quantum-confined active region becomes sublinear [10, 11]. Thus, the carrier accumulation in the waveguide region, which occurs due to the finite rate of their capture by the active region, can be one of the causes limiting the achievement of a high output power in a laser with a quantum-confined active region.

The mechanism of L–I characteristic nonlinearity in semiconductor lasers caused by delayed carrier capture by the quantum-confined active region was studied theoretically in [10, 11]. A universal analytical expression was derived for the internal quantum efficiency, which is applicable to QW, quantum-wire, and quantum dot lasers. In [10, 11], the following assumptions were made: (i) the internal optical loss α_{int} in the laser structure remains unchanged as the pump current density j increases, i.e., $\alpha_{int} = \text{const}(j)$; (ii) the electrical neutrality takes place separately in the active region and OCL—i.e., electron and hole concentrations are equal in both the active and waveguide regions. It immediately follows from these assumptions that the carrier concentration in the active region remains unchanged as j increases beyond the lasing threshold. The results of the general theoretical treatment were illustrated in [10, 11] with quantum dot lasers.

QW lasers represent the main and most actively used type of injection lasers, to which a large number of experimental and theoretical studies are devoted. Nevertheless, to our knowledge, in the available publications, there has been no systematic analysis of the dependence of the effect of charge-carrier capture from the waveguide region by the QW on the laser power characteristics. We give such an analysis here, using the general theoretical approach developed in [10, 11] and considering the QW laser. The calculations are performed for the experimental Fabry–Perot cavity separate-confinement laser structure described in [12]. Good agreement between calculated and experimental L–I characteristics (see below) is attained up to a very high injection current density of 45 kA/cm^2, which confirms the validity of the assumptions used in [10, 11] and in this study for such values of j.

2. INTERNAL DIFFERENTIAL QUANTUM EFFICIENCY AND LIGHT–CURRENT CHARACTERISTIC OF A QUANTUM-WELL LASER

The output optical power of the laser is determined by the expression [10, 11]

$$P = \frac{\hbar\omega}{e} S(j - j_{th})\eta_{int}\frac{\beta}{\beta + \alpha_{int}}, \quad (1)$$

where $\hbar\omega$ is the photon energy, e is the elementary charge, $S = LW$ is the contact stripe area, L is the Fabry–Perot cavity length, W is the contact stripe width, j is the injection current density, j_{th} is the threshold current density, $\beta = (1/L)\ln(1/R)$ is the loss due to emission output from the cavity, R is the mirror reflectivity, and α_{int} is the internal optical loss in the laser structure.

The internal differential quantum efficiency η_{int} of stimulated emission entering (1) is defined by the ratio of the current density j_{stim} of stimulated recombination to the excess injection current density over the threshold current density j–j_{th} [6],

$$\eta_{int}(j) = \frac{j_{stim}(j)}{j - j_{th}}. \quad (2)$$

In the structure under consideration, the waveguide layer material is GaAs, which makes it possible to disregard the Auger recombination in this layer. In [10, 11], the following expression was obtained for such a case:

$$\eta_{int} = \left\{\frac{1}{2} + \frac{j_{th}^{OCL}}{j_{capt, th}} + \sqrt{\left(\frac{1}{2} + \frac{j_{th}^{OCL}}{j_{capt, th}}\right)^2 + \frac{j_{th}^{OCL}}{j_{capt, th}}\frac{j - j_{th}}{j_{capt, th}}}\right\}^{-1}, \quad (3)$$

where j_{th}^{OCL} is the parasitic component of the threshold current density, caused by spontaneous radiative recombination in the OCL; $j_{capt, th}$ is the current density of carrier capture from the OCL by a quantum-confined active region, also taken at the lasing threshold.

The expression for j_{th}^{OCL} is given by

$$j_{th}^{OCL} = ebB_{3D}(n_{th}^{OCL})^2, \quad (4)$$

where b is the OCL width, B_{3D} is the coefficient of spontaneous radiative recombination in the bulk region (OCL), and n_{th}^{OCL} is the free carrier concentration in the OCL at the lasing threshold.

The current density of carrier capture from the OCL by the QW at the lasing threshold is given by [10, 11]

$$j_{capt, th} = en_{th}^{OCL}(1 - f_n)v_{capt, 0}, \quad (5)$$

where f_n is the filling factor (population) of the state corresponding to the bottom edge of the size quantization subband in the QW, $v_{capt, 0}$ is the velocity of capture by the unoccupied (at $f_n = 0$) single QW, measured in cm/s. The factor $(1 - f_n)$ in (5) accounts for the filling of the size quantization subband in the QW.

Despite the fact that $v_{capt, 0}$ is the only parameter adequately describing carrier capture from the bulk region (OCL) by the two-dimensional (2D) region (QW) (see [11, 13], where this problem is discussed), there is small number of studies devoted to this parameter (see [14–18]). It should also be noted that, in a certain sense, the capture velocity is an analogue of the surface recombination velocity.

The threshold current density j_{th} entering (1) and (3) is given by

$$j_{th} = j_{th}^{QW} + j_{th}^{OCL}, \quad (6)$$

where j_{th}^{OCL} is given by expression (4), and j_{th}^{QW} is the recombination current density in the nanoscale QW. As in the case of the GaAs OCL, we disregard Auger recombination in the InGaAs QW; this means that j_{th}^{QW} is controlled by spontaneous radiative recombination,

$$j_{th}^{QW} = eB_{2D}(n^{QW})^2, \quad (7)$$

where B_{2D} is the coefficient of spontaneous radiative recombination in the 2D region (QW) and n^{QW} is the 2D carrier concentration in the QW. Within the theoretical model of [10, 11], used in the present study (see the next Section), n^{QW} remains unchanged as the pump current increases beyond the lasing threshold.

3. CARRIER CONCENTRATIONS IN THE QUANTUM WELL, WAVEGUIDE REGION AND CURRENT DENSITIES $j_{th}^{OCL}, j_{th}, j_{capt, th}$

To determine the internal differential quantum efficiency and then the output optical power, the cur-

rent densities j_{th}^{OCL}, j_{th}, and $j_{capt,\,th}$ entering Eq. (3) should be determined. In this section, we show that the carrier concentration in the OCL at the lasing threshold; and, hence, the current densities j_{th}^{OCL}, j_{th}, and $j_{capt,\,th}$ are analytically expressed in terms of the carrier concentration n^{QW} in the QW.

The lasing condition (equality of the modal gain to the total optical loss) in the structure with the QW can be written as [19]

$$g^{max}\left[1-\exp\left(-\frac{n^{QW}}{N_c^{2D}}\right)-\exp\left(-\frac{m_e^{QW}}{m_{hh}^{QW}}\frac{n^{QW}}{N_c^{2D}}\right)\right] = \beta+\alpha_{int}, \quad (8)$$

where

$$N_c^{2D} = \frac{m_e^{QW}k_BT}{\pi\hbar^2} \quad (9)$$

is the 2D effective density of states in the QW conduction band, m_e^{QW} and m_{hh}^{QW} are the effective masses of electrons and heavy holes in the QW, k_B is the Boltzmann constant, and T is the temperature.

The maximum modal gain of the QW laser, entering (8) is given by [19]

$$\begin{aligned} g^{max} &= \pi\frac{\alpha}{\sqrt{\epsilon}}\frac{2m_{ehh}^{QW}(P_{QW}/\hbar)^2}{E_0}I_{overlap}\frac{\Gamma}{a} \\ &= \pi\frac{\alpha}{\sqrt{\epsilon}}\frac{m_{hh}^{QW}}{m_e^{QW}+m_{hh}^{QW}}\left[1-\frac{m_e^{QW}}{m_0}\right] \\ &\times\frac{E_g^{QW}(E_g^{QW}+\Delta_0^{QW})}{E_g^{QW}+(2/3)\Delta_0^{QW}}\frac{1}{E_0}I_{overlap}\frac{\Gamma}{a}, \end{aligned} \quad (10)$$

where $\alpha = e^2/\hbar c$ is the fine-structure constant, $\sqrt{\epsilon}$ is the refractive index of the waveguide region material, $m_{ehh}^{QW} = m_e^{QW}m_{hh}^{QW}/(m_e^{QW}+m_{hh}^{QW})$ is the reduced electron and heavy hole mass in the QW, $E_0 = E_g^{QW}+\varepsilon_n+\varepsilon_p$ is the energy of the laser transition in the QW, E_g^{QW} is the band gap of the QW material, $\varepsilon_{n,\,p}$ are the energies of bottom edges of the size quantization subbands of electrons and holes in the QW (measured from the well bottom), Γ is the optical confinement factor in the QW, a is the QW width, m_0 is the free electron mass, and Δ_0^{QW} is the energy of spin–orbit splitting in the QW material.

The quantity $I_{overlap}$ in expression (10) is the squared overlap integral of electron and hole wave functions in the QW [19]. In the calculations, we set it equal to unity, which is valid for not very thin the QW.

In (10), the following expression for the Kane parameter P_{QW} is used:

$$(P_{QW})^2 = \frac{\hbar^2}{2}\left(\frac{1}{m_e^{QW}}-\frac{1}{m_0}\right)\frac{E_g^{QW}(E_g^{QW}+\Delta_0^{QW})}{E_g^{QW}+(2/3)\Delta_0^{QW}}. \quad (11)$$

The coefficient of spontaneous radiative recombination in the 2D region (QW), measured in $cm^2\ s^{-1}$ and entering expression (7), is written as [20]

$$B_{2D} = \frac{4}{3}\pi\alpha\sqrt{\epsilon}\frac{\hbar}{(m_e^{QW}+m_{hh}^{QW})k_BT}E_0\left(\frac{P_{QW}}{\hbar c}\right)^2. \quad (12)$$

The coefficient of spontaneous radiative recombination in the bulk region (OCL), measured in cm^3/s and entering expression (4), is written as [20, 21]

$$\begin{aligned} B_{3D} = \frac{4}{3}\sqrt{2}\pi^{3/2}\alpha\sqrt{\epsilon}&\frac{\hbar^2}{[(m_e^{OCL}+m_{hh}^{OCL})k_BT]^{3/2}} \\ &\times E_g^{OCL}\left(\frac{P_{OCL}}{\hbar c}\right)^2, \end{aligned} \quad (13)$$

where m_e^{OCL} and m_{hh}^{OCL} are the electron and heavy hole effective masses, E_g^{OCL} is the band gap, and P_{OCL} is the Kane parameter for the OCL material.

Expression (8), which is satisfied at the lasing threshold ($j = j_{th}$) and above it ($j > j_{th}$), is an algebraic equation for determining n^{QW}. Since the injection current density j does not enter this equation, its solution for n^{QW} is independent of j; i.e., the carrier concentration in the QW remains unchanged as j increases beyond the lasing threshold. As is noted above and seen directly from (8), the n^{QW} independence of j is a consequence of the assumptions that the internal optical loss coefficient α_{int} is independent of j and electrical neutrality takes place separately in the active region ($n^{QW} = p^{QW}$) and OCL ($n^{OCL} = p^{OCL}$).

Assuming that the carrier distribution in the structure is equilibrium below the lasing threshold and at the threshold itself, both the carrier concentration n^{QW} in the QW and the free carrier concentration n_{th}^{OCL} in the OCL at the lasing threshold can be expressed in terms of the filling factor f_n of the size quantization subband edge in the QW. Thus, the carrier concentration in the QW is written as [22–24]

$$n^{QW} = N_c^{2D}\ln\frac{1}{1-f_n}. \quad (14)$$

The free-carrier concentration in the OCL is given by [21, 25]

$$n_{th}^{OCL} = n_1^{OCL}\frac{f_n}{1-f_n}, \quad (15)$$

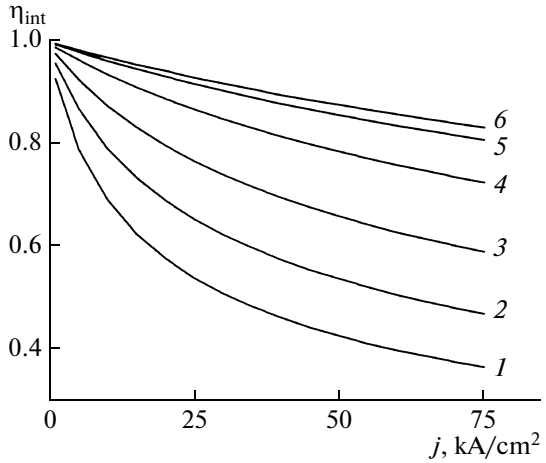

Fig. 1. Dependences of the internal differential quantum efficiency on the pump current density at various capture velocities into the QW, $v_{capt,\,0}$ = (*1*) 0.5, (*2*) 0.7, (*3*) 1, (*4*) 1.5, (*5*) 2, and (*6*) 3×10^6 cm/s.

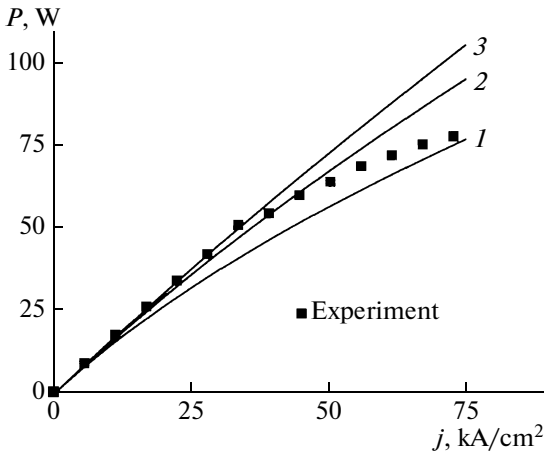

Fig. 2. Dependences of the output optical power on the pump current density at various capture velocities into the QW, $v_{capt,\,0}$ = (*1*) 1.2, (*2*) 2, and (*3*) 3×10^6 cm/s. Dots correspond to the experimental L–I characteristic [12].

where

$$n_1^{OCL} = N_c^{3D} \exp\left(-\frac{\Delta E_c - \varepsilon_n}{k_B T}\right). \quad (16)$$

In (16), ΔE_c is the conduction band edge offset at the OCL–QW heterojunction, and the effective bulk density of states in the OCL conduction band is given by

$$N_c^{3D} = 2\left(\frac{m_e^{OCL} k_B T}{2\pi\hbar^2}\right)^{3/2}. \quad (17)$$

From Eq. (14), we can express f_n in terms of the carrier concentration in the QW,

$$f_n = 1 - \exp\left(-\frac{n^{QW}}{N_c^{2D}}\right). \quad (18)$$

Substituting (18) into (15), we obtain the following expression for the free-carrier concentration in the OCL at the lasing threshold as a function of the 2D carrier concentration in the QW

$$n_{th}^{OCL} = n_1^{OCL}\left[\exp\left(\frac{n^{QW}}{N_c^{2D}}\right) - 1\right]. \quad (19)$$

Thus, the single equation requiring a numerical solution in the used model is algebraic equation (8) to determine n^{QW}. Having solved this equation, we immediately determine n_{th}^{OCL} using (19). Then we easily calculate all quantities entering expression (3) for the internal differential quantum efficiency: the component of the total threshold current density j_{th}^{OCL} (expression (4)), the total threshold current density j_{th} (expression (6)), and the current density $j_{capt,\,th}$ of carrier capture from the OCL by the QW at the lasing threshold (expression (5)).

4. EFFECT OF THE CAPTURE VELOCITY INTO THE QUANTUM WELL ON THE LINEARITY OF THE LIGHT–CURRENT CHARACTESTIC

In this section, we study the effect of the velocity of carrier capture by the QW on the laser L–I characteristic linearity. Using the theoretical model of Section 2, the internal differential quantum efficiency η_{int} is calculated (see (3)) as a function of the pump current density j (Fig. 1), and then the L–I characteristic is calculated (see (1) and Fig. 2). The calculations are performed at various velocities $v_{capt,\,0}$ of carrier capture from the OCL by the QW. The chosen range $v_{capt,\,0}$ = $(0.5–3) \times 10^6$ cm/s corresponds to published data [14, 16–18].

As an example of calculations, we consider an experimental Fabry–Perot cavity separate-confinement laser structure with a GaAs-based wide waveguide [12]. The active region consists of a single strained 80 Å-thick QW based on $In_{0.28}Ga_{0.72}As$. The n- and p-type emitter material is AlGaAs alloy. The following values of the parameters are used: the waveguide region width is $b = 1.7$ μm, the cavity length is L = 1.5 mm, the stripe contact width is $W = 100$ μm, the mirror reflectivity is $R = 0.32$, and the internal optical loss is $\alpha_{int} = 1$ cm^{-1}.

The calculated lasing wavelength is 1.044 μm. The experimentally measured wavelength at the intensity maximum of the lasing spectrum is 1.04 μm [12]. The carrier concentration in the QW determined from

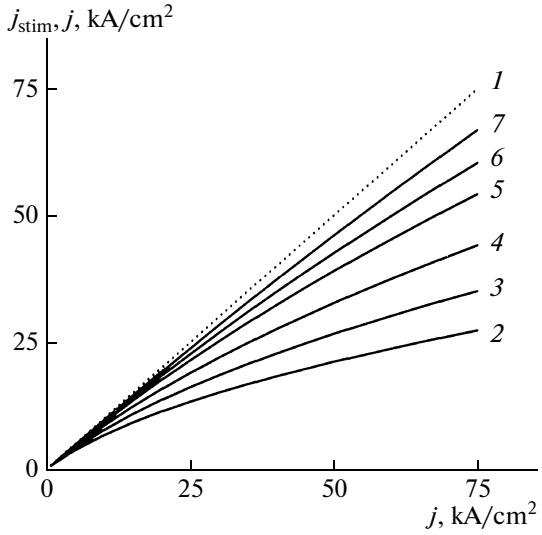

Fig. 3. Dependences of the current density of stimulated recombination on the pump current density at various capture velocities into the QW, $v_{capt,0}$ = (*2*) 0.5, (*3*) 0.7, (*4*) 1, (*5*) 1.5, (*6*) 2, and (*7*) 3×10^6 cm/s; (*1*) pump current density.

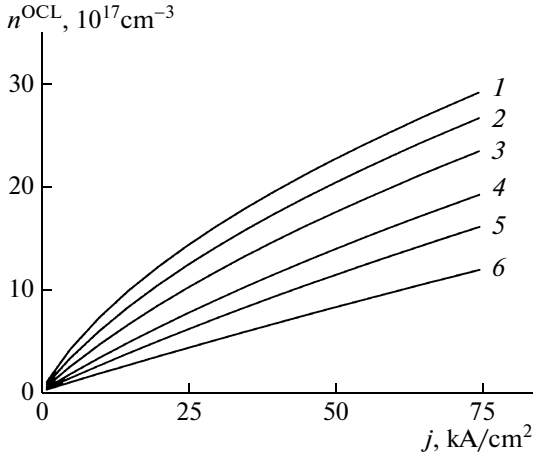

Fig. 4. Dependences of the carrier concentration in the waveguide region on the pump current density at various capture velocities into the QW, $v_{capt,0}$ = (*1*) 0.5, (*2*) 0.7, (*3*) 1, (*4*) 1.5, (*5*) 2, and (*6*) 3×10^6 cm/s.

Eq. (8) is $n^{QW} = 1.36 \times 10^{12}$ cm^{-2} and the free carrier concentration in the OCL at the lasing threshold, determined from (19), is $n_{th}^{OCL} = 2.8 \times 10^{16}$ cm^{-3}. The coefficients of spontaneous radiative recombination in the 2D and bulk regions, calculated by formulas (12) and (13) are $B_{2D} = 2.51 \times 10^{-4}$ cm^2/s and $B_{3D} = 2.04 \times 10^{-10}$ cm^3/s. The calculated threshold current density controlled only by spontaneous radiative recombination in the QW and OCL is $j_{th} = 78$ A/cm^2. The experimental threshold current density is 80 A/cm^2.

We can see in Fig. 1 that the internal differential quantum efficiency decreases with the injection current. This decrease is especially pronounced at low carrier capture velocities into the QW.

Figure 2 shows the dependences of the output optical power P on the pump current density j (L–I characteristic), calculated at various capture velocities $v_{capt,0}$. We can see that a decrease in $v_{capt,0}$ leads to a larger L–I characteristic sublinearity. For comparison, there is also shown the experimental L–I characteristic from [12] for the laser with the above parameters. The measurements in [12] were performed in the pulsed mode, which excluded the heating effects and associated L–I characteristic sublinearity disregarded in the model under consideration. The good agreement (up to very high injection current densities $j = 45$ kA/cm^2) of calculated and experimental L–I characteristics is attained at $v_{capt,0} = 2 \times 10^6$ cm/s. The deviation of the calculated L–I characteristic from experimental one at even higher j correlates with the observed broadening of the lasing spectrum [26] and can be caused by other factors (in particular, an increase in the carrier concentration in the QW) ignored in the used model.

Figure 3 shows the current density of stimulated recombination in the QW as a function of the injection current density at various $v_{capt,0}$, calculated according to the equation (see (2))

$$j_{stim}(j) = (j - j_{th})\eta_{int}(j). \quad (20)$$

We can see the large deviation of j_{stim} from $j - j_{th}$ at high j and small $v_{capt,0}$.

Figure 4 shows the dependence of the carrier concentration in the OCL on j, which is given by (see [10, 11])

$$n^{OCL}(j) = n_{th}^{OCL}\left[1 + \frac{j_{stim}(j)}{j_{capt,th}}\right]. \quad (21)$$

We can see that the effect of carrier accumulation in the waveguide region beyond the lasing threshold is pronounced even at high velocities of capture into the the QW: n^{OCL} at high pump currents is significantly (tens of times) higher than the threshold value n_{th}^{OCL}.

An increase in the carrier concentration in the waveguide region beyond the lasing threshold (Fig. 4), especially at low capture velocities, results in the enhancement of the "parasitic" process, i.e., spontaneous radiative recombination in the waveguide region. Consequently, the fraction of carriers involved in the "useful" stimulated recombination in the QW accordingly decreases. The current density of spontaneous radiative recombination in the waveguide region beyond the lasing threshold is given by

$$j_{spon}^{OCL}(j) = ebB_{3D}[n^{OCL}(j)]^2, \quad (22)$$

where $n^{OCL}(j)$ given by expression (21) is shown in Fig. 5 for various capture velocities. The increase in spontaneous radiative recombination in the OCL with the pump current density is in agreement with the experimental results [26, 27] at the current density as

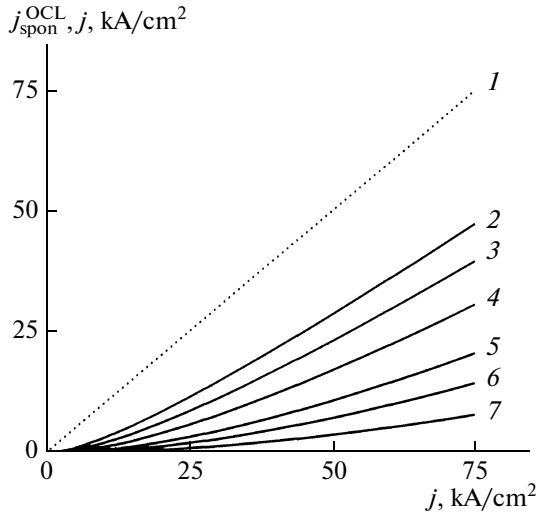

Fig. 5. Dependences of the current density of spontaneous recombination in the waveguide region on the pump current density at various capture velocities into the QW, $v_{capt,0}$ = (*2*) 0.5, (*3*) 0.7, (*4*) 1, (*5*) 1.5, (*6*) 2, and (*7*) 3×10^6 cm/s; (*1*) pump current density.

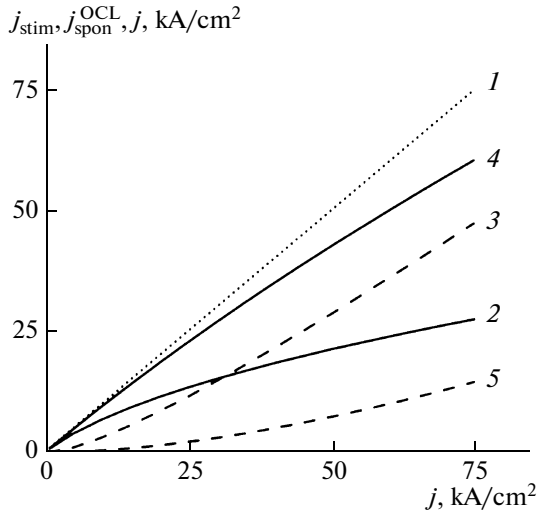

Fig. 6. Dependences of the current densities of (*2*, *4*) stimulated recombination in the QW and (*3*, *5*) spontaneous recombination in the waveguide region on the pump current density at two capture velocities into the QW, $v_{capt,0}$ = (*2*, *3*) 0.5 and (*4*, *5*) 2×10^6 cm/s; (*1*) pump current density.

high as $j \approx 45$ kA/cm^2. The substantial increase in spontaneous emission from the waveguide region at even higher pump current densities, observed in [26, 27], can be associated with the increase in the carrier concentration in the QW, which is disregarded in this study.

For comparison, Fig. 6 shows the current densities of stimulated recombination (in the QW) and spontaneous recombination (in the waveguide region). At $v_{capt,0} = 2 \times 10^6$ cm/s, j_{spon}^{OCL} is low in comparison with j_{stim} in the entire range of j shown in the figure. However, as the capture velocity decreases to 5×10^5 cm/s, j_{spon}^{OCL} begins to exceed j_{stim} even at the pump current density $j = 32$ kA/cm^2.

5. CONCLUSIONS

It is shown that noninstantaneous carrier capture from the waveguide region by the QW is a factor that significantly affects the laser power characteristics. The velocity of carrier capture from the bulk (waveguide) region by the 2D region (the QW) is used as the main parameter of the theoretical model. The lower the capture velocity, the stronger the carrier accumulation in the waveguide region. As the carrier concentration increases, the parasitic spontaneous radiative recombination in the waveguide region, i.e., the injection current fraction expended to this recombination, is enhanced. Accordingly, the fraction of injection current expended to stimulated recombination in the QW decreases; i.e., the internal differential quantum efficiency decreases, which results in sublinearity of the the laser L–I characteristic. Good agreement between calculated and experimental L–I characteristics was attained up to a very high injection current density of 45 kA/cm^2. The results of this study can be used to optimize QW lasers for generating high output optical powers.

ACKNOWLEDGMENTS

Z.N. Sokolova and I.S. Tarasov acknowledge the support of the federal targeted program “Scientific and Pedagogical Personnel of Innovative Russia” (contract no. P2319); L.V. Asryan acknowledges the support of the U.S. Army Research Office, grant no. W911-NF-08-1-0462.

REFERENCES

1. D. Z. Garbuzov, A. V. Ovchinnikov, N. A. Pikhtin, Z. N. Sokolova, I. S. Tarasov, and V. B. Khalfin, Sov. Phys. Semicond. **25**, 560 (1991).
2. W. Rideout, W. F. Sharfin, E. S. Koteles, M. O. Vassell, and B. Elman, IEEE Photon. Technol. Lett. **3**, 784 (1991).
3. N. Tessler, R. Nagar, G. Eisenstein, S. Chandrasekhar, C. H. Joyner, A. G. Dentai, U. Koren, and G. Raybon, Appl. Phys. Lett. **61**, 2383 (1992).
4. H. Hirayama, J. Yoshida, Y. Miyake, and M. Asada, Appl. Phys. Lett. **61**, 2398 (1992).
5. H. Hirayama, J. Yoshida, Y. Miyake, and M. Asada, IEEE J. Quantum Electron. **30**, 54 (1994).
6. L. A. Coldren and S. W. Corzine, *Diode Lasers and Photonic Integrated Circuits* (Wiley, New York, 1995).
7. G. W. Taylor and P. R. Claisse, IEEE J. Quantum Electron. **31**, 2133 (1995).

8. P. M. Smowton and P. Blood, IEEE J. Sel. Top. Quantum Electron. **3**, 491 (1997).
9. G. W. Taylor and S. Jin, IEEE J. Quantum Electron. **34**, 1886 (1998).
10. L. V. Asryan, S. Luryi, and R. A. Suris, Appl. Phys. Lett. **81**, 2154 (2002).
11. L. V. Asryan, S. Luryi, and R. A. Suris, IEEE J. Quantum Electron. **39**, 404 (2003).
12. A. V. Lyutetskii, K. S. Borshchev, N. A. Pikhtin, S. O. Slipchenko, Z. N. Sokolova, and I. S. Tarasov, Semiconductors **42**, 104 (2008).
13. D.-S. Han and L. V. Asryan, Nanotechnology **21**, 015201 (2010).
14. I. N. Yassievich, K. Schmalz, and M. Beer, Semicond. Sci. Technol. **9**, 1763 (1994).
15. C.-Y. Tsai, Y. H. Lo, R. M. Spencer, and L. F. Eastman, IEEEJ. Sel. Top. Quantum Electron. **1**, 316 (1995).
16. S. A. Solov'ev, I. N. Yassievich, and V. M. Chistyakov, Semiconductors **29**, 654 (1995).
17. A. Dargys and J. Kundrotas, Semicond. Sci. Technol. **13**, 1258 (1998).
18. R. A. Suris, NATO ASI Series E **323**, 197 (1996).
19. L. V. Asryan, N. A. Gun'ko, A. S. Polkovnikov, G. G. Zegrya, R. A. Suris, P.-K. Lau, and T. Makino, Semicond. Sci. Technol. **15**, 1131 (2000).
20. L. V. Asryan, Quantum Electron. **35**, 1117 (2005).
21. L. V. Asryan and R. A. Suris, Semicond. Sci. Technol. **11**, 554 (1996).
22. K. J. Vahala and C. E. Zah, Appl. Phys. Lett. **52**, 1945 (1988).
23. L. V. Asryan and S. Luryi, Appl. Phys. Lett. **83**, 5368 (2003).
24. L. V. Asryan and S. Luryi, IEEE J. Quantum Electron. **40**, 833 (2004).
25. L. V. Asryan and R. A. Suris, Semiconductors **38**, 1 (2004).
26. S. O. Slipchenko, Z. N. Sokolova, N. A. Pikhtin, K. S. Borshchev, D. A. Vinokurov, and I. S. Tarasov, Semiconductors **40**, 990 (2006).
27. D. A. Vinokurov, V. A. Kapitonov, A. V. Lyutetskii, N. A. Pikhtin, S. O. Slipchenko, Z. N. Sokolova, A. L. Stankevich, M. A. Khomylev, V. V. Shamakhov, K. S. Borshch¸v, I. N. Arsent'ev, and I. S. Tarasov, Semiconductors **41**, 984 (2007).

Translated by A. Kazantsev

ISSN 1063-7826, Semiconductors, 2012, Vol. 46, No. 8, pp. 1044–1050. © Pleiades Publishing, Ltd., 2012.
Original Russian Text © Z.N. Sokolova, I.S. Tarasov, L.V. Asryan, 2012, published in Fizika i Tekhnika Poluprovodnikov, 2012, Vol. 46, No. 8, pp. 1067–1073.

PHYSICS OF SEMICONDUCTOR DEVICES

Effect of the Number of Quantum Wells in the Active Region on the Linearity of the Light–Current Characteristic of a Semiconductor Laser

Z. N. Sokolova[a]^, I. S. Tarasov[a], and L. V. Asryan[b]

[a] *Ioffe Physical–Technical Institute, Russian Academy of Sciences, St. Petersburg, 194021 Russia*

^ *e-mail: Zina.Sokolova@mail.ioffe.ru*

[b] *Virginia Polytechnic Institute and State University, Blacksburg, Virginia 24061, USA*

Submitted February 1, 2012; accepted for publication, February 27, 2012

Abstract—The light–current characteristic of a semiconductor laser with multiple quantum wells (QWs) is calculated, with the delayed capture of charge carriers from the waveguide region into the wells taken into account. It is shown that increasing the number of QWs is a more effective way to improve the power characteristics of a laser, compared with an increase in the velocity of carrier capture into each of the wells. For example, using two QWs as the active region leads to a substantial increase in the internal quantum efficiency of stimulated emission and to a significantly better linearity of the light–current characteristic of the laser, compared with a single-well structure. At the same time, using three or more QWs only slightly improves the power characteristics of the laser, compared with the double-well structure. Thus, a double-well structure is the optimal as regards high output power and simplicity of growth.

DOI: 10.1134/S1063782612080222

1. INTRODUCTION

Increasing the power of output optical emission is one of the most topical tasks in the development of semiconductor lasers. Lasers with a nanosize active region consisting of one or multiple quantum wells (QWs) exhibit "saturation" of the emission power at high pump currents and the light–current (L–I) characteristic becomes sublinear [1, 2]. According to [3, 4], a possible reason for this behavior is the delayed capture of charge carriers from the waveguide region of a separate-confinement laser structure into the QWs. In [5], the effect of the carrier-capture velocity into a single QW on the optical output power of a laser with a Fabry–Perot cavity was theoretically studied.

The present study is concerned with the effect of delayed carrier capture on the power characteristics of a laser with multiple QWs. It is shown that the use of two QWs as the active region significantly improves the linearity of the L–I characteristic and the output power, compared with a structure with a single QW. At the same time, a further increase in the number of QWs leads only to a slight improvement of the laser's power characteristics. Thus, with consideration for the fact that the growth of a defect-free structure with a larger number of QWs may be technologically more complicated, a conclusion is made that a double-well structure is optimal for high-power lasing.

2. INTERNAL QUANTUM EFFICIENCY AND L–I CHARACTERISTIC OF A LASER WITH MULTIPLE QWs

This study employs the model described in detail in [5]. The general theoretical approach was developed in [3, 4]. Calculations were made for a separate-confinement laser heterostructure with a GaAs waveguide region and an active region consisting of multiple $In_{0.28}Ga_{0.72}As$ QWs of the same thickness (80 Å). Charge carriers are delivered to the active region of a structure of this kind indirectly, via injection from AlGaAs emitters into the waveguide region (optical confinement layer, OCL) and further via capture from the OCL into the QWs. The capture velocity being finite, carriers accumulate in the OCL as the pump current increases to above the lasing threshold [3–5]. As the carrier concentration in the OCL, n^{OCL}, increases, the parasitic spontaneous recombination in this layer becomes more pronounced [6–13]. Because the dependence of the velocity of this recombination on n^{OCL} is superlinear (quadratic or cubic in cases when spontaneous radiative recombination or Auger recombination is the dominant recombination mechanism), the internal quantum efficiency of stimulated emission from QWs decreases with increasing current. As a result, the L–I characteristic of the laser becomes sublinear.

The L–I characteristic of a semiconductor laser (the output emission power as a function of the pump current density) is given by the expression

$$P(j) = \frac{\hbar\omega}{e} S(j - j_{th}) \eta_{int}(j) \frac{\beta}{\beta + \alpha_{int}}, \qquad (1)$$

where $\hbar\omega$ is the photon energy; e is the elementary charge; $S = LW$ is the stripe-contact area; L is the length of the Fabry–Perot cavity; W is the stripe-contact width; j is the injection current density; j_{th} is the threshold current density; $\beta = (1/L)\ln(1/R)$ is the mirror loss; R is the mirror reflectance; and α_{int} is the internal optical loss. The following values were used in our calculations: $L = 1.5$ mm, $W = 100$ μm, and $R = 0.32$. The photon energy $\hbar\omega = 1.188$ eV and, accordingly, the lasing wavelength $\lambda_0 = 1.044$ μm.

The internal differential quantum efficiency of stimulated emission, η_{int}, is defined as the ratio of the current density of stimulated recombination $j_{stim}(j)$ to the excess of the injection current density j over the threshold current density j_{th}: $\eta_{int}(j) = j_{stim}(j)/(j - j_{th})$. For η_{int}, the following expression has been derived [3, 4]:

$$\eta_{int}(j) = \frac{1}{\frac{1}{2} + \frac{j_{th}^{OCL}}{j_{capt,\,th}} + \sqrt{\left(\frac{1}{2} + \frac{j_{th}^{OCL}}{j_{capt,\,th}}\right)^2 + \frac{j_{th}^{OCL}}{j_{capt,\,th}}\frac{j - j_{th}}{j_{capt,\,th}}}}, \quad (2)$$

where

$$j_{th}^{OCL} = ebB_{3D}(n_{th}^{OCL})^2 \quad (3)$$

is the parasitic component of the threshold current density, due to spontaneous radiative recombination in the OCL; b is the OCL width; B_{3D} is the spontaneous radiative recombination coefficient in the OCL (see an expression for B_{3D} in [14, 15]; and n_{th}^{OCL} is the free carrier concentration in the OCL at the lasing threshold.

The current density of carrier capture (at the lasing threshold) from the OCL into N_{QW} identical (with the same width and composition) QWs is written as

$$j_{capt,\,th} = en_{th}^{OCL}N_{QW}(1 - f_n)v_{capt,\,0}, \quad (4)$$

where f_n is the degree of filling (occupancy) of the state corresponding to the lower edge of the quantum-confinement subband in a QW; $v_{capt,\,0}$ is the capture velocity into a single empty (at $f_n = 0$) QW, measured in cm s^{-1}. The capture velocity plays a key role in our theoretical model. We use here $v_{capt,\,0}$ values in the range $(0.5–2) \times 10^6$ cm s^{-1}, which is in agreement with [16–19].

The threshold current density is equal to the sum

$$j_{th} = j_{th}^{QW} + j_{th}^{OCL}, \quad (5)$$

in which the parasitic component j_{th}^{OCL} is given by (3), and the component caused by the spontaneous radiative recombination in the QWs is

$$j_{th}^{QW} = eN_{QW}B_{2D}(n^{QW})^2, \quad (6)$$

where B_{2D} is the spontaneous radiative recombination coefficient in a 2D region (QW) (see expression for B_{2D} in [14]), and n^{QW} is the 2D carrier concentration in each QW (we remind that we consider the case of identical QWs, i.e., n^{QW} is the same in all QWs). In terms of the model used here and in [3–5], n^{QW} remains unchanged as the current increases to above the lasing threshold (for this reason we do not use the subscript "th" (stemming from "threshold") in the designation n^{QW}).

Provided that, below and up to the lasing threshold, there is equilibrium charge-carrier distribution in the structure [15, 20], not only j_{th}^{QW} [see (6)], but also the current densities j_{th}^{OCL} (and, consequently, j_{th}) and $j_{capt,\,th}$ appearing in expression (2) for η_{int} are analytically expressed in terms of the carrier concentration in the QW, n^{QW}. This concentration is found from the following lasing condition (equality of the modal gain coefficient to the total optical loss) [5, 21, 22]:

$$N_{QW}g^{max}\left[1 - \exp\left(-\frac{n^{QW}}{N_c^{2D}}\right) - \exp\left(-\frac{m_e^{QW}}{m_{hh}^{QW}}\frac{n^{QW}}{N_c^{2D}}\right)\right] = \beta + \alpha_{int}, \quad (7)$$

where g^{max} is the maximum modal gain coefficient of the laser per QW (see expressions (10) and (3) for g^{max} in [5] and [22], respectively); m_e^{QW} and m_{hh}^{QW} are the effective electron and hole masses in the QW; and N_c^{2D} is the 2D effective density of states in the conduction band of a single QW.

It can be seen from (2) that, at a given excess of the injection current density over the threshold current density, $j - j_{th}$, the internal quantum efficiency is governed by the ratio $j_{th}^{OCL}/j_{capt,\,th}$. The smaller this parameter, the higher η_{int} (see [4], where this parameter is discussed for a quantum-dot semiconductor laser). Taking into account (3) and (4), we have for $j_{th}^{OCL}/j_{capt,\,th}$ the following

$$\frac{j_{th}^{OCL}}{j_{capt,\,th}} = \frac{bB_{3D}}{v_{capt,\,0}}\frac{n_{th}^{OCL}}{N_{QW}(1 - f_n)}. \quad (8)$$

The first fraction on the right-hand side combines quantities independent of N_{QW}, and the second, those N_{QW}-dependent.

The free carrier concentration in the OCL at the lasing threshold is expressed in terms of the 2D carrier concentration in the QW, n^{QW} [5, 22]:

$$n_{th}^{OCL} = n_1^{OCL}\left[\exp\left(\frac{n^{QW}}{N_c^{2D}}\right) - 1\right], \quad (9)$$

where

$$n_1^{OCL} = N_c^{3D}\exp\left(-\frac{\Delta E_c - \varepsilon_n}{k_B T}\right). \quad (10)$$

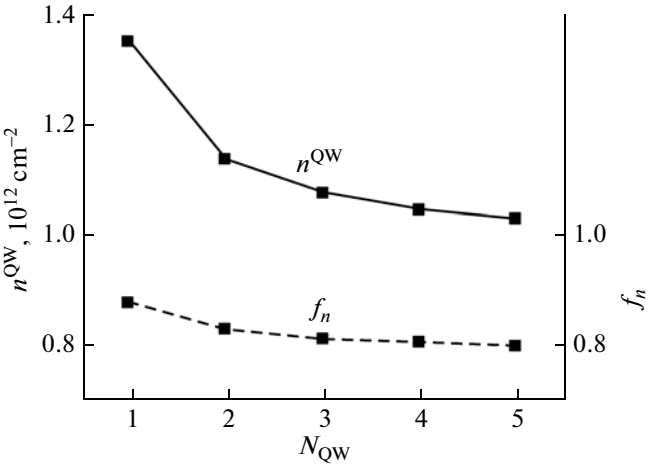

Fig. 1. 2D carrier concentration (left-hand axis, solid line) and degree of filling of the quantum-confinement subband (right-hand axis, dashed line) in each QW vs. the number of QWs, N_{QW}. Throughout the study the internal loss α_{int} was assumed to be independent of the number of QWs and equal to 1 cm^{-1}.

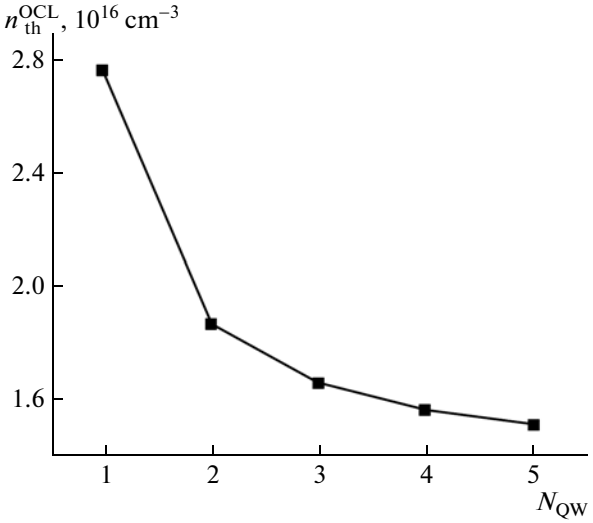

Fig. 2. Free carrier concentration in the waveguide region at the lasing threshold vs. the number of QWs.

Here, N_c^{3D} is the bulk effective density of states in the conduction band of the OCL; ΔE_c is the conduction band offset at the OCL–QW heterointerface; ε_n is the lower edge energy of the electron quantum-confinement subband, reckoned from the well bottom; k_B is the Boltzmann constant; and T is the temperature.

The degree of filling of the edge of the quantum-confinement subband in the QW is also expressed in terms of n^{QW} [5, 23–25]:

$$f_n = 1 - \exp\left(-\frac{n^{QW}}{N_c^{2D}}\right). \quad (11)$$

Using (9) and (11), we can represent expression (8) for the $j_{th}^{OCL}/j_{capt,\,th}$ ratio as

$$\frac{j_{th}^{OCL}}{j_{capt,\,th}} = \frac{bB_{3D}n_1^{OCL}}{v_{capt,\,0}}\frac{1}{N_{QW}}\exp\left(\frac{n^{QW}}{N_c^{2D}}\right)\left[\exp\left(\frac{n^{QW}}{N_c^{2D}}\right) - 1\right]. \quad (12)$$

Here, it can be seen from the lasing condition (7) that the 2D carrier concentration n^{QW} in each QW is independent of the capture velocity $v_{capt,\,0}$ into a single QW, but falls with increasing number of QWs, N_{QW} (Fig. 1, left-hand axis, solid line). Accordingly, with increasing N_{QW}, the degree of filling of the edge of the quantum-confinement subband in the QW decreases [11] (Fig. 1, right-hand axis, dashed line). This result is a natural consequence of our assumption that the total optical loss (right-hand part of expression (7)) is independent of the number of QWs, which means that, with increasing N_{QW}, lower filling of each of the QWs by charge carriers is required to provide the modal gain coefficient (left-hand part of expression (7)) at a given loss level.

Because n^{QW} decreases with increasing number of QWs, the free carrier concentration n_{th}^{OCL} in the OCL at the lasing threshold also decreases (see (9)) (Fig. 2). Thus, as follows from (8) and (12), the parameter $j_{th}^{OCL}/j_{capt,\,th}$ decreases both with increasing capture velocity $v_{capt,\,0}$ into a single QW and with increasing number of QWs (Fig. 3). At a given excess of the injection current density over the threshold current density, $j - j_{th}$, a decrease in the parameter $j_{th}^{OCL}/j_{capt,\,th}$ results in an increase in the internal quantum efficiency (see (2)) and a weakening of its dependence on the injection current density, i.e., the linearity of the L–I characteristic is improved (see (1)) . The possibility of improving the linearity of the L–I characteristic by using a greater number of QWs is an extremely important result. The point is that, in the case when the OCL and QW compositions and the QW size are specified (which may be governed by technological factors or by the required emission wavelength), the capture velocity $v_{capt,\,0}$ into a single QW is fixed, whereas the number of QWs can be varied.

It should also be noted that, because the 2D carrier concentration n^{QW} depends on the number N_{QW} of QWs and is independent of $v_{capt,\,0}$, the dependence of the parameter $j_{th}^{OCL}/j_{capt,\,th}$ (see (12)) on the number of QWs is stronger than that on the capture velocity into a single QW. This means that, for example, doubling the N_{QW} will improve the linearity of the L–I characteristic to a greater extent than a similar increase in $v_{capt,\,0}$ (see Figs. 10, 11).

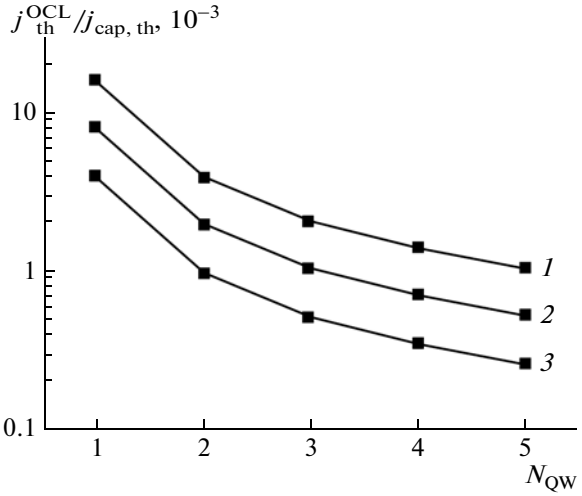

Fig. 3. Parameter $j_{th}^{OCL}/j_{capt,\,th}$ governing the linearity of the L–I characteristic (see (12) and (2))] vs. the number of QWs at various carrier capture velocities into a single QW, $v_{capt,\,0}$ (10^6 cm s^{-1}): (*1*) 0.5, (*2*) 1, and (*3*) 2.

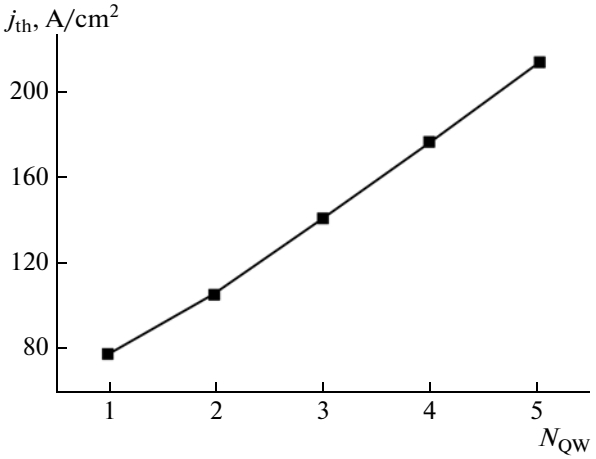

Fig. 4. Threshold current density vs. the number of QWs.

The above condition of a fixed difference $j - j_{th}$ appearing in (1) and (2) does not greatly restrict the validity of the conclusion that η_{int} increases and the linearity of the L–I characteristic is improved with increasing number of QWs. Indeed, despite the fact that threshold current density j_{th} depends on N_{QW} (see below), of primary interest are high levels of emission power, i.e., pump current densities j that greatly exceed the threshold current density j_{th}. At these j, j_{th} in expressions (1) and (2) can be disregarded.

The increase in the carrier concentration n^{OCL} in the OCL to above the lasing threshold with increasing j is described by the following expression [3–5]:

$$n^{OCL}(j) = n_{th}^{OCL}\left[1 + \frac{j_{stim}(j)}{j_{capt,\,th}}\right] = n_{th}^{OCL}\left[1 + \frac{j - j_{th}}{j_{capt,\,th}}\eta_{int}(j)\right], \quad (13)$$

where the threshold concentration n_{th}^{OCL} is given by (9) (see Fig. 2 for the dependence of n_{th}^{OCL} on the number of QWs).

3. DISCUSSION

In this section, we present the results of calculations in terms of the model described above. Throughout our study, the internal optical loss coefficient α_{int} was assumed to be independent of the number of QWs and equal to 1 cm^{-1}.

The 2D carrier concentration and the degree of filling of the edge of the quantum-confinement subband in each of the QWs are shown in Fig. 1 as functions of the number of QWs. The dependence of the free carrier concentration in the OCL at the lasing threshold on the number of QWs is shown in Fig. 2.

Figure 3 shows the parameter $j_{th}^{OCL}/j_{capt,\,th}$ as a function of the number of QWs. As demonstrated in Section 2 (and can be seen in Figs. 3 and 5–8), this parameter governs the dependence of the internal differential quantum efficiency on the pump current and, consequently, also the linearity of the L–I characteristic.

The threshold current density j_{th} is shown in Fig. 4 as a function of the number of QWs. It can be seen that j_{th} steadily grows with increasing N_{QW} in the structure under consideration. At certain N_{QW}, j_{th} may also have a minimum (see, e.g., [21]).

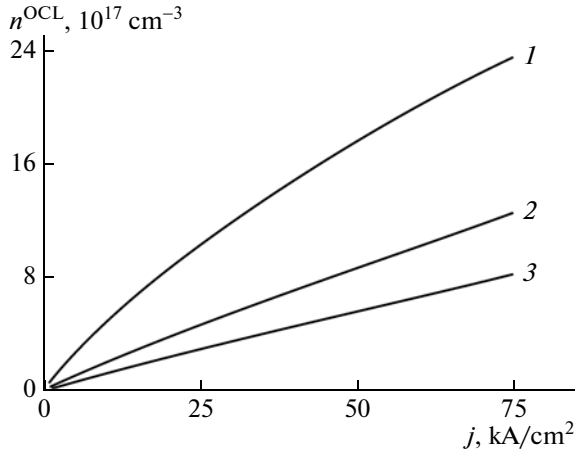

Fig. 5. Carrier concentration in the waveguide region vs. the pump current density for structures with (*1*) one, (*2*) two, and (*3*) three QWs. The capture velocity into a single well $v_{capt,\,0} = 10^6$ cm s^{-1}.

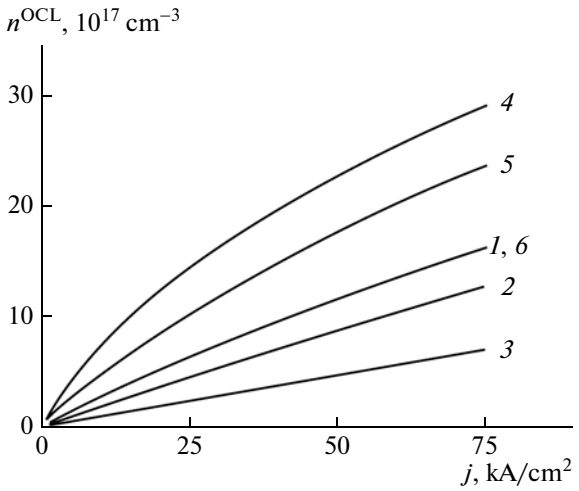

Fig. 6. Carrier concentration in the waveguide region vs. the pump current density for structures with (*1–3*) two and (*4–6*) one QW at various carrier capture velocities into a single QW, $v_{capt,0}$ (10^6 cm s^{-1}): (*1*) 0.7, (*2*, *5*) 1, (*3*, *6*) 2, and (*4*) 0.5.

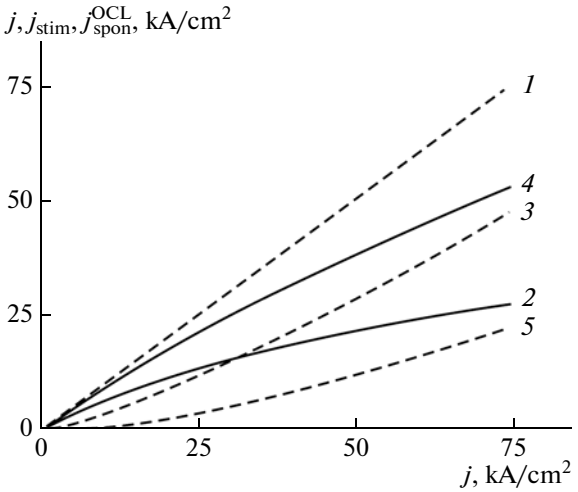

Fig. 7. Current densities of (*2*, *4*) stimulated recombination in QWs and (*3*, *5*) spontaneous recombination in the waveguide region in structures with (*2*, *3*) one and (*4*, *5*) two QWs vs. the pump current density at a capture velocity into a single QW of $v_{capt,0} = 5 \times 10^5$ cm s^{-1}. (*1*) Pump current density.

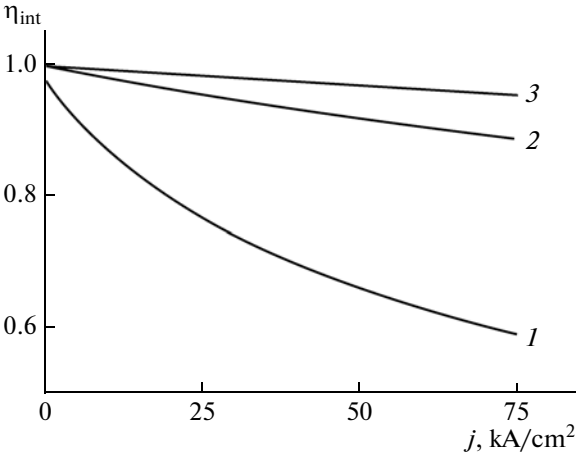

Fig. 8. Internal differential quantum efficiency vs. the pump current density for structures with (*1*) one, (*2*) two, and (*3*) three QWs. Capture velocity into a single QW, $v_{capt,0} = 10^6$ cm s^{-1}.

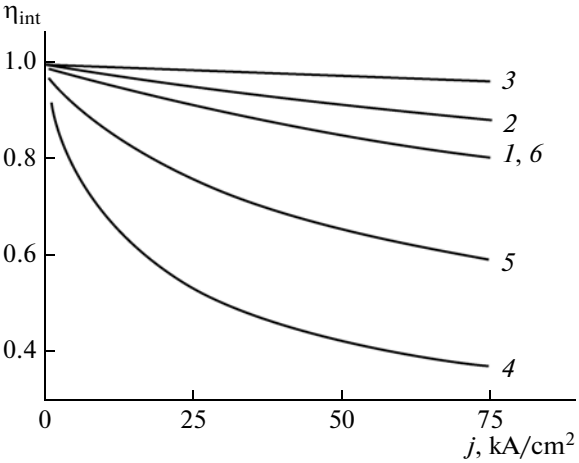

Fig. 9. Internal differential quantum efficiency vs. the pump current density for structures with (*1–3*) two and (*4–6*) one QW at various carrier capture velocities into a single QW, $v_{capt,0}$ (10^6 cm s^{-1}): (*1*) 0.7, (*2*, *5*) 1, (*3*, *6*) 2, and (*4*) 0.5.

The dependences of the charge-carrier concentration in the waveguide region on the pump current density are shown in Fig. 5 for structures with one (curve *1*), two (curve *2*), and three (curve *3*) QWs at a capture velocity $v_{capt,0} = 10^6$ cm s^{-1}. It can be seen that, at high pump levels, the carrier concentration in the OCL, n^{OCL}, above the lasing threshold is tens of times the threshold value of this concentration, n_{th}^{OCL}. The effect of carrier accumulation in the waveguide region is strong even in structures with multiple QWs and at high capture velocities. However, the n^{OCL} in double- and triple-well structures is multiple times lower than in that with a single well (Fig. 5). The difference between the triple- and double-well structures is substantially smaller than that between the double- and single-well structures.

Figure 6 compares the dependences $n^{OCL}(j)$ for structures with two QWs (curves *1–3*) and one QW (curves *4–6*) at various capture velocities $v_{capt,0}$: (*1*) 7×10^5, (*2*, *5*) 10^6, (*3*, *6*) 2×10^6, and (*4*) 5×10^5 cm s^{-1}. It can be seen in both Figs. 5 and 6 that, if two QWs are used in a laser structure instead of a single QW, the carrier accumulation effect in the waveguide region is manifested to a considerably lesser extent. The near coincidence of curves *1* and *6* in Fig. 6 means that the

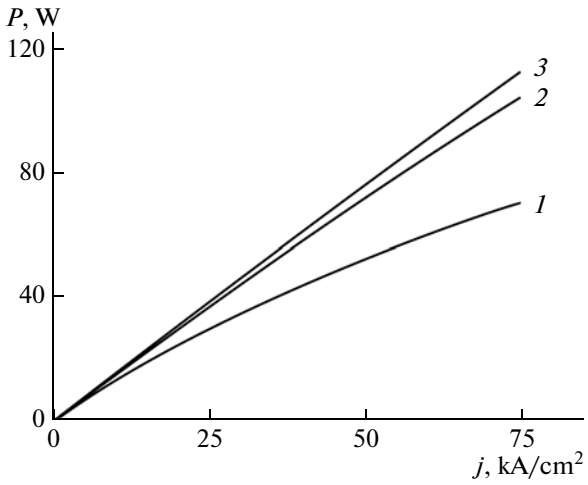

Fig. 10. Output optical power vs. the pump current density (L–I characteristic) for structures with (*1*) one, (*2*) two, and (*3*) three QWs. Capture velocity into a single QW, $v_{capt,0} = 10^6$ cm s^{-1}.

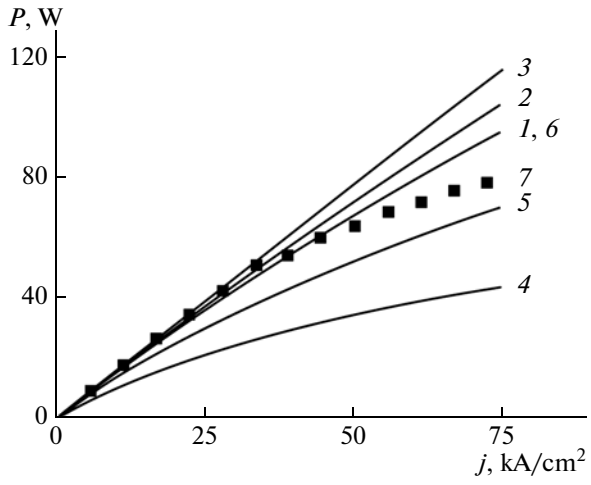

Fig. 11. Output optical power vs. the pump current density (L–I characteristic) for structures with (*1–3*) two and (*4–6*) one QW at various carrier capture velocities into a single QW, $v_{capt,0}$ (10^6 cm s^{-1}): (*1*) 0.7, (*2*, *5*) 1, (*3*, *6*) 2, and (*4*) 0.5. (*7*) Experimental L–I characteristic for a structure with one QW [26].

use of two QWs instead of a single one approximately corresponds to a threefold increase in the capture velocity for a single-well structure.

An increase in the carrier concentration in the waveguide region above the lasing threshold (Figs. 5 and 6) results, especially at low capture velocities, in the enhancement of the parasitic process in this region, i.e., spontaneous radiative recombination. Accordingly, the fraction of carriers involved in the beneficial stimulated recombination in the QW becomes smaller. Figure 7 shows for comparison the recombination current densities: stimulated in the QWs (j_{stim}, curves *2* and *4*) and spontaneous in the OCL (j_{spon}^{OCL}, curves *3* and *5*) in structures with one (curves *2* and *3*) and two (curves *4* and *5*) QWs. In the double-well laser structure (curves *4* and *5*), j_{spon}^{OCL} is small as compared with j_{stim} in the whole range of j values even at a low capture velocity $v_{capt,0} = 5 \times 10^5$ cm s^{-1}. At the same capture velocity in a structure with a single QW (curves *2* and *3*), the effect of carrier accumulation in the OCL is manifested to a considerably greater extent: at $j > 32$ kA cm^{-2}, j_{spon}^{OCL} exceeds j_{stim}.

Figure 8 shows the internal quantum efficiency η_{int} as a function of the pump current density j for laser structures with one (curve *1*), two (curve *2*), and three (curve *3*) QWs. The capture velocity $v_{capt,0}$ into an empty single QW was considered to be 10^6 cm s^{-1} for all three structures. It can be seen in the figure that, with the use of two QWs as the active region of the laser, instead of a single one, the internal efficiency markedly increases and its decay with increasing pump current becomes substantially slower. With the number of QWs increasing from two to three, η_{int} is improved further, but changes in the value of η_{int} and in the nature of its dependence on j are less significant.

Figure 9 compares the dependences $\eta_{int}(j)$ for structures with two QWs (curves *1–3*) and one QW (curves *4–6*) at various capture velocities $v_{capt,0}$ (cm s^{-1}): (*1*) 7×10^5, (*2*, *5*) 10^6, (*3*, *6*) 2×10^6, and (*4*) 5×10^5. As already noted, the parameter $j_{th}^{OCL}/j_{capt,th}$ governing $\eta_{int}(j)$ and the linearity of the L–I characteristic is more dependent on the number of QWs than on the capture velocity into a single QW. Just this circumstance is illustrated by comparison of curves *1* and *6* in Fig. 9. It can be seen that use of two QWs in the laser structure under consideration, instead of a single one, approximately corresponds to a threefold increase in the carrier capture velocity in a single-well structure.

Figure 10 shows the L–I characteristic (the dependence of the output power P on j, given by expression (1)) for structures with one (curve *1*), two (curve *2*), and three (curve *3*) QWs. The curves were calculated at a capture velocity of $v_{capt,0} = 10^6$ cm s^{-1}. It can be seen in the figure that, with two, instead of one, QWs used in the active region of the laser, the optical power at high pumping levels strongly increases, with the L–I characteristic remaining practically linear at any j in the range under study. With the number of QWs increasing from two to three, the emission power grows only slightly.

Figure 11 compares the L–I characteristics for structures with two (curves *1–3*) and one (curves *4–6*) QW at various capture velocities $v_{capt,0}$ (cm s^{-1}): (*1*) 7×10^5, (*2*, *5*) 10^6, (*3*, *6*) 2×10^6, and (*4*) 5×10^5. As also in Fig. 9, the proximity of curves *1* and *6* in Fig. 11 means

that using two QWs, instead of one, is approximately equivalent to a fivefold increase in the carrier capture velocity in a single-well structure. It can be seen in the figure that the increase in the sublinearity of the L–I characteristic with decreasing $v_{capt,0}$ is manifested in the single-well structure much more strongly, compared with the double-well structure. (The squares in Fig. 11 represent the experimental L–I characteristic from [26] for a structure with one QW ($\lambda_0 = 1.04$ μm).) Good agreement between the experimental and calculated (up to injection current densities of j = 45 kA cm^{-2}) L–I characteristics is achieved for a single-well structure at $v_{capt,0} = 2 \times 10^6$ cm s^{-1}. To describe the experimental L–I characteristics [26, 27] at even higher pump currents, it is be necessary to additionally take into account other factors, e.g., a possible increase in the carrier density in QWs themselves with increasing pump current.

4. CONCLUSIONS

It has been demonstrated that using two quantum wells (QWs) in a laser structure, instead of one, improves the efficiency of carrier capture into QWs, owing to which the component of the injection current, "spent" on stimulated recombination in the QWs, substantially exceeds that spent on spontaneous recombination in the waveguide region. This leads to an increase in the internal differential quantum efficiency and better linearity of the light–current characteristic in a double-well structure, compared with that of a single-well structure.

It has been shown for the structures with a GaAs waveguide region and $In_{0.28}Ga_{0.72}As$ QWs, considered in this study, that, to obtain the same output power in lasers with one and two QWs, the carrier capture velocity in the former must be approximately three times that in the latter. This means that the use of two QWs instead of one in our laser structures is approximately equivalent to a threefold increase in the carrier capture velocity.

It was demonstrated that a further increase in the number of QWs (i.e., the use of three or more QWs) only slightly improves the power characteristics of the laser. Thus, with consideration for the fact that the filling of the wells by carriers may be nonuniform at a greater number of QWs [28] and with the growth simplicity factor taken into account, it seems that the double-well structure is the most optimal for high-power lasing.

ACKNOWLEDGMENTS

The study was carried out by Z.N. Sokolova and I.S. Tarasov under the research plan of the Ioffe Physical–Technical Institute, Russian Academy of Sciences. It was in part supported by the Program OFN-III.7 and Program no. 24 of the Presidium of the Russian Academy of Sciences. L.V. Asryan thanks the U.S. Army Research Office for support of the present study (grant no. W911-NF-08-1-0462).

REFERENCES

1. S. O. Slipchenko, Z. N. Sokolova, N. A. Pikhtin, K. S. Borshchev, D. A. Vinokurov, and I. S. Tarasov, Semiconductors **40**, 990 (2006).
2. I. S. Tarasov, Quantum Electron. **40**, 661 (2010).
3. L. V. Asryan, S. Luryi, and R. A. Suris, Appl. Phys. Lett. **81**, 2154 (2002).
4. L. V. Asryan, S. Luryi, and R. A. Suris, IEEE J. Quantum Electron. **39**, 404 (2003).
5. Z. N. Sokolova, I. S. Tarasov, and L. V. Asryan, Semiconductors **45**, 1494 (2011).
6. D. Z. Garbuzov, A. V. Ovchinnikov, N. A. Pikhtin, Z. N. Sokolova, I. S. Tarasov, and V. B. Khalfin, Sov. Phys. Semicond. **25**, 560 (1991).
7. W. Rideout, W. F. Sharfin, E. S. Koteles, M. O. Vassell, and B. Elman, IEEE Photon. Technol. Lett. **3**, 784 (1991).
8. N. Tessler, R. Nagar, G. Eisenstein, S. Chandrasekhar, C. H. Joyner, A. G. Dentai, U. Koren, and G. Raybon, Appl. Phys. Lett. **61**, 2383 (1992).
9. H. Hirayama, J. Yoshida, Y. Miyake, and M. Asada, Appl. Phys. Lett. **61**, 2398 (1992).
10. H. Hirayama, J. Yoshida, Y. Miyake, and M. Asada, IEEE J. Quantum Electron. **30**, 54 (1994).
11. G. W. Taylor and P. R. Claisse, IEEE J. Quantum Electron. **31**, 2133 (1995).
12. P. M. Smowton and P. Blood, IEEE J. Sel. Top. Quantum Electron. **3**, 491 (1997).
13. G. W. Taylor and S. Jin, IEEE J. Quant. Electron. **34**, 1886 (1998).
14. L. V. Asryan, Quantum Electron. **35**, 1117 (2005).
15. L. V. Asryan and R. A. Suris, Semicond. Sci. Technol. **11**, 554 (1996).
16. I. N. Yassievich, K. Schmalz, and M. Beer, Semicond. Sci. Technol. **9**, 1763 (1994).
17. S. A. Solov'ev, I. N. Yassievich, and V. M. Chistyakov, Semiconductors **29**, 654 (1995).
18. A. Dargys and J. Kundrotas, Semicond. Sci. Technol. **13**, 1258 (1998).
19. R. A. Suris, NATO ASI Ser. E **323**, 197 (1996).
20. L. V. Asryan and R. A. Suris, Semiconductors **38**, 1 (2004).
21. L. V. Asryan, N. A. Gun'ko, A. S. Polkovnikov, G. G. Zegrya, R. A. Suris, P.-K. Lau, and T. Makino, Semicond. Sci. Technol. **15**, 1131 (2000).
22. L. V. Asryan, N. V. Kryzhanovskaya, M. V. Maximov, A. Yu. Egorov, and A. E. Zhukov, Semicond. Sci. Technol. **26**, 055025 (2011).
23. K. J. Vahala and C. E. Zah, Appl. Phys. Lett. **52**, 1945 (1988).
24. L. V. Asryan and S. Luryi, Appl. Phys. Lett. **83**, 5368 (2003).
25. L. V. Asryan and S. Luryi, IEEE J. Quantum Electron. **40**, 833 (2004).
26. A. V. Lyutetskii, K. S. Borshchev, N. A. Pikhtin, S. O. Slipchenko, Z. N. Sokolova, and I. S. Tarasov, Semiconductors **42**, 104 (2008).
27. D. A. Vinokurov, V. A. Kapitonov, A. V. Lyutetskii, N. A. Pikhtin, S. O. Slipchenko, Z. N. Sokolova, A. L. Stankevich, M. A. Khomylev, V. V. Shamakhov, K. S. Borshchev, I. N. Arsent'ev, and I. S. Tarasov, Semiconductors **41**, 984 (2007).
28. N. Tessler and G. Eisenstein, Appl. Phys. Lett. **62**, 10 (1993).

Translated by M. Tagirdzhanov